

# A Review of the Models and Mechanisms for Environmentally-Assisted Crack Growth of Pressure Vessel and Piping Steels in PWR Environments

---

Prepared by W. Cullen, G. Gabetta, H. Hanninen

Materials Engineering Associates, Inc.

Prepared for  
U.S. Nuclear Regulatory  
Commission

## NOTICE

This report was prepared as an account of work sponsored by an agency of the United States Government. Neither the United States Government nor any agency thereof, or any of their employees, makes any warranty, expressed or implied, or assumes any legal liability of responsibility for any third party's use, or the results of such use, of any information, apparatus, product or process disclosed in this report, or represents that its use by such third party would not infringe privately owned rights.

## NOTICE

### Availability of Reference Materials Cited in NRC Publications

Most documents cited in NRC publications will be available from one of the following sources:

1. The NRC Public Document Room, 1717 H Street, N.W.  
Washington, DC 20555
2. The Superintendent of Documents, U.S. Government Printing Office, Post Office Box 37082,  
Washington, DC 20013-7082
3. The National Technical Information Service, Springfield, VA 22161

Although the listing that follows represents the majority of documents cited in NRC publications, it is not intended to be exhaustive.

Referenced documents available for inspection and copying for a fee from the NRC Public Document Room include NRC correspondence and internal NRC memoranda, NRC Office of Inspection and Enforcement bulletins, circulars, information notices, inspection and investigation notices, Licensee Event Reports, vendor reports and correspondence, Commission papers, and applicant and licensee documents and correspondence.

The following documents in the NUREG series are available for purchase from the GPO Sales Program: formal NRC staff and contractor reports, NRC sponsored conference proceedings, and NRC booklets and brochures. Also available are Regulatory Guides, NRC regulations in the *Code of Federal Regulations*, and *Nuclear Regulatory Commission Issuances*.

Documents available from the National Technical Information Service include NUREG series reports and technical reports prepared by other federal agencies and reports prepared by the Atomic Energy Commission, forerunner agency to the Nuclear Regulatory Commission.

Documents available from public and special technical libraries include all open literature items, such as books, journal and periodical articles, and transactions. *Federal Register* notices, federal and state legislation, and congressional reports can usually be obtained from these libraries.

Documents such as theses, dissertations, foreign reports and translations, and non-NRC conference proceedings are available for purchase from the organization sponsoring the publication cited.

Single copies of NRC draft reports are available free, to the extent of supply, upon written request to the Division of Technical Information and Document Control, U.S. Nuclear Regulatory Commission, Washington, DC 20555.

Copies of industry codes and standards used in a substantive manner in the NRC regulatory process are maintained at the NRC Library, 7920 Norfolk Avenue, Bethesda, Maryland, and are available there for reference use by the public. Codes and standards are usually copyrighted and may be purchased from the originating organization or, if they are American National Standards, from the American National Standards Institute, 1430 Broadway, New York, NY 10018.

---

# A Review of the Models and Mechanisms for Environmentally-Assisted Crack Growth of Pressure Vessel and Piping Steels in PWR Environments

---

Manuscript Completed: September 1985  
Date Published: December 1985

Prepared by  
W. Cullen, G. Gabetta\*, H. Hanninen\*\*

Materials Engineering Associates, Inc.  
9700-B George Palmer Highway  
Lanham, MD 20706-1837

\*Centro Informazioni Studii Esperienze (CISE)  
\*\*Technical Research Centre of Finland (VTT)

Prepared for  
Division of Engineering Technology  
Office of Nuclear Regulatory Research  
U.S. Nuclear Regulatory Commission  
Washington, D.C. 20555  
NRC FIN B8900

## ABSTRACT

The crack-tip micromechanisms and the computational models for environmentally-assisted cracking in pressure vessel and piping steels in high-temperature, low-oxygen (PWR), reactor-grade water are described and evaluated in this report. The report begins with a brief description of the critical variables which are known to affect environmentally-assisted subcritical cracking in these metal/environment systems. The micromechanistic models are discussed in some detail, with anodic dissolution and hydrogen assistance being the prime candidates for the successful explanation of the observed phenomena. The anodic dissolution model offers far better quantification of the environmentally-assisted crack growth rates, but tends to overpredict the rates for a large number of conditions. The hydrogen assistance models qualitatively could account for a wider range of effects, but quantification of the model is virtually nonexistent. A variety of calculational models are in various stages of development; all of them are far from use as a predictive tool. Crack-tip strain rate models have received the most attention, and the approach to their use has been to partition the environmentally-assisted growth rates into a mechanically-driven component, with the environmental enhancement superposed. The environment component is then correlated with a calculated crack-tip strain rate. At the present time, these models predict monotonically increasing growth rates with increases in the cyclic period, which is incorrect, although for cases in which the environment assistance is significant, the strain rate models, with a suitable choice of fitting parameters, correlate with the data reasonably well.

## CONTENTS

	<u>Page</u>
ABSTRACT.....	iii
LIST OF FIGURES.....	vii
ACKNOWLEDGEMENT.....	xi
1. INTRODUCTION.....	1
2. REVIEW OF CRITICAL TEST VARIABLES.....	2
2.1 Load Ratio and Test Frequency Effects.....	3
2.2 Waveform Effects.....	3
2.3 Material Chemistry and Microstructural Effects.....	3
2.4 Temperature Effects.....	9
2.5 Irradiation.....	9
2.6 Water Chemistry - Dissolved Oxygen Content.....	9
2.7 Fractography, Metallography and Oxide Analysis.....	12
3. MECHANISMS FOR ENVIRONMENTALLY-ASSISTED CRACKING.....	18
3.1 Anodic Dissolution Mechanisms.....	20
3.2 Hydrogen-Induced Cracking Mechanisms.....	27
3.3 Summary and Discussion of Mechanisms.....	39
4. COMPUTATIONAL MODELS FOR ENVIRONMENTALLY-ASSISTED CRACK GROWTH RATES.....	47
4.1 Crack Tip Strain Rate.....	49
4.2 Finite Element Model (FEM) Calculations.....	74
4.3 Slip Controlled (Deformation) Models.....	84
5. SUMMARY OF MECHANISMS AND MODELS.....	91
6. RECOMMENDED RESEARCH.....	93
REFERENCES.....	96

LIST OF FIGURES

<u>Figure</u>		<u>Page</u>
1	Fatigue crack growth rate for A 106 Gr. C steel....	4
2	Effect of frequency on fatigue crack growth rates....	5
3	Fatigue crack growth rates for two different loading waveforms.....	6
4	fatigue crack growth rate for medium sulfur steel....	7
5	Fatigue crack growth rates for steels of three sulfur levels.....	8
6	Fatigue crack growth rates vs. inverse temperature....	10
7	Fatigue crack growth rate for irradiated pressure vessel steels.....	11
8	Fatigue crack growth rate for higher oxygen and near-zero oxygen environment.....	13
9	Fatigue crack growth rate vs. inverse temperature....	14
10	Fatigue fracture surface of A 508-2 tested at 288°C....	15
11	Matching fatigue fracture surfaces for high sulfur A 533-B.....	16
12	Circular area fatigue fracture surface.....	17
13	Schematic of possible effects of environment.....	19
14	Average crack propagation rate and the oxidation kinetics.....	22
15	Factors of importance in the constant-charge criterion for SCC crack propagation.....	23
16	Oxidation charge density and penetration with time....	25
17	Crack-tip penetration with time.....	26
18	Crack growth rate/crack-tip strain rate relationships....	27
19	Theoretical and observed $da/dN$ vs. $\Delta K$ relationships.....	29
20	Comparison between ASME XI and the theoretical rates....	30
21	Hydrogen assistance during cyclic crack growth....	31
22	Environment/metal interaction model.....	37
23	Schematic illustrations of crack growth mechanisms....	38

LIST OF FIGURES

<u>Figure</u>		<u>Page</u>
24	Stress corrosion crack growth according to the slip-dissolution model.....	40
25	Fatigue crack growth data in hydrogen and upper bound growth predictions.....	46
26	Formation of a micronotch from underfilm crevice attack.....	48
27	Cylindrical slow strain rate specimens and the $\dot{\epsilon}$ calculation.....	50
28	Strain evaluation in smooth specimens.....	51
29	Strain evaluation in notched specimens.....	51
30	Strain vs. time and the $\dot{\epsilon}$ formulation.....	52
31	Crack tip strain rates for sinusoidal and triangular fatigue cycles.....	54
32	Average, maximum and minimum crack tip strain rates....	56
33	"Plateau" rates of environmentally-assisted crack growth.....	57
34	Schematic of a compact fracture specimen.....	58
35	Behavior of $K$ , $\delta$ , and $\delta^{\circ}$ during the loading part of sine and ramp cycles.....	60
36	Plot of the average $\dot{\epsilon}$ as a function of $a/W$ .....	61
37	Environmental $da/dt$ plotted vs. $\epsilon_{sc}$ .....	62
38	Crack growth rate curves for different frequencies....	64
39	Plastic strain at different positions with respect to the crack tip.....	65
40	Plastic strain and $\dot{\epsilon}$ as a function of crack length....	66
41	Crack growth rate as a function of $\dot{\epsilon}$ .....	68
42	Bounding crack growth curves.....	69
43	Environmental component of crack growth rate.....	71
44	Environmental component of crack growth rate.....	72
45	Environmental component of crack growth rate.....	73

LIST OF FIGURES

<u>Figure</u>	<u>Page</u>
46	Coordinate scheme for a crack tip blunting model.... 75
47	Undeformed and deformed crack tip..... 75
48	Fine mesh finite element model of a crack tip region.... 77
49	Cyclic stress-strain curve for A 508..... 78
50	Blunted crack in A 508-2 steel at 300°C..... 79
51	Crack tip root strain and crack tip opening width for A 508 steel at 300°C..... 80
52	Blunted crack in A 508-2 steel at 300°C..... 81
53	Crack tip root strain for A 508..... 82
54	Crack tip root stress and strain as a function of time..... 83
55	Crack tip at the $\Delta K_{eff}$ just exceeding the threshold.... 86
56	Crack tip at a large $\Delta K_{eff}$ showing four and a half slip lines..... 86
57	Measurement method used to quantify the stereoimaged displacements..... 88
58	Effective strain range ahead of the crack in 304 stainless steel..... 89
59	Computed crack-tip strain rates for crack closure and threshold stress intensity..... 90



#### ACKNOWLEDGEMENT

The authors would like to acknowledge the time, effort and contributions made by three individuals who reviewed this report. These were: Dr. John Atkinson, Central Electricity Research Laboratories, Leatherhead, Surrey, UK; Dr. Peter Ford, General Electric Corporation Research and Development Laboratory, Schenectady, New York, USA; and Dr. Peter Scott, United Kingdom Atomic Energy Authority, Harwell Laboratories, Didcot, UK. The CISE contribution to this report was supported by ENEL-CRTN. The ENEL-CISE program was managed by Dr. Stefano Ragazzoni and Dr. Vittorio Regis. Dr. Frank Loss is to be acknowledged for his plan of action for this report, and for continued encouragement during the assembly of the document. All the authors appreciate the continued interest and support of Mr. Milton Vagins, the NRC program manager.

## 1. INTRODUCTION

The prediction of fatigue crack growth rates of pressure vessel and piping steels in the high temperature water environment in which they are employed involves consideration of a huge number of variables and their mutual interactions. Over the last 15 years or so, the effects of load ratio, waveform, material and environment chemistries, and loading frequencies have been determined to a reasonable degree of accuracy. However the certainty of safety assurance calculations has not improved as rapidly as our knowledge of fatigue crack growth rates and what influences them. This is largely because of the following factors:

- (1) Crack Growth rates have been determined at rather high levels of maximum stress intensity factor  $K_{max}$ , which in fact addresses the final stages of flaw growth, but not the initial stages, and it is in the initial stages that most of the available lifetime is used up. Also, laboratory tests are conducted using rather high cyclic frequencies (in the millihertz range) whereas most pressure-induced load transients are in the microhertz range, and crack growth rates in high temperature, deoxygenated environments (i.e., PWR coolants) do not scale with frequency as well as those for example, of structural steels in marine environments.
- (2) The critical variables interact in ways which have not been well determined. As an example, it is well known that "linearized" waveforms, such as triangular, or ramp/reset forms, generate lower crack growth rates in PWR environments, than do sinusoidal waveforms of the same cyclic period. However, it has not been sufficiently well determined that this conclusion holds for all load ratios. In fact, the conclusion about wave shape is valid currently only for load ratio (R) = 0.2.
- (3) Laboratory tests are conducted in model, or idealized environments, which, for the most part, are reasonably well maintained and characterized. But actual operating conditions vary, albeit over presumably narrow ranges, but ones for which growth rates may also exhibit wide variations. As an example, growth rates in pressure vessel steels vary by about a factor of eight with temperature changes from 200°C (growth rates at a minimum) to about 340°C (the maximum investigated). Included in this area of concern are the possibly damaging effects of off-chemistry transients, such as contaminant intrusions or oxygen excursions, which might severely affect crack growth characteristics.
- (4) Actual loading schemes are comprised of variable amplitude, variable frequency cycles, while laboratory tests are usually constant load amplitude, or constant applied cyclic stress intensity factor (constant  $\Delta K$ ) tests, with only occasional changes in test frequency. The influence of load interactions has not been determined to the degree necessary to support reasonable calculational accuracy.

- (5) Laboratory testing is usually carried out using compact tension fracture specimens, which are useful because they have a sensitive compliance to crack length relationship. However, they also exhibit a large crack mouth opening, a large bending moment, and crack extension in only one dimension, as compared with "real" cracks, which exist (usually) in a predominately tensile stress field, propagate in two dimensions, and have a very small aperture. The difference in stress field, and stress gradient, at the crack tip, may also influence the distribution of carbon and hydrogen atoms, resulting perhaps in mechanistic changes in environmentally-assisted crack growth.

While great progress has been made in identifying the critical variables which influence fatigue crack growth rates in high temperature water environments, these studies are a classic case of the more you know, the more you know there is to know. It is reasonably clear that it is impossible to test for all the combinations of variables and conditions which may obtain under even a reasonable spectrum of operating reactor conditions, let alone transients due to unexpected events. For this reason, it has long been recognized that if the micromechanisms and associated reaction rates responsible for the environmental component of the fatigue cracking could be identified or calculated, that analytical models of cracks in structures could be constructed, and crack growth rates could be computed with some certainty.

The objective of this report is to review briefly the variables which influence fatigue crack growth rates in high temperature, deoxygenated (PWR) environments, in order to identify what the mechanisms must account for as a minimum. Secondly, the suggested mechanisms are described, along with their advantages and disadvantages and the calculational models which are available are reviewed. In the final sections of the report, some research approaches are suggested which may lead to additional confirmation of the mechanisms or their limitations.

## 2. REVIEW OF CRITICAL TEST VARIABLES

In order to set the stage appropriately for the discussion of mechanisms and associated models, a brief review of the known critical variables will be presented. This provides the basis for consideration of the mechanisms by identifying the trends in fatigue crack growth rates which have been observed in the cumulative research of the last 10 to 15 years. For contrast, the reader may be referred to an earlier review (Ref. 1), which described the state-of-the-art knowledge of both critical variables and micromechanisms in 1980, together with one of the earliest suggestions that hydrogen assistance may be responsible principally for environmentally-enhanced fatigue crack growth in PWR environments.

## 2.1 Load Ratio and Test Frequency Effects

For many metal alloy/environment combinations, these two well-known variables could be considered separately. But it has been clearly demonstrated that there is a strong interaction between the two for PWR water. As shown in Fig. 1, as load ratio, R, increases, crack growth rates increase also. However, Scott has determined (Ref. 2) that increasing the test frequency from 17 mHz to 5, 10 or 20 Hz, produced increased crack growth rates at the high load ratio of 0.7 to 0.9. Van Der Sluys (Ref. 3) has made a careful determination of these effects, using constant  $\Delta K$  test and a wide range of cyclic frequencies. As illustrated in Fig. 2, he found that a maximum in crack growth rates could be obtained at some frequency, which depended on R (and possibly also the material chemistry). For load ratios of 0.2, 17 mHz sinusoidal waveforms give a maximum in fatigue crack growth rates. Although these findings are reasonably well accepted now, they have been slow in gaining credibility since there is no analogy for this phenomenon for other better known and more investigated alloy steels in aqueous environments. Also, these results are rather recent, and their full importance has not been carefully determined.

## 2.2 Waveform Effects

As above, there is no historical basis for expecting that the waveform should have any influence on environmentally-assisted crack growth rates. The work of Barsom (Ref. 4) established such a strong precedent in this area that experimental focus is usually on rise times of the waveform rather than shape of the waveform. Additionally, many reactor transients are supposed to have a saw-toothed shape, and some laboratories adopted saw-toothed waveforms as the basis for their research, in an attempt to provide more realistic simulation of reactor conditions in their test parameter matrix. However, it has been conclusively shown, in experiments replicated at several laboratories, that sinusoidal waveforms consistently provide higher crack growth rates than triangular or ramp waveforms of equivalent cyclic period or rise time (Refs. 5 and 6). An example of this is shown in Fig. 3. Thus, while linearized waveforms may be more realistic, sinusoidal waveforms maximize the effects of the environment, making these effects easier to study, and providing more conservative data.

## 2.3 Material Chemistry and Microstructural Effects

Shortly after the waveform dependence was sorted out in 1979, it became clear that the sulfur content had an important effect on crack growth rates, with the higher sulfur steels ( $> 0.012\% S$ ) often showing high crack growth rates, compared to steels of lower sulfur content. Bamford (Ref. 7) has published results from an extensive test matrix involving sulfur contents of A 533-B steel, and crack plane and propagation orientation with respect to the rolling direction of the plate. Some of these results are shown in Fig. 4; other, independently acquired results are shown in Figs. 5a and 5b. Steels of low sulfur content generally exhibit only a slight increase in crack growth rates compared with those in air, but this may be due as much to the fact that the manganese sulfide inclusions in these steels are

APPLIED CYCLIC STRESS INTENSITY FACTOR,  $\text{ksi}\sqrt{\text{in}}$

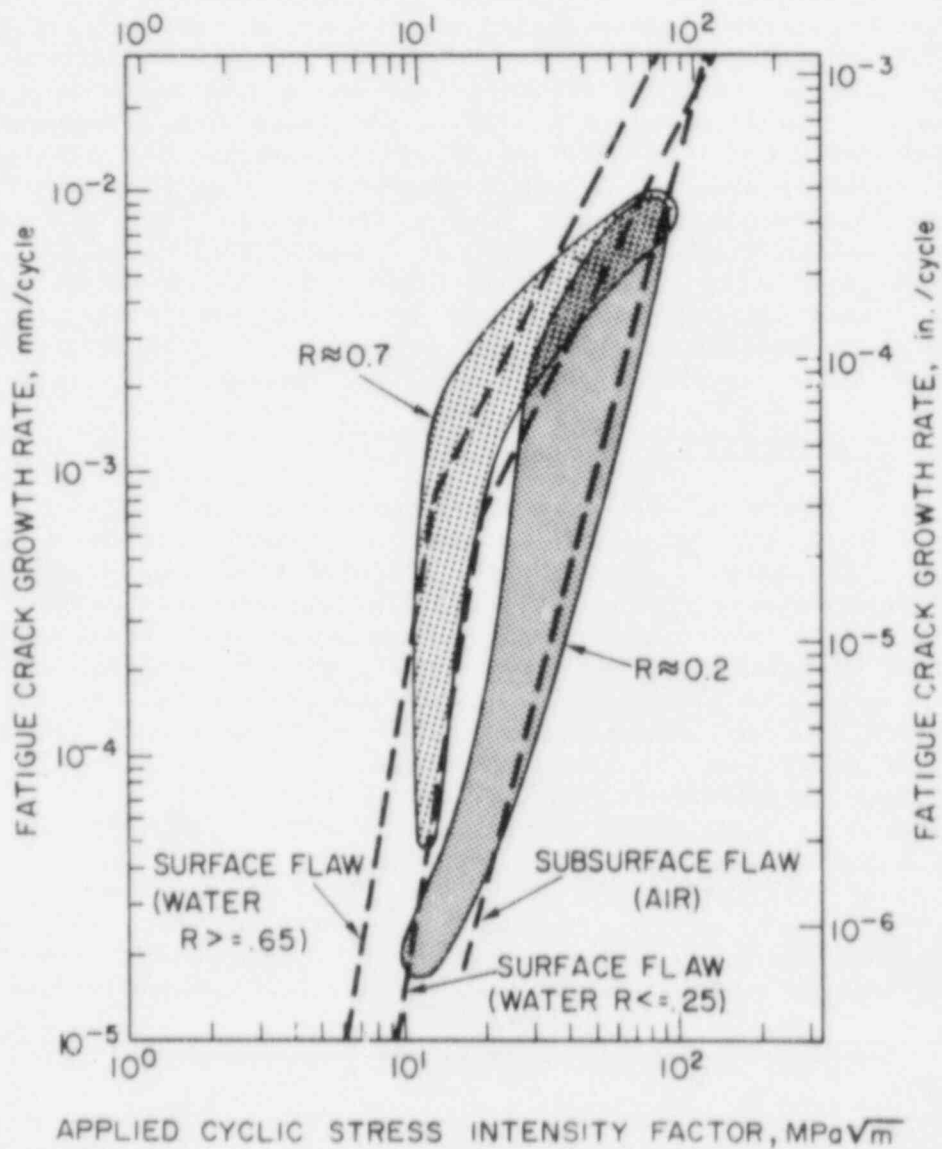


Fig. 1 Fatigue crack growth rate vs. applied cyclic stress intensity factor for A 106 Gr. C steel in 288 C PWR environment, for load ratios of 0.2 and 0.7.

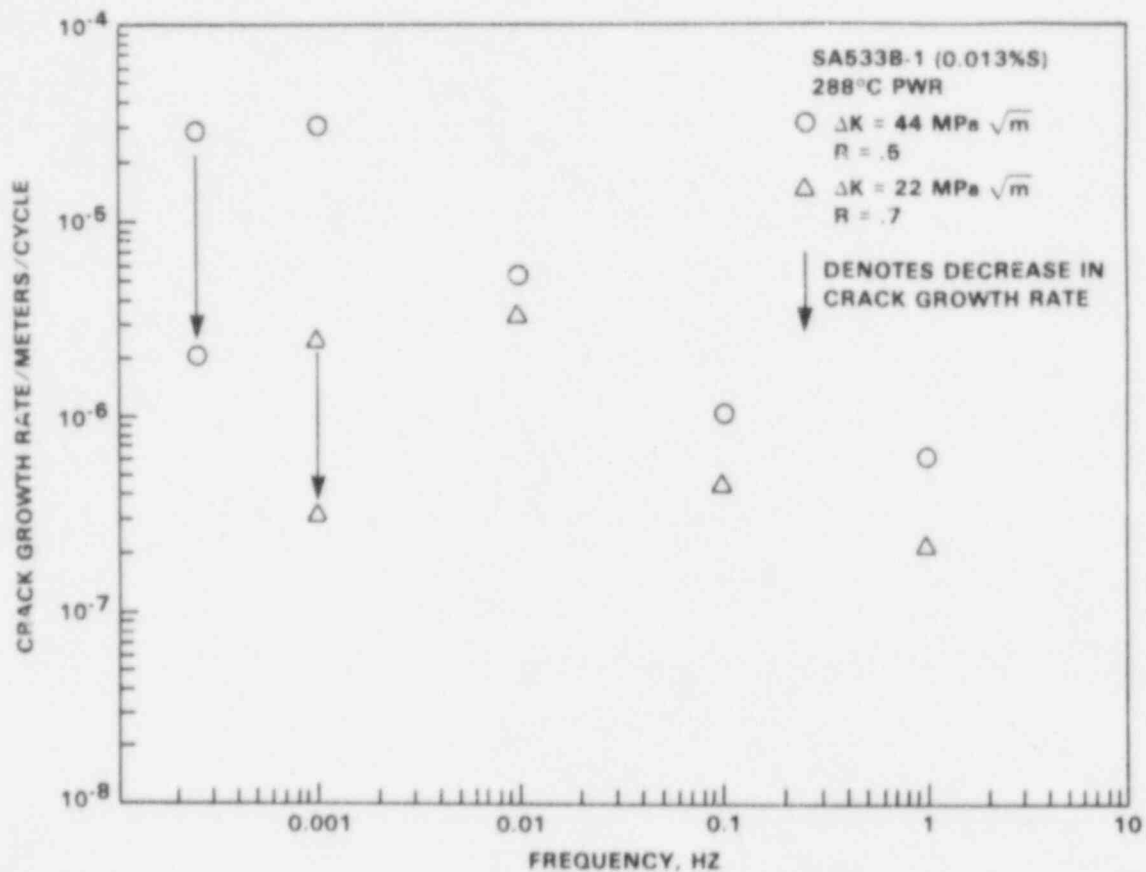


Fig. 2 Effect of frequency on fatigue crack growth rates from a series of constant  $\Delta K$  experiments. Note the maximum in growth rate at a test frequency of about 0.001 Hz (Ref. 3).

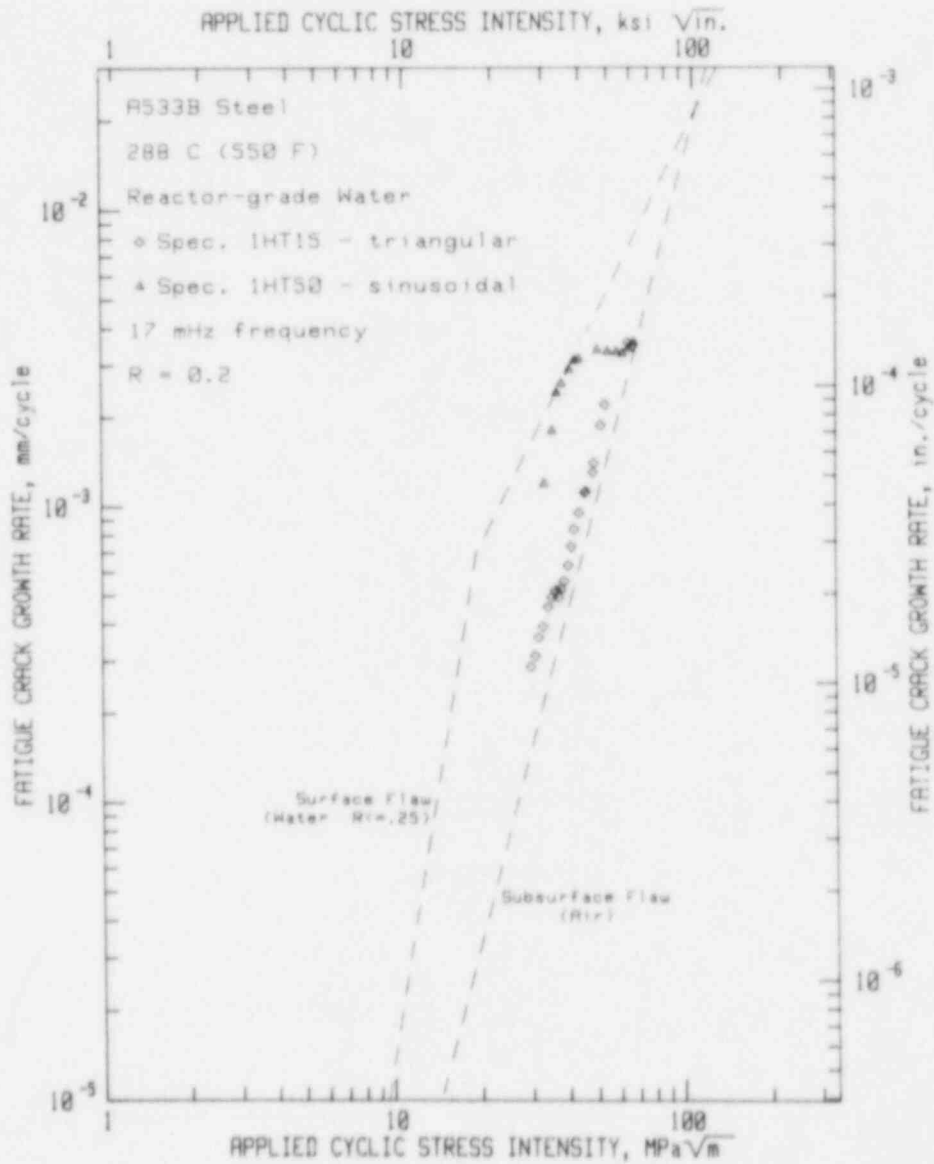


Fig. 3 Fatigue crack growth rates vs. applied cyclic stress intensity factor for tests of two different loading waveforms. Note that the growth rates are much slower for the triangular waveform, even though the cyclic period is the same as for the sinusoidal waveform (Ref. 5).

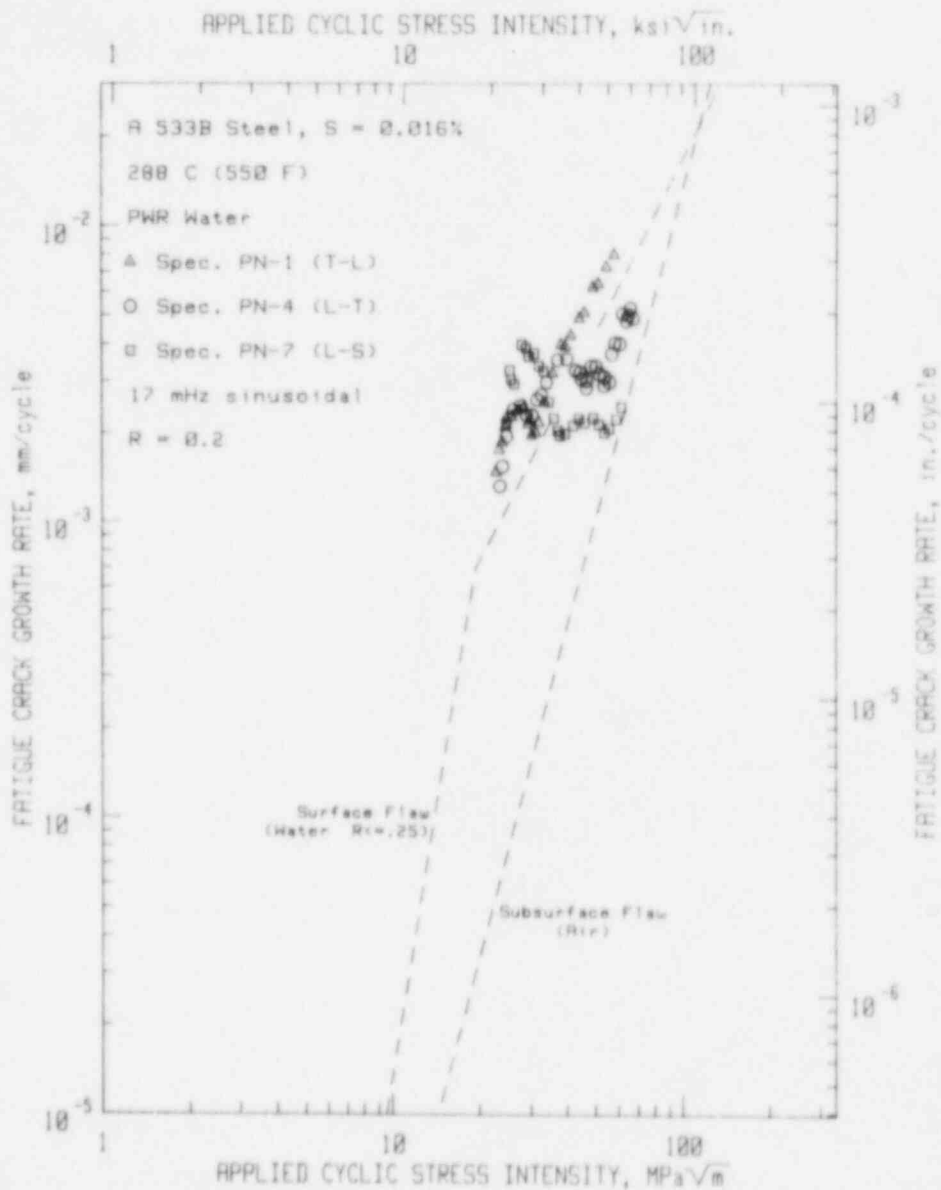


Fig. 4 Fatigue crack growth rate vs. applied cyclic stress intensity factor for a steel of medium sulfur content tested at a load ratio of 0.2. These results show a high degree of environmental assistance, and a strong orientation effect (Ref. 7).



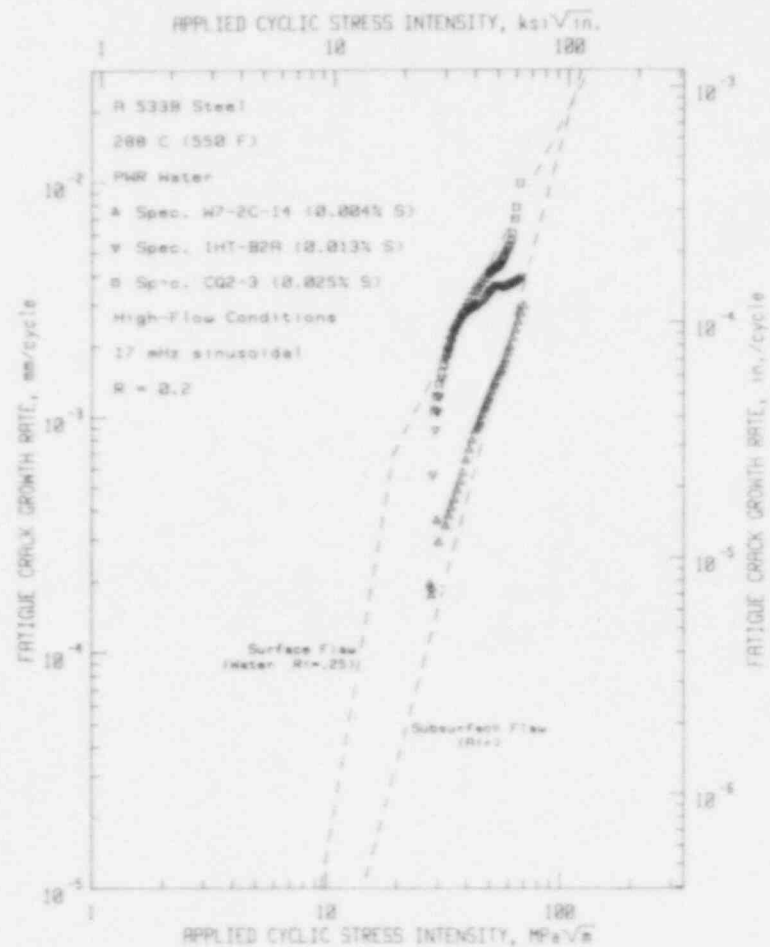
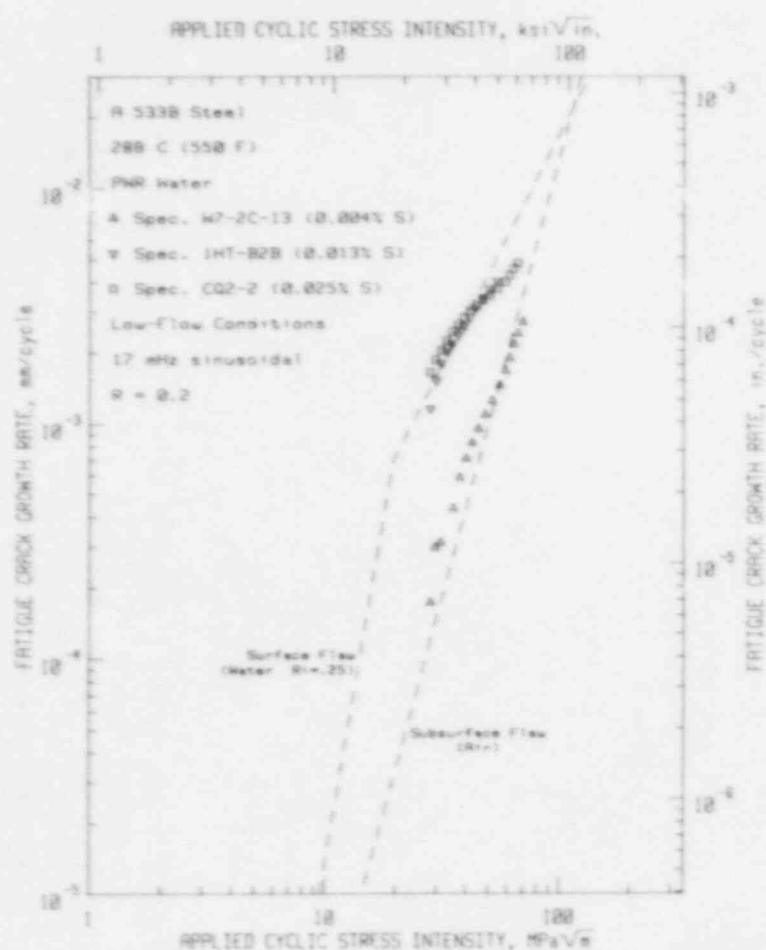


Fig. 5 Fatigue crack growth rates vs. applied cyclic stress intensity factor for multispecimen tests of steels of three sulfur levels but identical crack plane orientation at two environmental flow rates: (a) 50 liters/hour and (b) 3000 liters/hour. Note that low rate appears to have no effect, but growth rates are strongly dependent on sulfur content of steels (Ref. 8).

more spheroidal in shape, rather than elongated or plate-like. Equally important is the orientation of the crack plane with respect to the inclusion axes. When the crack plane contains the long axis of the inclusions, the degree of environmental assistance is increased, often dramatically. There is some evidence that steels of low sulfur content can produce high crack growth rates (Ref. 9), and conversely, that steels of medium sulfur content exhibit little environmental effect (Ref. 10). There is active research in this area at present, and it is likely that these variables will become much better defined in the near future.

#### 2.4 Temperature Effects

Research on the effect of temperature on environmentally-assisted fatigue crack growth in PWR environment has shown that for low alloy pressure vessel steels, there is a minimum in crack growth rates at about 200°C, with growth rates increasing rapidly and linearly above that temperature, but rising to a plateau below that temperature (Ref. 11). This is shown in Fig. 6, in which growth rates are plotted for specific values of  $\Delta K$ . While this basic finding was confirmed at two other laboratories (Refs. 12 and 13), there is some indication that the effect might vary for different materials. Since this research was conducted using 17 MHz sinusoidal waveforms, thus maximizing the environment effects, it is likely that changes in test frequency would alter the degree of this effect.

#### 2.5 Irradiation

It was feared that irradiation would seriously aggravate the amount of environmental enhancement to fatigue crack growth rates, but the data base currently available fails to support that fear (Ref. 14). Data sets for two pressure vessel steels are shown in Figs. 7a to 7c. The data in Fig. 7b may be compared with Fig. 7d, indicating that for this set of conditions (i.e., product form, test frequency and temperature), irradiation has little observable effect. Obviously, there is a whole spectrum of other conditions which should be investigated before this becomes a generic conclusion.

#### 2.6 Water Chemistry-Dissolved Oxygen Content

Although this review is concerned only with operating PWR (low dissolved oxygen) environments, it is worthwhile to mention that the dissolved oxygen content of the water and thus the electrochemical potential is one of the most critical variables, and that the effects described above are almost all different for water containing 200 ppb or more dissolved oxygen (BWR environments). For this reason, it is surmised that the principal mechanism (if there is only one) is likely to be quite different in each case. As examples of this difference it should be pointed out that crack growth rates increase monotonically with increases in ramp time (Ref. 13), as shown in Fig. 8a. Over approximately the same frequency range, growth rates for linearized waveforms in PWR environments show little environmental effects at all (Ref. 6) and, if anything, exhibit a slight decrease in growth rate as the cyclic period increases (Fig. 8b). Temperature effects in higher

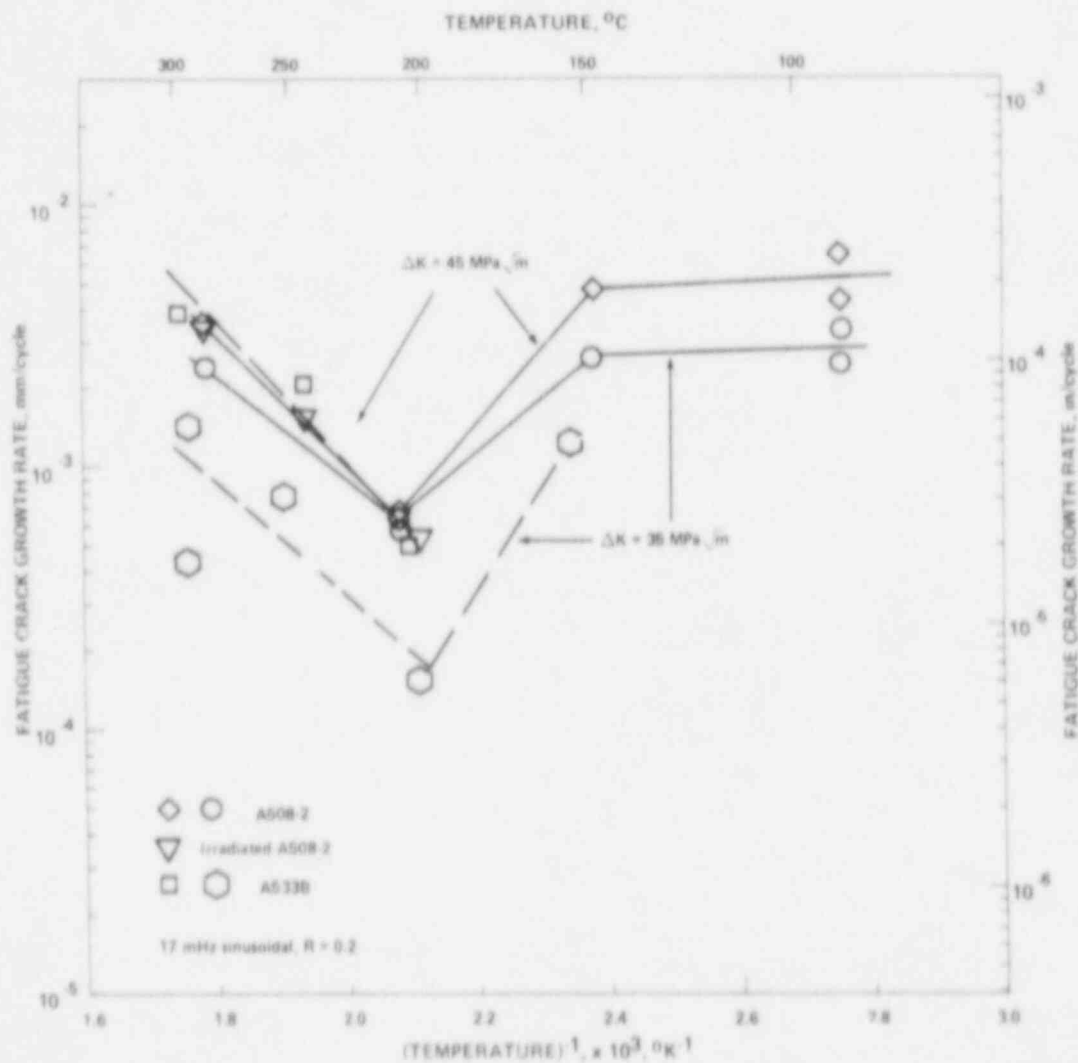


Fig. 6 Fatigue crack growth rate for fixed values of applied cyclic stress intensity factor versus inverse temperature, showing the minimum in growth rates for the load ratio and temperature of about 200°C in PWR environment (Ref. 11).

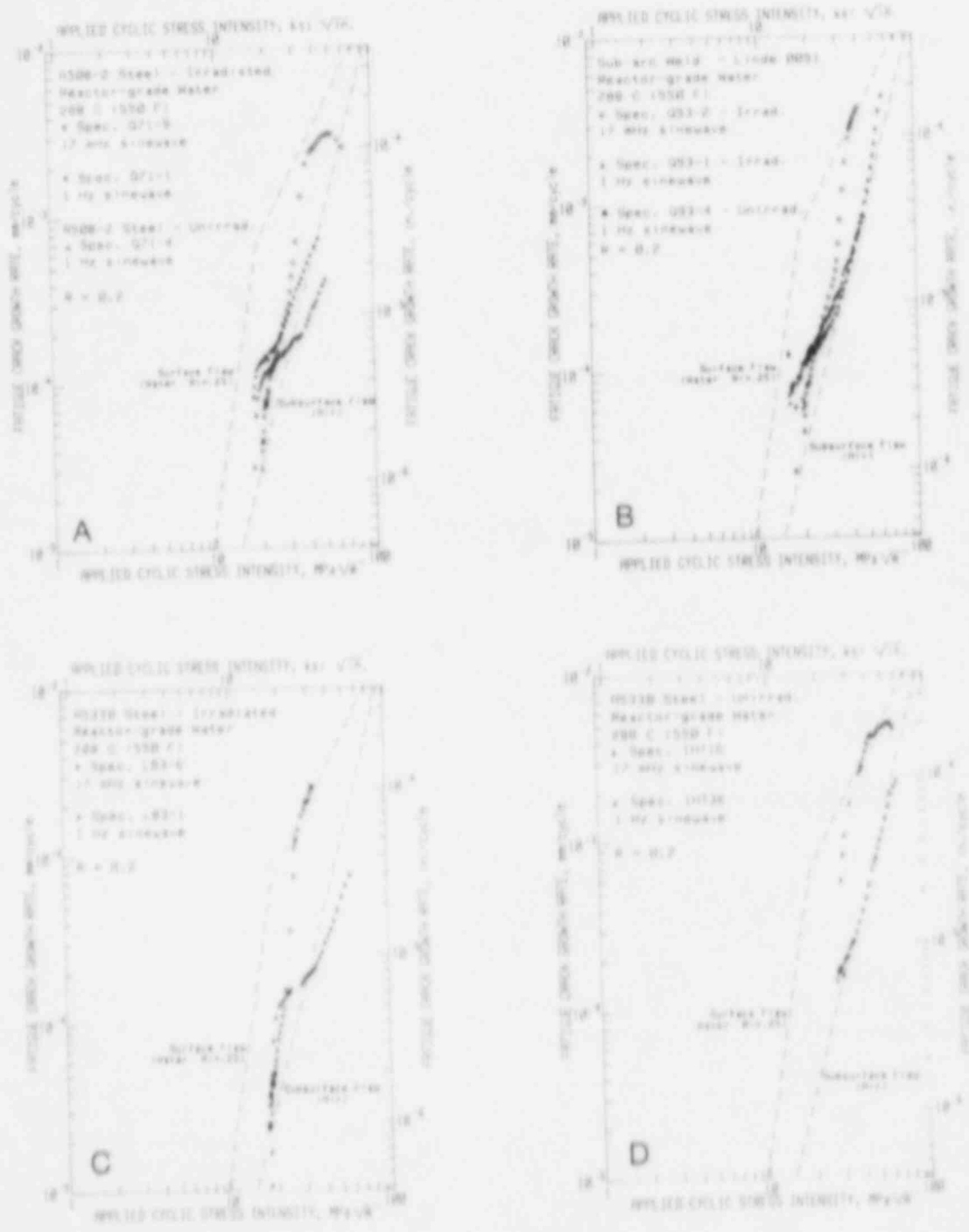


Fig. 7 Fatigue crack growth rate vs. applied cyclic stress intensity factor for irradiated pressure vessel steels (a through c) and an unirradiated companion steel. These data sets show that irradiation appears to have little effect on environmentally-assisted fatigue crack growth rates for the load ratio and temperature range explored (Ref. 14).

dissolved oxygen environments are quite different also. The benchmark research on this topic was conducted by Kondo in the early 1970's (Ref. 15) and is contrasted in Fig. 9 with the more recent PWR results described in Section 2.4. More recent results in BWR environments (Ref. 16), showing a more complex temperature dependence, suggest that material chemistry may also play an important role in the magnitude and trend of temperature effects. Research on irradiation effects in BWR environments will be underway shortly in Japan (Ref. 17).

### 2.7 Fractography, Metallography and Oxide Analysis

Fractographic observations have played a very important role in the delineation of the microprocesses which have taken place at the crack tip. It was first observed in 1978-1979 (Ref. 6) that the fatigue fracture surface of specimens tested in PWR environments appeared to have a brittle-like structure when the associated data exhibited a large degree of environmental enhancement. These brittle-like features included fan-shaped areas and brittle striations, but did not include intergranular cracking. The fan-shaped areas shown in Fig. 10 usually emanate from a manganese sulfide inclusion site, and the MnS inclusions are often dissolved, particularly if they have been exposed for some time. Since that time, a significant data base of fractographic studies has emerged (Ref. 18), and it has been determined additionally that fatigue fracture surfaces match almost exactly, as shown in Fig. 11 indicating minor or no dissolution of the metal matrix, and that what appears to be evidence of hydrogen-induced blister cracking is scattered over the fatigue fracture surface (Fig. 12), and in fact may be also found in locations ahead of the crack front (Ref. 8). Similar features are found on the fracture surfaces of specimens tested in hydrogen sulfide gas environments. It has been postulated that the dissolving MnS inclusions form hydrogen sulfide, resulting in this similarity (Ref. 19).

Metallographic research has also contributed several clues to the mechanistic studies. Cross-sectioning studies of environmentally-assisted fatigue cracks have shown that the cracking is fully transgranular, and is seldom accompanied by microbranching (Ref. 18). Cracks often change direction in order to intersect manganese sulfide inclusions. It is unclear whether this is due to increase in the local stress field due to the poorly-bonded and weak inclusion (Ref. 20), or whether the inclusion has acted as an extremely strong hydrogen trap (Ref. 21). Recent recrystallization studies indicated that the plastic zone associated with environmentally-assisted cracking is discontinuously formed along the flanks of the crack, and that there is extensive carbon depletion within this zone (Ref. 22). Companion studies on specimens tested in high temperature air environments showed no such carbon depletion and a plastic zone which was continuously formed and which monotonically increased in size with increasing  $K_{max}$ .

Studies of the oxide formed on the flanks of fatigue cracks can be used to infer the nature of the chemical processes which might have taken place at the time of fatigue fracture or soon afterward. These studies have revealed that the basic oxide is magnetite regardless of

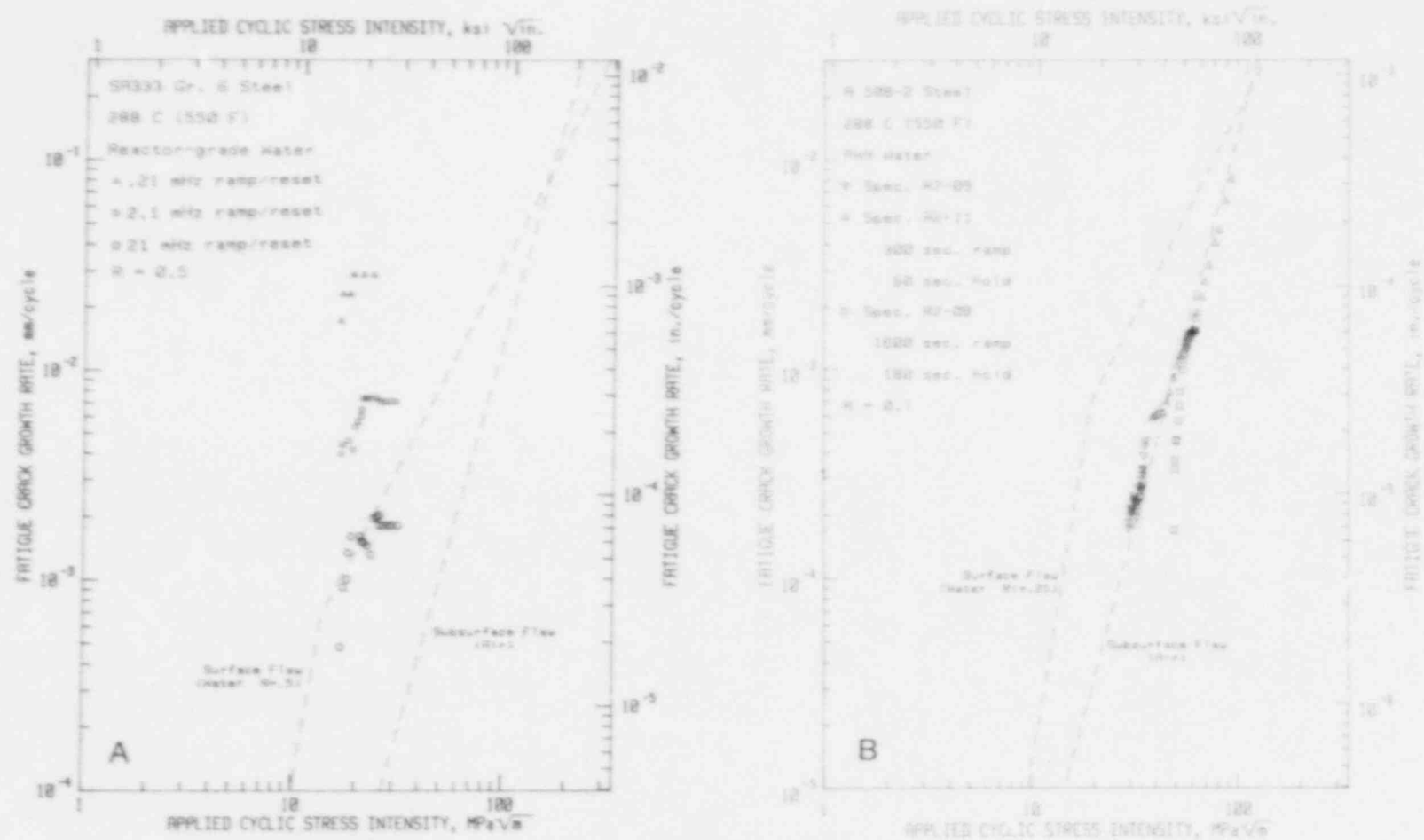


Fig. 8 Fatigue crack growth rate vs. applied cyclic stress intensity factor for both higher oxygen (BWR-typical) environment (a) and near-zero oxygen (PWR-typical) environment (b) as a function of cyclic period. Note that, as in Fig. 2, long cyclic periods result in a decrease in growth rates for the PWR conditions, but an increase in growth rates for the BWR conditions (Refs. 1 and 13).

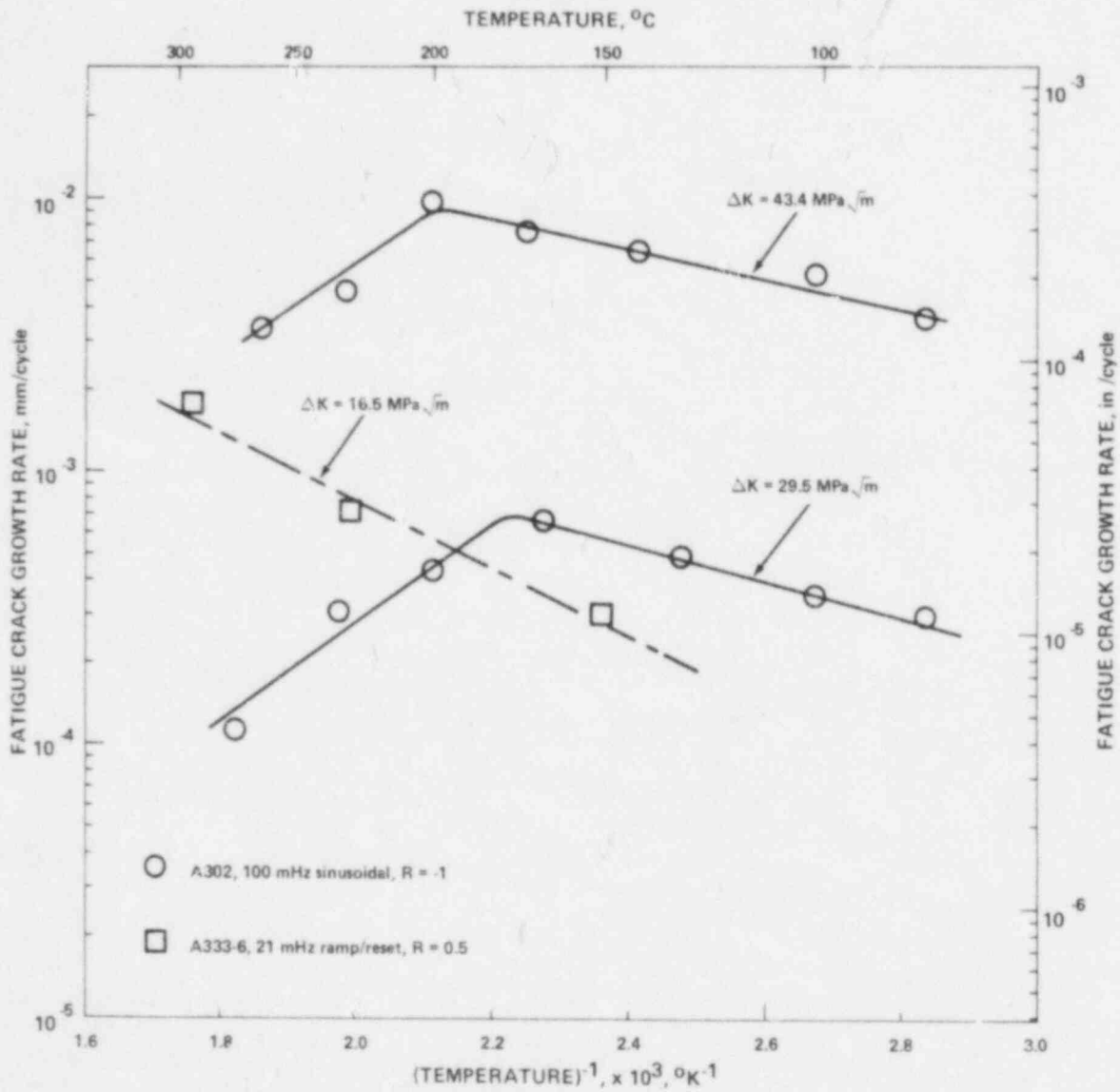
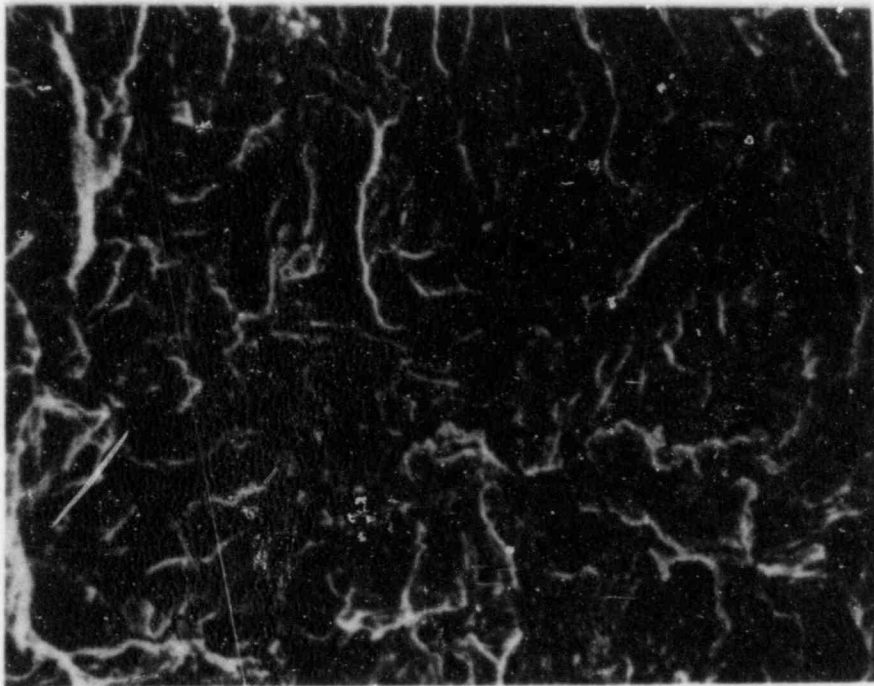
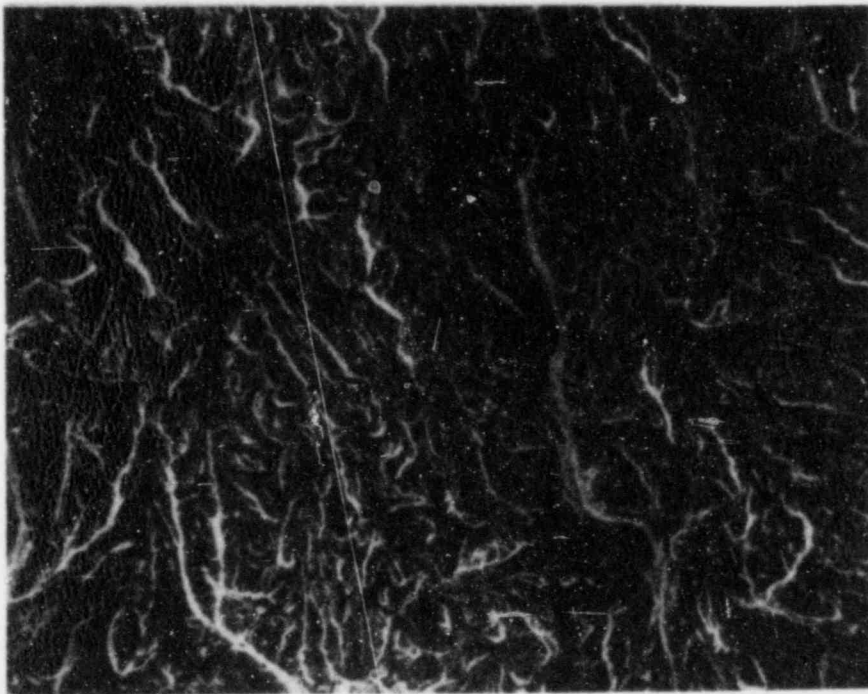


Fig. 9 Fatigue crack growth rate for fixed values of applied cyclic stress intensity factor versus inverse temperature for high oxygen environment (Refs. 13 and 15). Note the maximum in growth rates and compare these results with those in Fig. 6.



1000X



300X

Fig. 10 Fatigue fracture surface of A 508-2 tested at 288°C in reactor-grade water. Growth direction indicated by the arrow. The value of applied cyclic stress intensity factor at this crack length was 30.3 MPa $\sqrt{m}$ . Note the brittle-like character on the alluvial or fan-shaped facets (Ref. 6).



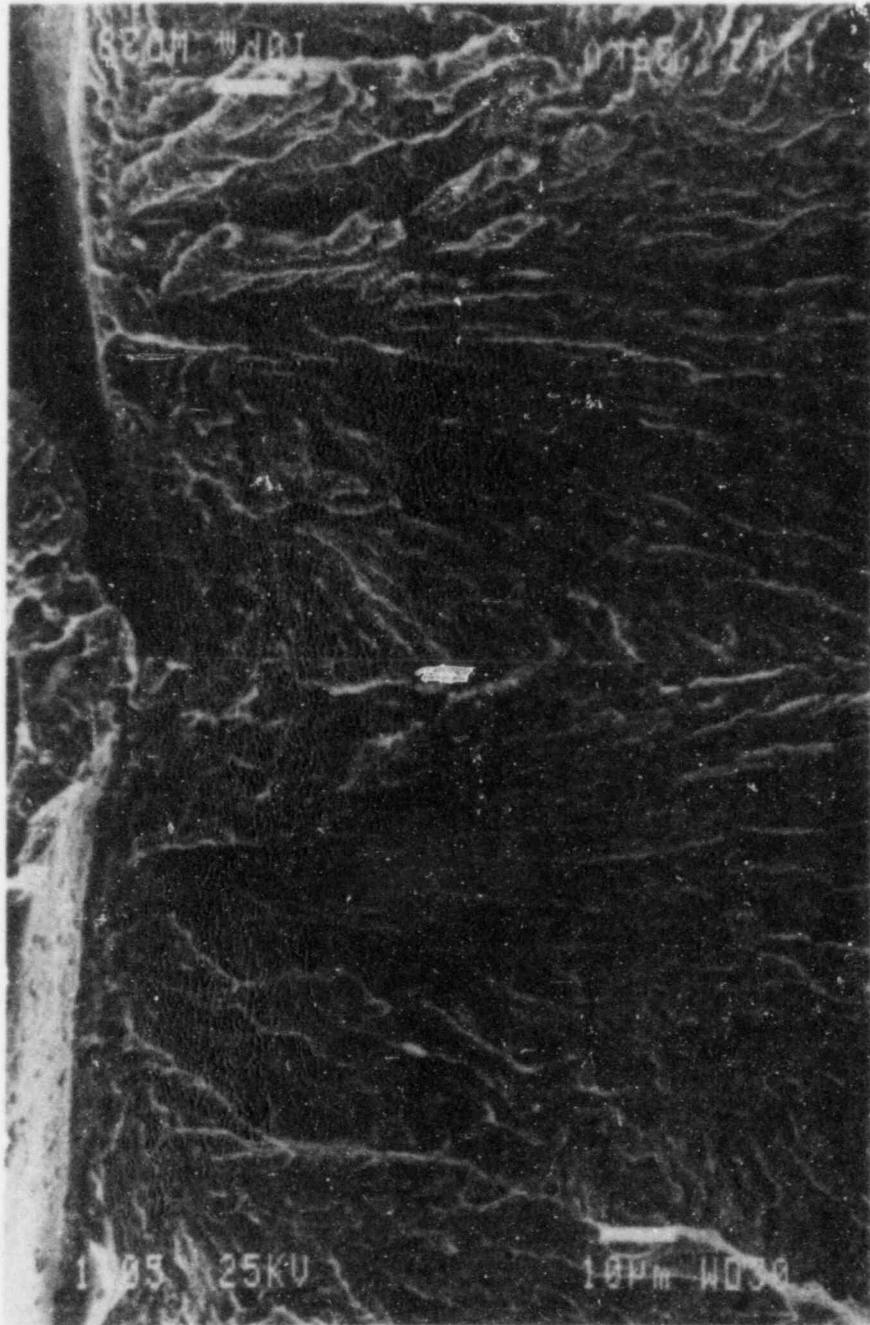


Fig. 11 Scanning electron micrographs of matching fatigue fracture surfaces for a high sulfur A 533 B steel specimen ( $S = 0.025\%$ ). The complementary match of the various features is nearly perfect (Ref. 8).

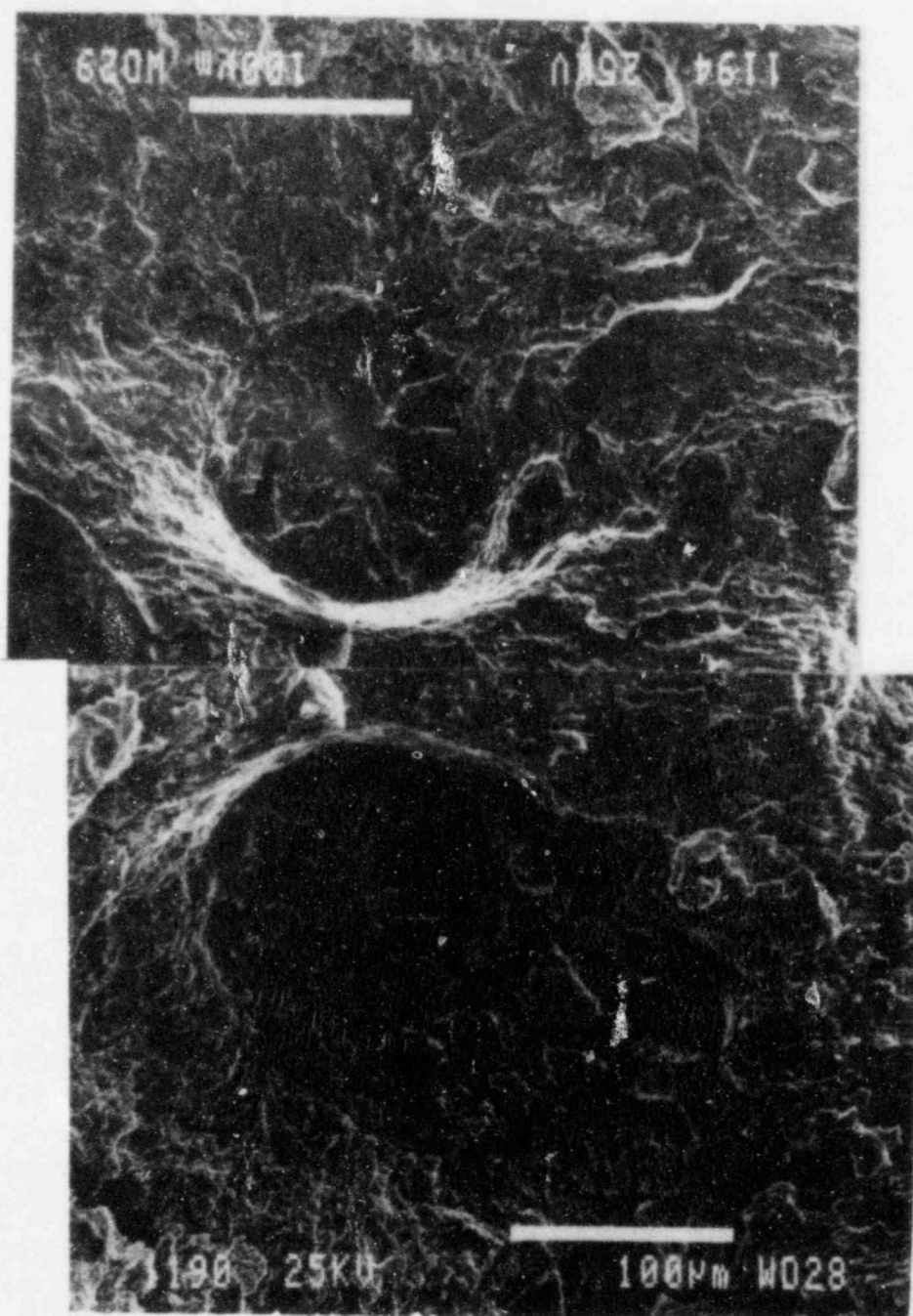


Fig. 12 Fractograph of a matching, nearly circular area of brittle-like appearance on a corrosion fatigue fracture surface, showing no evidence of striations or slow crack growth. This region, found on the low sulfur A 533 B steel, is presumed to have formed by hydrogen induced blister cracking (Ref.8).

the test temperature (Ref. 11), as long as the level of dissolved oxygen in the bulk environment remained very low. On the other hand, the presence of hematite on the fatigue fracture surface is usually an indication that an oxygen intrusion occurred during the test. X-ray photoelectron spectroscopy studies (Ref. 8) have shown that two solid phases, FeS and FeS<sub>2</sub>, coexist in the magnetite layer. Reference to the Pourbaix diagram for the Fe-H<sub>2</sub>O-S system shows that conditions of near-neutral pH (>4) and low corrosion potential (<-500mV<sub>SHE</sub>) must exist for both species to be stably formed at 300°C.

### 3.0 MECHANISMS FOR ENVIRONMENTALLY-ASSISTED CRACKING

In this section, the mechanistic knowledge of environment enhancement in corrosion fatigue (CF) crack growth of pressure vessel and piping steels in LWR environments is described. The mechanistic information from other environment-sensitive cracking phenomena (stress corrosion cracking, hydrogen-induced cracking and liquid metal embrittlement) is also used as background information. A mechanistic model that could be applied for prediction of subcritical crack growth rates in nuclear components would be extremely valuable, for example, in assessing the necessity of repairing cracks and defects during in-service inspections of the plants.

It is generally recognized that for understanding environment-sensitive crack growth an interdisciplinary approach is needed. The study of corrosion fatigue involves, in addition to mechanical engineering and materials science, various aspects of electrochemistry, surface science, physics and analytical chemistry. As described earlier, fractographic and metallographic studies reveal changes in the fracture mode, the fracture path, and the extent of plasticity and microcracking around the cracks. The information obtained by these techniques is considered very important in elucidating mechanisms of crack growth. Therefore, this review discusses, in particular, the recent advances in understanding mechanisms of crack growth based on fractographic and metallographic studies. Since the environment enhancement of the corrosion fatigue crack growth rate is affected by a number of variables, e.g., load ratio, load waveform, loading frequency,  $\Delta K$ , solution flow rate, sulfur content in both the alloy (including distribution, size and morphology of MnS inclusions) and the bulk environment, the effects of electrochemistry and local crack tip chemistry and their possible dependence on loading variables are also very important in understanding the mechanism of cracking. The generally proposed possible mechanisms of environment-sensitive cracking of materials are schematically shown in Fig. 13 (Ref. 23).

When corrosion fatigue crack growth in LWR environments is studied, generally, either the slip-dissolution or hydrogen-induced cracking mechanisms have been chosen as reasonable working hypotheses. Under high strain rate conditions, when the crack tip is continuously maintained in a bare surface condition, the crack growth can be identified atomistically with the bare surface reaction rates for either dissolution or hydrogen reduction. In the normal strain rate conditions,

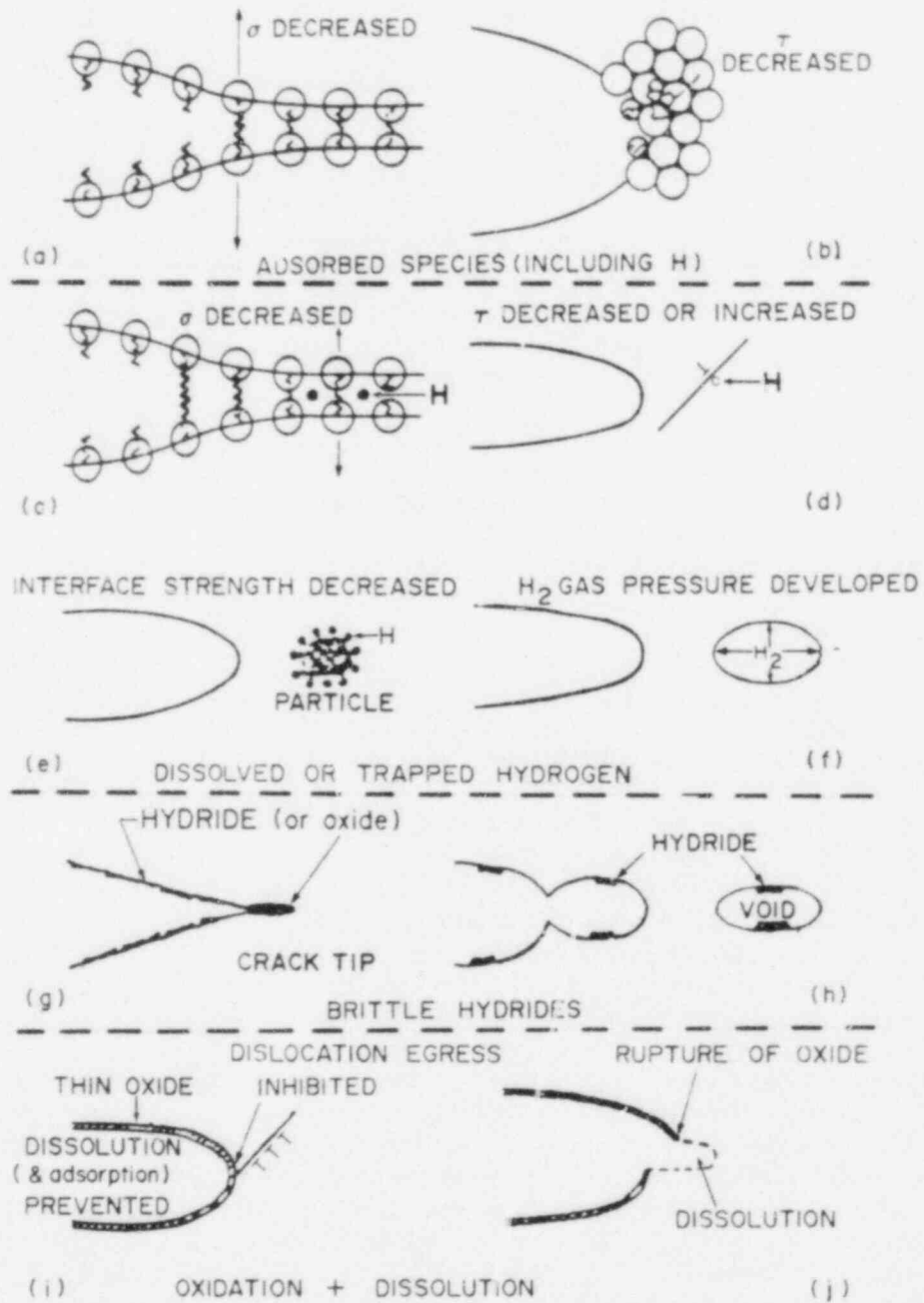


Fig. 13 Schematic presentation of possible effects of environment on fracture (Ref. 23).

however, the crack tip surface is not maintained continuously, in a bare condition. The crack growth rate is controlled by the oxide rupture, the repassivation rate, and the liquid diffusion rate at, or near, the crack tip (Ref. 24). Since these rate-determining parameters may control both slip-dissolution and hydrogen-induced cracking mechanisms, it has been difficult to differentiate experimentally between these two mechanisms. This has resulted in a situation where a fraction of the researchers has chosen the slip-dissolution model and others have chosen the hydrogen-induced cracking model as a working hypothesis. Adsorption models have been studied very little and brittle hydride models are considered to be inadequate for these conditions. In the following, the mechanisms are first outlined generally concentrating on basic requirements and attributes, but because the proposed mechanisms are controversial, also their advantages and disadvantages are discussed on the basis of supporting evidence for each mechanism -- fractography, electrochemistry, etc.

### 3.1 Anodic Dissolution Mechanisms

The film rupture/anodic dissolution model, which is also referred to as the slip-dissolution model, is a special variation of the general category of strain-assisted, active crack path formation models. It has been proposed that the dissolution at the film-free crack tip can be enhanced by the strain concentration (Refs. 25 to 29). This has been supported by TEM observations of stressed thin foils of austenitic stainless steels showing that dissolution occurs preferentially in regions of moving dislocations (Refs. 30 and 31). It was then demonstrated that the rate of film formation on a rapidly strained, bared surface correlated with the susceptibility to stress corrosion cracking (SCC). From the repassivation rate measurement experiments, qualitative explanations for the influence of various loading, environmental and metallurgical variables on environment sensitive cracking have been developed (Refs. 24, 32 to 38). In general, if the repassivation is too fast, no significant amount of dissolution can occur and if the repassivation is too slow, chemical blunting of a crack is expected to occur.

Recently Ford and Emigh (Ref. 39) have formulated a quantitative explanation of the slip-dissolution model for environment-sensitive crack growth in the low alloy steel/high temperature water system. They have calculated the maximum theoretical environment enhancement in crack growth which may be expected under specific combinations of alloy, environment and loading conditions. In the slip-dissolution model, the crack growth occurs by oxide rupture at the tip of the crack due to an increase of the strain in the underlying matrix (repeated rupture caused by fatigue, or creep-strain-induced rupture cause by sustained loading). In order to have a sharp crack, the sides of the crack must be passivated, even though the crack tip is in an active condition. The crack growth rate is related faradaically to the oxidation rate on the bared surface including both dissolution and oxide growth. The environment-sensitive part of the crack growth is reinitiated by a further increment of matrix strain which ruptures the crack-tip oxide again after a time period,  $t_f (= \epsilon_f / \dot{\epsilon}_{ct})$ , where  $\epsilon_f$

is the fracture strain of the oxide and  $\dot{\epsilon}_{ct}$  is the strain rate in the metal matrix at the crack tip (Ref. 39). The environment-sensitive component of the time-dependent crack growth,  $V_t$ , can be presented by the equation:

$$V_t = \frac{M}{npF} \cdot \frac{Q_f}{e_f} \cdot \dot{\epsilon}_{ct} \quad (3-1)$$

where M and  $\rho$  are the atomic weight and density values for the crack tip metal, F is Faraday's constant, n is the number of electrons/mole involved in the overall oxidation process and  $Q_f$  is the oxidation charge density passed between oxide rupture events. A strong support for the slip-dissolution model is that the observed crack growth rates of many different alloy/environment systems are in direct proportion to the experimentally-determined dissolution rates measured by straining electrodes (continuous supply of bared metal surface by film rupture) under the mechanical and chemical conditions expected at the crack tip, Fig. 14. Since the data cover a wide range of systems and over three orders of magnitude in crack rate, it has been thought that the slip-dissolution model has a rather wide applicability.

From stress corrosion studies, it has been observed that the strain rate at the crack tip is a critical parameter (Refs. 35 and 40). Crack tip strain rate generally includes both a time-dependent component (creep strain rate) and a time-independent component. Models of Parkins (Ref. 40) and Scully (Ref. 34), for instance, consider only the time-dependent strain rate, while models of Vermilyea (Ref. 41) and Vermilyea and Diegle (Ref. 42) consider only the time-independent strain rate. A more general approach would consider the total strain rate together with the specimen geometry and type of loading. Estimates of crack-tip strain rate based on the crack-tip opening displacement (CTOD rate) given by linear-elastic fracture mechanics for a static crack have been presented (Ref. 43), but reliable analyses which consider crack growth and cyclic loading ( $\Delta K$ , R, and frequency, etc.) are not yet available. This limitation should be kept in mind as an uncertainty for the  $\dot{\epsilon}_{ct}$  value in the following application of slip-dissolution model for corrosion fatigue crack growth in pressure vessel and piping steels in LWR conditions, as will be described in Section 4 of this report.

The analysis of Ford and Emigh (Ref. 39) is based on both theoretically and experimentally verified crevice conditions for A 533-B steel in deaerated water at 288°C, where the potential is  $\sim -620$  mV<sub>SHE</sub> and the pH value at 25°C is about 7.0, i.e., no significant difference between potential-pH conditions of the crack tip and outer surface is expected to occur. This has also been confirmed by Mager (Ref. 44). At the crack tip a dynamic equilibrium between the continued creation of bared surface and passivation is occurring, as shown in Fig. 15. Crack growth may be produced either by emission of dislocations from crack tips or attraction of dislocations toward crack tips. However, the probability of dislocations nucleated from near surface sources (Fig. 15) exactly intersecting crack tips would be low and dislocation activity on slip planes not intersecting the crack tip would produce general strain and extensive mechanical crack-tip blunting (Ref. 23), which would probably diminish crack propagation rates.

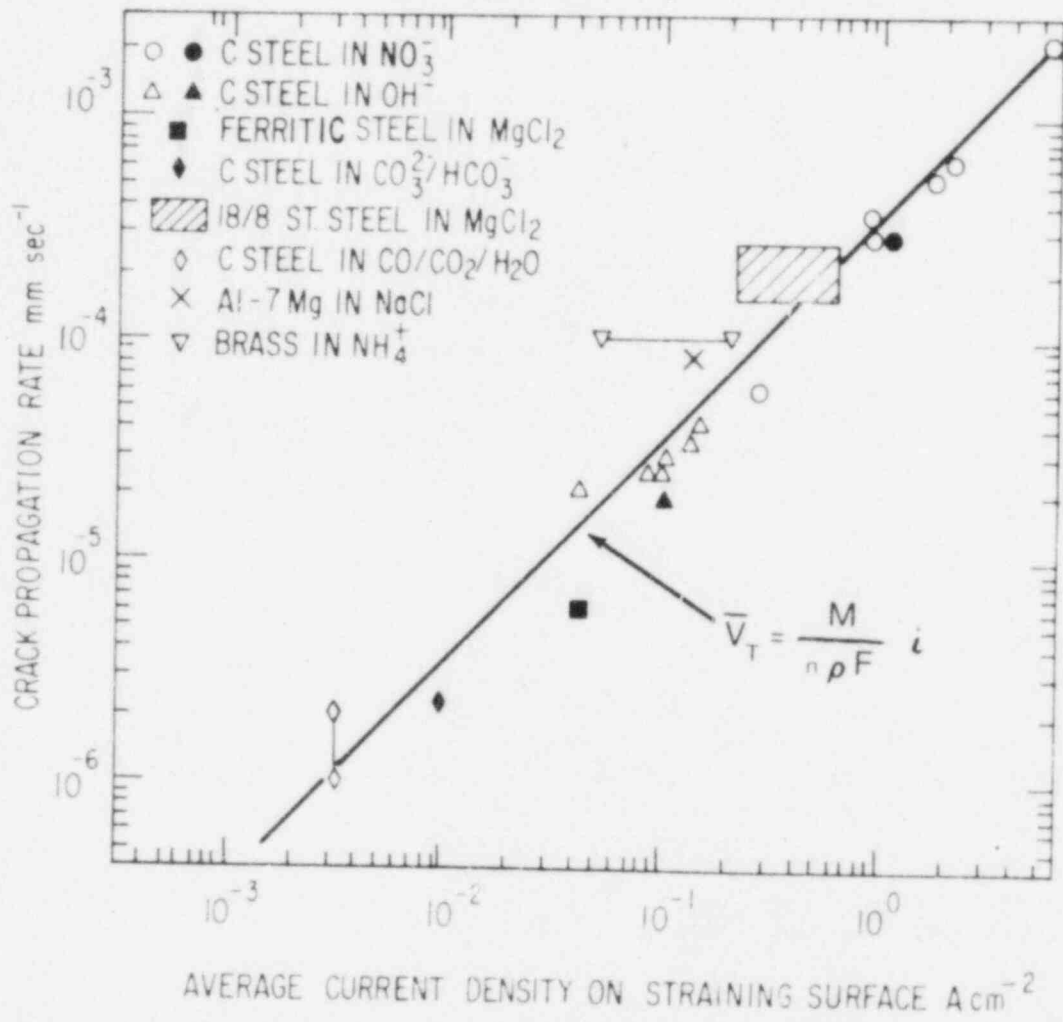


Fig. 14 Relationship between the average crack propagation rate and the oxidation (dissolution and oxide growth) kinetics on a straining surface for several ductile alloy/ aqueous environment systems known to be susceptible to SCC (Ref. 40).

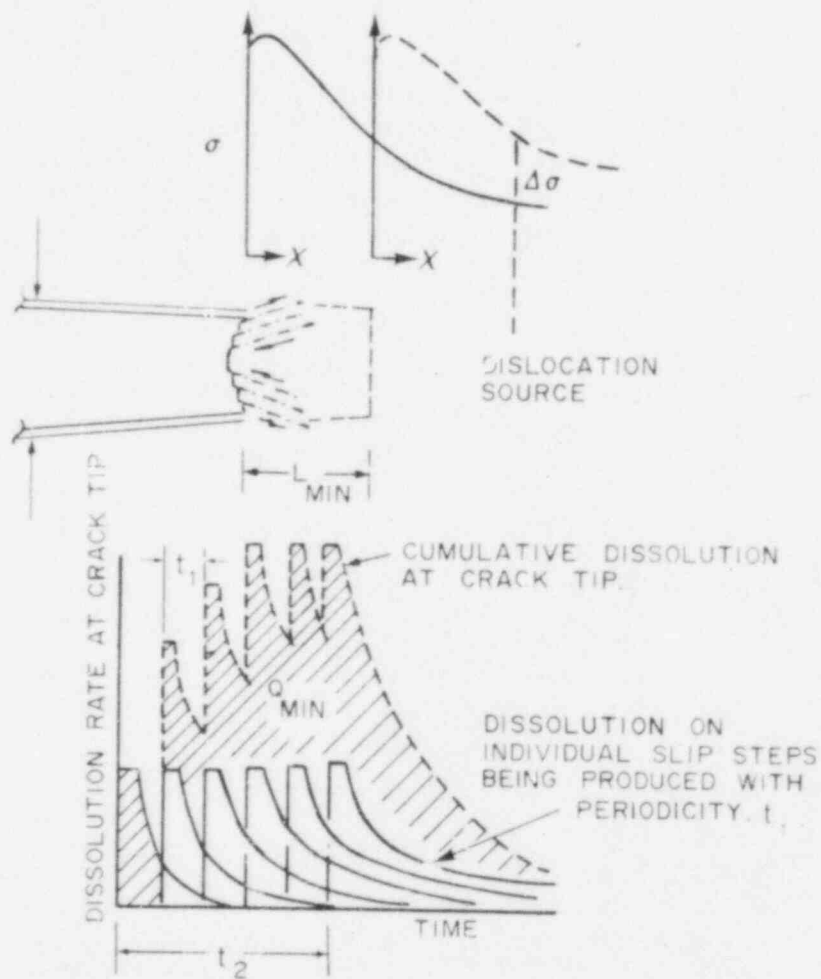


Fig. 15 Illustration of the factors of importance in the constant-charge criterion for SCC crack propagation. Propagation will occur in the statically loaded case only if a dislocation source is activated by the stress increment,  $\Delta\sigma$ , caused by the crack advance,  $L_{\text{min}}$ , associated with the passage of charge-density,  $Q_{\text{min}}$ , at the crack tip. This latter amount will be a function of the charge density increments caused by the individual oxide rupture events at the crack tip, the periodicity between their occurrence,  $t_1$ , and time,  $t_2$ , during which the plasticity is occurring (Ref. 24).



Figure 16 shows schematically the environmentally-enhanced crack growth in the low alloy steel/high temperature water system when it is purely governed by a film rupture/slip-dissolution model. Based on the recent concept of Sieradzki and Newman (Ref. 45), in addition to the crack growth due to oxidation reactions, an extra component of crack growth may be associated with the rapid fracture of crack-tip oxide and penetration of this "cleavage" crack into the underlying ductile matrix. Figure 17 shows schematically the effect of this additional cleavage component on the crack growth. The extent of this cleavage component,  $a^*$ , is believed to be in the range of 0.1 to 10  $\mu\text{m}$  for ductile alloys; in the study of Ford and Emigh (Ref. 39),  $a^* = 0.1 \mu\text{m}$  is used. When the measured oxidation rate transients are used to produce the oxidation charge density/time relationships shown schematically in Fig. 16, theoretical crack growth rate/crack-tip strain rate relationships for the film rupture/slip-dissolution model are obtained. Figure 18 shows the results for two different crack-tip conditions (low and high sulfur conditions). A  $\dot{\epsilon}_{ct}^n$  power-law relationship for crack growth rate is predicted with limitations at both the high and low strain rates. At crack-tip strain rates  $> 10^{-2} \text{ s}^{-1}$ , the crack growth rate is limited by the oxidation rate on the continuously bared surface, whereas at low strain rates a limit is set by the criterion that the crack tip must propagate faster ( $V_T$ ) than the dissolution rate on the adjacent crack sides ( $V_S$ ), if a sharp crack is to be maintained. In Fig. 18, three  $V_T/V_S$  ratios of 1, 5 and 10 are shown. Even though, according to the model, the environmental enhancement of the  $(da/dN)_{\Delta K}$  value should, in general, increase with decreasing loading frequency, at very low frequencies, the crack growth is limited by crack blunting and subsequent crack arrest. Ford and Emigh (Ref. 39) assumed that the crack blunting will become dominant if the  $V_T/V_S$  ratio is less than 5. Also an example of theoretical crack growth rate/crack-tip strain rate relationship for the situation where crack growth is occurring purely by the above-mentioned cleavage model of Sieradzki and Newman (Ref. 45) is shown in Fig. 17 in which the crack grows discontinuously a distance,  $a^*$  ( $= 0.1 \mu\text{m}$ ), every  $(\dot{\epsilon}_f/\dot{\epsilon}_{ct}^n)$  seconds. The chosen  $a^*$  -value is arbitrary, and if, e.g., the fractographically-observed brittle striation spacing 1 to 5  $\mu\text{m}$  (Ref. 18), is equated to a cleavage event, then the environmentally-assisted cleavage crack growth rates would be

Ford and Emigh (Ref. 39) come to the following main conclusion from the results shown in Fig. 18: the film-rupture/slip-dissolution model predicts a  $V_T/\dot{\epsilon}_{ct}^n$  relationship ( $n = 0.3$  to  $0.5$ , obtained from bared surface dissolution current decay experiments) with the constants in that relationship depending on the localized conditions at the crack tip (e.g., sulfur content). On the other hand, the environmentally-enhanced cleavage model would predict a  $V_T/\dot{\epsilon}_{ct}^{1.0}$  relationship with an undefined effect of crack-tip conditions on the relationship constants. Ford and Emigh (Ref. 39) found that the fracture strain of the oxide was independent of anion content ( $\sim 10^{-3}$ ), which was then interpreted as above. This value was measured for stainless steel and not for low alloy steel in high temperature water. Lenz (Ref. 46), however, determined the strain required to crack the magnetite layers on low alloy steels to be  $0.46 \cdot 10^{-3}$ . The use of this value would

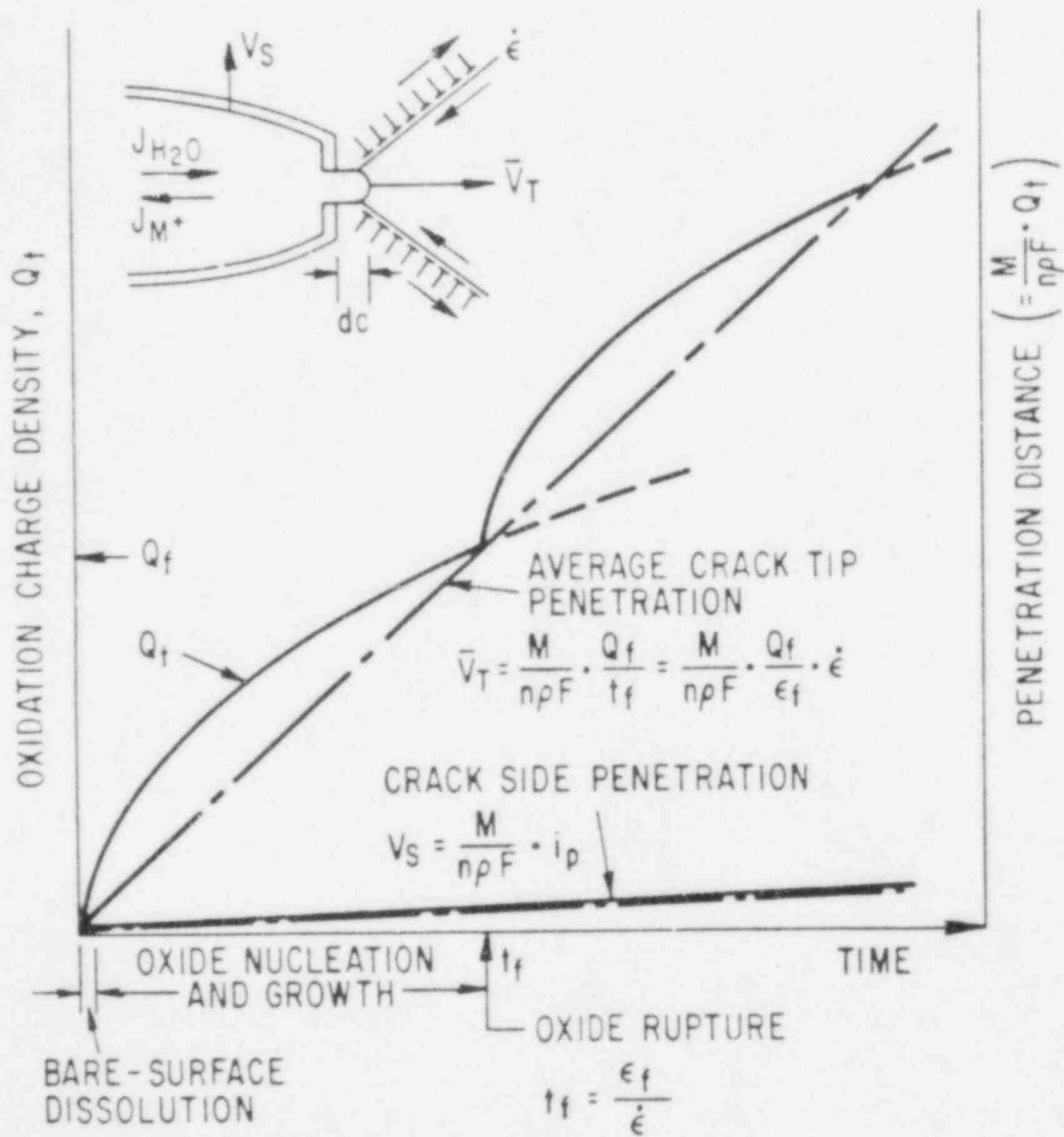


Fig. 16 Schematic variation of oxidation charge density and, hence, penetration with time following oxide rupture at strained crack tip. Note importance of the periodicity of oxide rupture ( $\epsilon_f/\dot{\epsilon}$ ), and of low oxidation rate on crack sides ( $V_s$ ), in maintaining propagation of a sharp crack ( $V_T$ ) (Ref. 39).

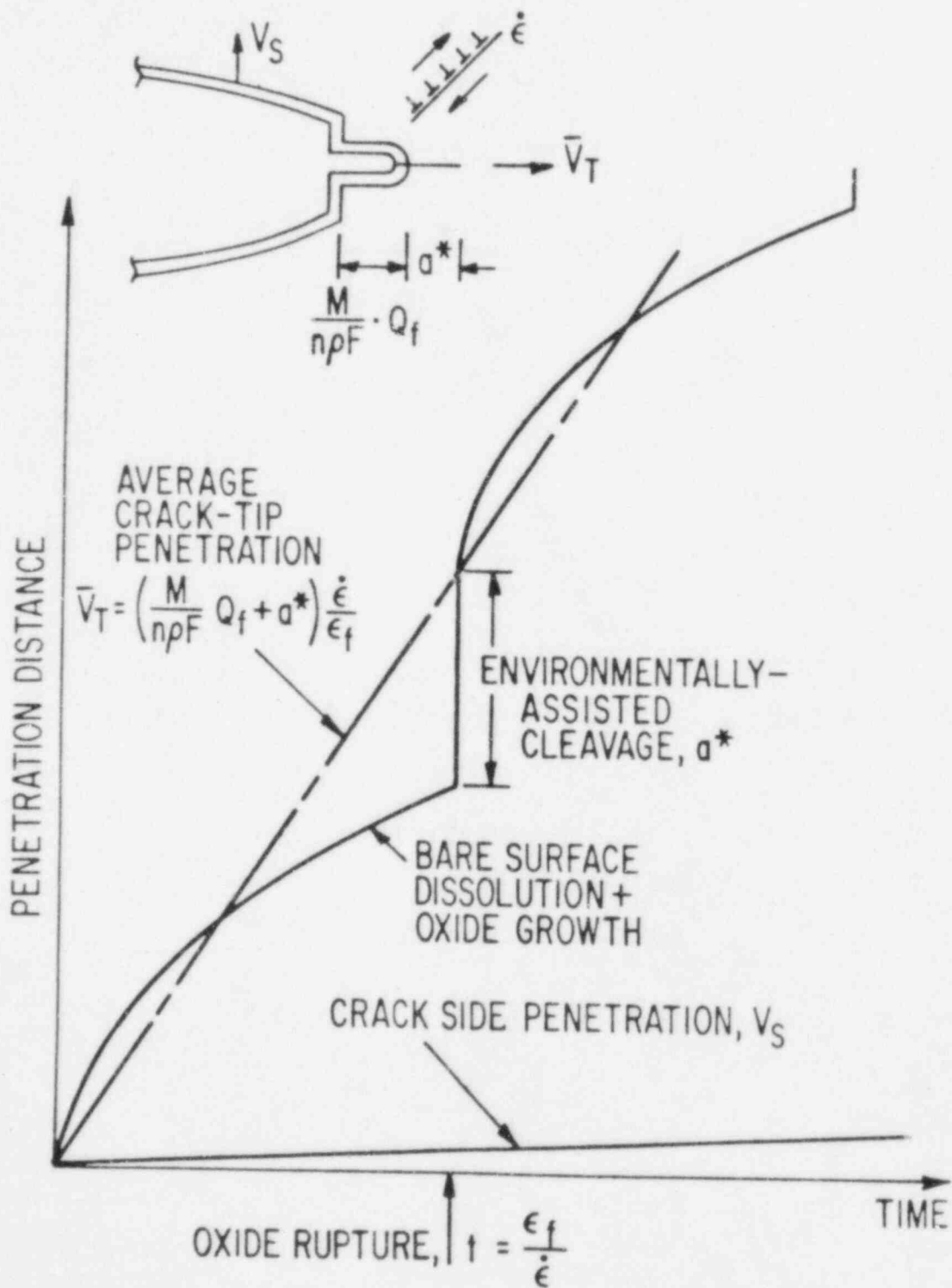


Fig. 17 Schematic variation of crack-tip penetration with time following oxide rupture, where crack advance due to environmentally-assisted cleavage,  $a^*$ , acts in addition to that associated with oxidation of the bared metal (Ref. 39).

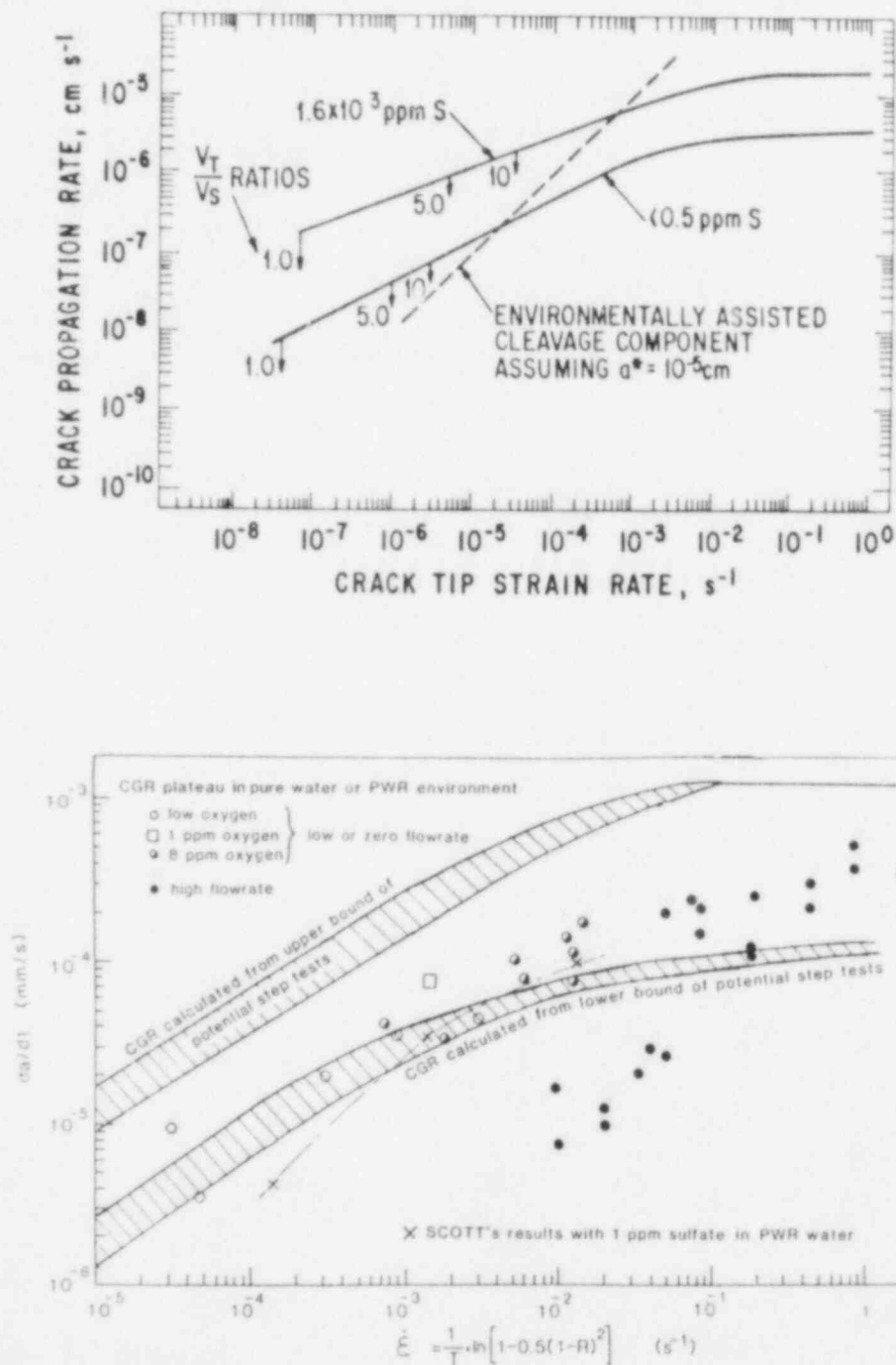


Fig. 18 (a) Theoretical crack growth rate/crack-tip strain rate relationships for low alloy steel in stagnant deaerated water at 288°C, in which either  $1.16 \times 10^3$  ppm or  $< 0.5$  ppm sulfur is created and maintained in crack-tip enclave. In addition to the predictions of the film rupture/slip-dissolution model, those of an environmentally-assisted cleavage model are also shown, in which it is assumed that cleavage distance is  $0.1 \mu\text{m}$  (Ref. 39). (b) Comparison of the predicted corrosion fatigue crack growth values with some experimental values (Ref. 44). Data found in Ref. 43.

result in underestimation of the crack growth by the model. Since the localized slip process at the crack tip ruptures the oxide, the actual meaning of the critical strain and strain rate may not be so clear.

A similar analysis of theoretical crack growth by slip-dissolution model of Mager (Ref. 44) is shown in Fig. 18b. Some experimental "plateau" values of corrosion fatigue crack growth of A 503 Cl. 3 steel and A 533-B steel are plotted vs. the average crack-tip strain rate (Ref. 43). The experimental crack growth rates are within the predicted scatter and reside near the lower bound of the calculated crack growth values.

A comparison between some observed  $da/dN$  vs.  $\Delta K$  values compared to predicted values from film rupture/slip-dissolution model are shown in Fig. 19. Ford and Emigh (Ref. 39) state here that the so-called "plateau" crack growth values of  $(da/dN)_{\Delta K, R}$  are observed only in the conditions predicted by their theory for sustaining a sharp crack. They have also compared the calculated maximum  $(da/dN)_{\Delta K, R}$  values for low alloy steel/deaerated water system at 288°C with the present ASME XI (1980) code values as shown in Figs. 20a and 20b for various combinations of load ratio and sulfur content of the steel. It can be seen that the present code values for low sulfur steels are in approximate agreement with the maximum theoretical values for both the high and low R conditions. In the case of high sulfur steel, this prediction based on the film rupture/slip-dissolution model exceeds the present ASME XI (1980) code reference lines.

### 3.2 Hydrogen-Induced Cracking Mechanisms

At the crack-tip conditions of potential, pH and anion content, both slip-dissolution and hydrogen-induced cracking mechanisms are thermodynamically and kinetically viable. Both mechanisms are dependent on oxide rupture rates, passivation rates and liquid diffusion rates, since these factors affect the charge transfer per time in the slip-dissolution model and the hydrogen ad-atom coverage and hydrogen evolution rate in the hydrogen-induced cracking models. As the rate-determining step in the slip-dissolution mechanism, the oxide rupture event was used. This same event is naturally very important in hydrogen-induced cracking models, since it affects directly the hydrogen entry into the metal. In the case of hydrogen embrittlement (HE) numerous other rate-determining parameters are possible depending on the exact mechanism considered. Therefore, calculation of maximum crack growth rate predictions (as presented above for slip-dissolution model) for hydrogen-induced cracking models are hampered by lack of quantitative knowledge of such events as hydrogen coverage at the crack tip, hydrogen diffusion ahead of the crack and possible dislocation transport phenomena including trapping and subsequent diffusion away from the supersaturated site, as well as specific details of the interatomic rupture event.

A hydrogen-induced cracking model is outlined in Fig. 21 (Ref. 10). This cracking model is based on the direct fractographic observations from an extensive fractographic study of ICCGR group round robin

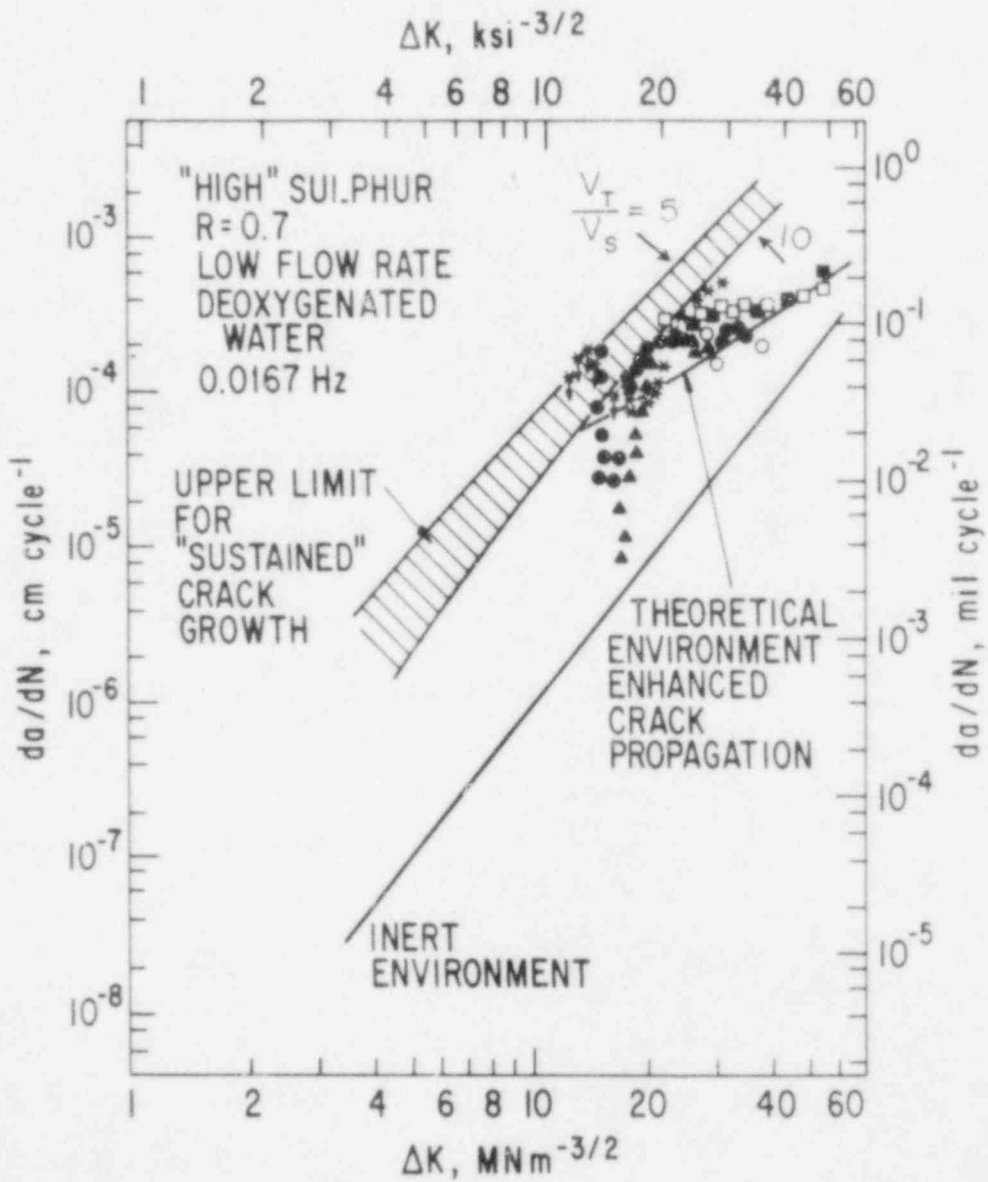


Fig. 19 Theoretical and observed  $da/dN$  vs.  $\Delta K$  relationships for high sulfur steels in deoxygenated water at 288°C. Loading condition is  $R = 0.7$  and frequency = 0.0167 Hz. The band of  $(da/dN)_{\Delta K}$  values shown as the limit for sustained crack growth is corresponding to  $V_T/V_S$  values of 5 and 10 (Ref. 39).

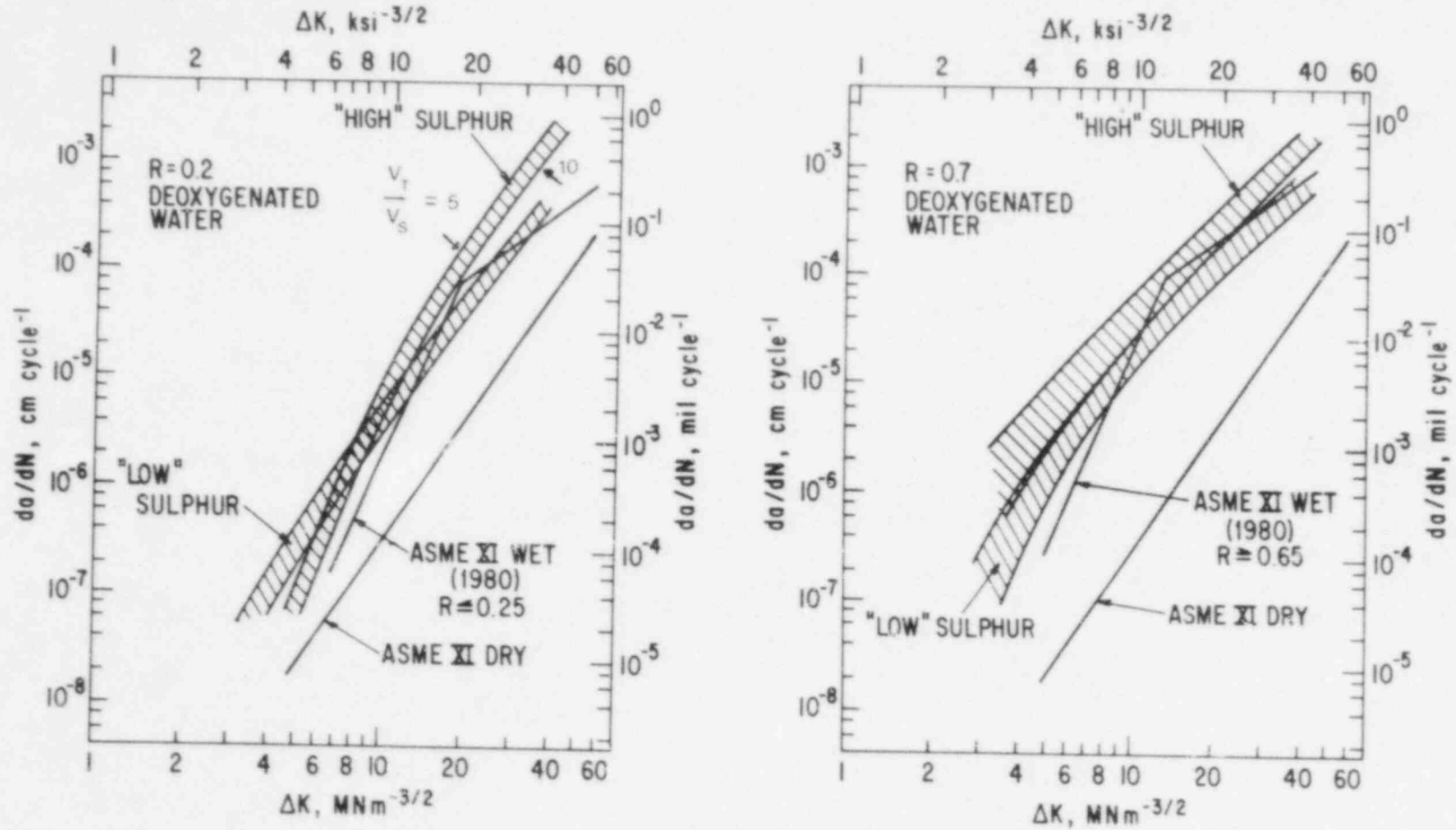


Fig. 20 Comparison between the ASME XI (1980) code values of  $(da/dN)_{\Delta K}$  and the theoretical maximum crack propagation rates obtained by slip-dissolution model for high and low sulphur content steels in deoxygenated water at 288°C. Loading conditions are either (a)  $R = 0.7$  or (b)  $R = 0.2$  (Ref. 39).

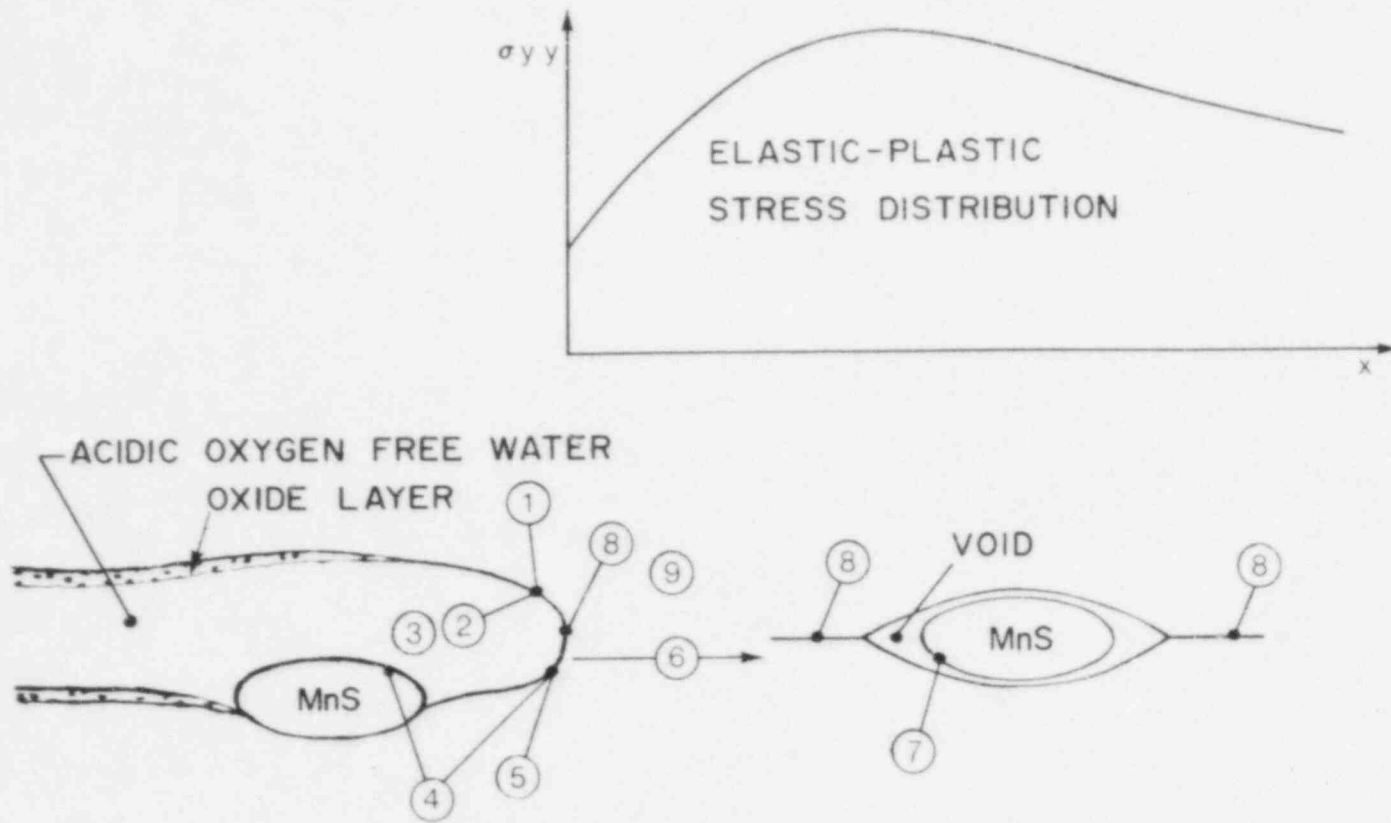


Fig. 21 Schematic illustration of hydrogen assistance during cyclic crack growth of pressure vessel steel in high temperature water (Ref. 48).



specimens (Ref. 18). The brittle-striated or striationless, cleavage-like fracture surface areas are considered to be produced by this model. Ductile, striated fracture morphology, which is similar to fracture surface morphology produced in air, often exists together with the brittle fracture morphology. In these ductile areas no environmental enhancement is considered to have occurred. Also the detailed stereofractography of mating fracture surfaces (Ref. 47) couples with similar fracture surfaces obtained in hydrogen charging experiments (Ref. 10) strongly supports this model. In this model for low alloy steel/high temperature deaerated water system, the oxidation reaction produces hydrogen at or near the crack tip. This hydrogen is first adsorbed and then partly evolved and partly absorbed into the metal. The absorbed hydrogen diffuses to the region of elastic-plastic stress distribution just ahead of the crack tip and interacts with any MnS inclusions which may reside there, causing mechanical failure at the inclusion/matrix interface and brittle crack growth of the immediately surrounding metal matrix. Evidence of cracks in front of the main crack tip, the appearance of brittle striations on the corrosion fatigue fracture surface and a relationship between the amount of brittle cracking mode and the environmental-enhancement factor are three important pieces of experimental evidence which support the hydrogen-induced cracking mechanism in the corrosion fatigue crack growth of low alloy steels in high temperature deaerated water. Also, the observed incubation times and transient crack growth phenomena, the effects of pre-immersion and precracking of test specimens in high-temperature water, specimen size effects and steel sulfur content correlations can be best explained by hydrogen-induced cracking mechanisms.

Manganese sulfide inclusions (including size, form and distribution parameters) play an extremely important role in this mechanism (Ref. 10 and 48). The dissolution of MnS inclusions produces  $H_2S$  and  $HS^-$  in the crack-tip enclave (Ref. 49). It is proposed that these species are good hydrogen donors and enhance hydrogen absorption through their adsorption on the bare metal surface. Commonly the brittle, cleavage-like cracking starts from MnS inclusions and spreads like a fan during crack growth, which indicates the importance of local chemistry in environmentally-enhanced crack growth. Kobayashi and Shockey (Ref. 47) observed that the corrosion fatigue crack front is not a simple line separating fractured and unfractured material, but rather a band about 200- $\mu m$  wide containing fracture and unfractured areas. Crack growth occurs by the formation of narrow channels of separated material extending through the process zone ahead of the main crack tip. Especially in fast crack growth regions large unconnected microcracks appear well in advance of the crack tip process zone. Narrow channels form from these microcracks and extend backwards to the main crack tip. According to the above model, these microcracks ahead of the main crack are most likely formed by hydrogen-induced cracking. Thus, the hydrogen-induced crack growth is anticipated to occur both at the crack tip in the process zone and well in advance of the crack tip from strong hydrogen traps, the MnS inclusions. High resolution topographs need to be examined to ascertain the relative proportion of the slip-dissolution and hydrogen-induced crack growth mechanisms in the process zones and at

the crack tip both in either the slow or fast crack growth regions. Reference specimens fatigued in an inert environment should also be studied.

In the following section, the hydrogen interactions in metal, i.e., hydrogen-induced fracture processes and hydrogen transport, are briefly reviewed with reference to the possible mechanism for corrosion fatigue of low alloy steels in LWR environments.

### 3.2.1 Decohesion Mechanism

The most popular of hydrogen embrittlement mechanisms is the decohesion mechanism which proposes that hydrogen can affect the interatomic cohesive forces at or near a crack tip (Refs. 50 to 52). In this mechanism, hydrogen accumulates at regions of high triaxial stress ahead of the crack tip. Sufficiently large local hydrogen concentrations are formed over some critical length which may affect the bond strength between metal atoms, e.g., by the model suggested by Troiano (Ref. 50), where hydrogen donates its electron to the unfilled d-bands of the metallic cores. The increase in electron density leads to an increase in the repulsive forces between adjacent metal cores and a decrease in the cohesive interatomic strength of the lattice. Tiller (Ref. 53) has shown that high tensile stresses at the crack-tip region result in a higher electron affinity and electro-negativity there. Due to chemical interaction, hydrogen will diffuse to regions of high tensile stress in a metal lattice.

The decohesion mechanism can be thought of as continuous crack growth by bond rupture at the crack tip. Hydrogen-induced bond rupture occurs also ahead of the crack tip, at points of stress concentration, producing cracks which link up with the main crack possibly with some degree of plastic tearing of ligaments, giving rise to discontinuous crack growth. Gerberich (Refs. 54 and 55) has presented a discussion of the decohesion mechanism applied to bond rupture ahead of the main crack tip, where localized fracture occurs when the hydrogen content reaches a critical value throughout a critical volume.

This mechanism can be incorporated into the above mentioned corrosion fatigue model as follows: it has been recognized that the MnS inclusions provide accumulation sites for hydrogen within the region of the crack-tip stress field. If the interatomic force model (Ref. 51) is generalized (Ref. 56) to include the bonds at grain boundaries, interphase boundaries and inclusions, the sometimes observed local intergranular cracking, as well as crack initiation from inclusions ahead of the crack tip and subsequent brittle propagation across several grains, can be qualitatively explained.

### 3.2.2 Hydrogen Adsorption Mechanism

The hydrogen adsorption mechanism proposes that adsorbed hydrogen lowers the surface energy of the metal, and according to the Griffith criterion for crack growth facilitates crack growth at a lower fracture stress level (Refs. 57 and 58). Plasticity effects were not addressed by developers of the mechanism, which reduces to a special

case of the decohesion mechanism when the crack growth occurs only at the crack tip (Ref. 51).

In corrosion fatigue this hydrogen adsorption-induced surface energy reduction may be important on internal interfaces (particle/matrix interfaces and grain boundaries), where it affects interface separation, hydrogen recombination, and interaction with other locally accumulated species like sulfur on MnS inclusions. It is unclear if this mechanism can operate at the main crack tip in the crack tip solution or if it can produce brittle cracking starting from inclusion matrix interfaces ahead of the main crack tip. Since Kobayashi and Shockey (Ref. 47) reported that cracking occurs mainly in the solid matrix in front of the main crack at regions corresponding to maximum stress triaxiality, the surface adsorption of hydrogen may not account for all the observed phenomena.

### 3.2.3 Hydrogen Pressure Mechanism

The hydrogen pressure mechanism proposes formation of high pressure molecular hydrogen within the metal (Ref. 59). The resulting gas pressure in the internal voids and cracks exerts an internal stress which lowers the apparent fracture stress. This mechanism is not thought to be a general one, since brittle crack growth can occur under hydrogen partial pressures well below one atmosphere (Ref. 60). However, if hydrogen transport by mobile dislocations is a major component of the fracture process, then significant quantities of hydrogen can be transported to some sites in the metal, especially if the sites are strong hydrogen attractors, leading to development of a localized, non-equilibrium, very high fugacity of hydrogen. Even though the rapid transport of hydrogen by dislocations can occur, it would probably not concentrate hydrogen along planes or at particles directly ahead of the crack tip plane, but along the slip planes positioned at an angle from the fracture plane. The significant internal hydrogen pressure can affect, e.g., ductile fracture behavior through the effect on void growth rates.

In corrosion fatigue, the formation of high pressure molecular hydrogen can affect the inclusion matrix separation ahead of the main crack tip and void growth around inclusions (Ref. 10). Also in some cases, ductile-dimple cracking has been found on the fracture surfaces of weld metal, thus supporting the hydrogen-induced, ductile-cracking mechanism (Ref. 61). Since internal pressures of the order of  $10^3$  atmospheres can be attained (Ref. 62), the observed brittle cracking around MnS inclusions ahead of the crack tip appears to serve as a mechanism which reduces the internal pressure. However, the brittle, cleavage-like fracture mode cannot be explained by this model.

### 3.2.4 Deformation Mechanism

Deformation mechanisms of hydrogen embrittlement propose that hydrogen can reduce the local stress required for dislocation generation and motion (Ref. 63). This mechanism has been supported by fractography (Ref. 64) and direct HVEM observations (Refs. 65 and 66), which show extremely localized crack tip plasticity. The operation of this

mechanism can result in a lower stress intensity for crack growth. For more brittle cracking the role of a reduced flow stress is not as apparent, unless the effect is related to the hydrogen transport in the vicinity of the crack tip. It has also been recognized that any reduction in interatomic cohesion will also reduce the shear stress necessary to move dislocations (Ref. 67). Thus, the decohesion and deformation mechanisms are difficult to test unequivocally, since cracking can be formulated in terms of reduced normal stress across lattice planes or in terms of reduced shear stress for flow. Since there have been no observations of hydrogen effects in plastic deformation of pressure vessel steels, it is currently not known if hydrogen-induced localized plasticity at the crack tip would be a viable possible mechanism.

### 3.2.5 Brittle Hydride Mechanism

Brittle hydride mechanism in hydrogen embrittlement has not been taken seriously outside the Group IVa and Va metals, since stable hydrides have not been identified in connection with cracking. Fujita (Ref. 68) has proposed that hydrogen in iron accumulates into plate-shaped clusters in a way which is enhanced by stress. Clustering occurs most readily under high triaxial stress. The formation of an interface is energetically favored and hydride-like cracking occurs. However, the hydrogen platelets are unstable under normal conditions and are therefore difficult to observe experimentally. In corrosion fatigue, the crystallography of brittle cracking is unknown and therefore cannot be correlated with hydrogen-induced cracking. This type of hydrogen clustering may be a possible mechanism but is still waiting experimental evidence.

As shown above, there is some dispute as to the location of the critical region of hydrogen damage and none of the hydrogen-induced cracking mechanisms are yet sufficiently general to be used quantitatively for a special case of environment-sensitive cracking in the same way as the slip-dissolution mechanism was used quantitatively for corrosion fatigue of low alloy steels in LWR condition. Moreover, the general examination of the mechanisms suggests that hydrogen can exhibit many influences on fracture behavior so that the different proposed mechanisms may be operative simultaneously and in various proportions. In some cases an internal flaw ahead of the main corrosion fatigue crack might be pressurized by hydrogen gas. The interface between the inclusion and the matrix would be weakened by adsorbed hydrogen like also the tip of the main crack, while the atomic bonds in the surrounding lattice might be weakened by dissolved hydrogen. The enhanced dislocation mobility is a consequence of lowering of the local stress by localized plasticity. Thus, the hydrogen-induced crack growth could, in some cases, be a conjoint action of various mechanisms.

### 3.2.6 Adsorption Mechanisms

Adsorption of surface active species other than hydrogen has been proposed to reduce the fracture stress in various embrittlement phenomena. In adsorption related mechanisms the influence of adsorption is limited to one or two atomic distances from the surface of the metal. Adsorption can, thus, only influence the tensile strength and shear strength of the interatomic bonds at the crack tip, Fig. 22. A crack can grow rapidly by cleavage or slowly by slip depending on whether the tensile fracture stress,  $\sigma$ , for the interatomic bond or the shear stress,  $\tau$ , to cause slip on a favorable slip system is achieved first. Hence, as the ratio of  $\sigma/\tau$  decreases, cleavage becomes more probable and, conversely, shear failure becomes more likely as the ratio increases (Ref. 69). Hence, this criterion is inapplicable in cases where both ductile and "brittle" fracture occur by slip and distribution of slip around crack tip determines fracture behavior.

Adsorption can promote crack growth by facilitating tensile-decohesion as stated before in the case of hydrogen, when chemisorption of an environmental species on the crack tip reduces the surface energy term  $\gamma_s$ , in the equilibrium Griffith relationship and thereby reduces the local fracture stress of the metal lattice. Such an argument has been used for hydrogen embrittlement, liquid metal embrittlement, and for the effects of specific anions in aqueous solutions where the adsorbed atom coverage is dependent on electrode potential (Ref. 70). However in plastically-deforming materials, the plastic work expended in crack growth would be at least an order of magnitude greater than the surface energy. Therefore adsorption is best discussed in terms of its effects on interatomic bond strengths rather than in terms of its effects on surface energy. Lynch (Ref. 23) explains that adsorption reduces the shear strength of interatomic bonds and thereby facilitates nucleation of dislocations at crack tips, although the mechanism by which this occurs is unclear. Theoretical shear strengths for ductile materials are much lower than theoretical tensile strengths and, hence, adsorption-induced crack growth probably involves dislocation emission rather than tensile decohesion. Inhibition of dislocation nucleation by adsorption would lead to crack growth by tensile-decohesion rather than slip, but would probably not produce subcritical crack growth.

Lynch (Ref. 71) has proposed a corrosion fatigue fracture mechanism in which chemisorption of environmental species intensifies localized slip at the crack tip only, thus inhibiting the formation of a more generalized slip field, and results in the extensive blunting observed in the absence of the environment, Fig. 23. Fatigue crack growth occurs by a slip process at the crack tip only on planes intersecting the crack tip, and during unloading slip occurs behind the crack tip. In this way, part of the fracture surface produced during the previous loading is deformed by reverse slip and crack tips are resharpended. Slip during unloading generally concentrates just behind the crack tip with less deformation farther from the crack tip.

Ductile striations are produced in a manner similar to brittle striations. The difference in spacing and profile of the two types of

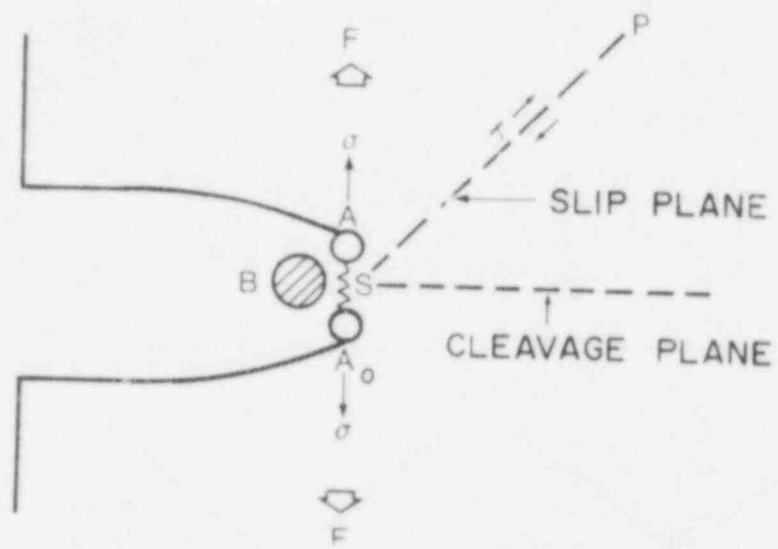


Fig. 22 Environment/metal interaction model (Ref. 69).

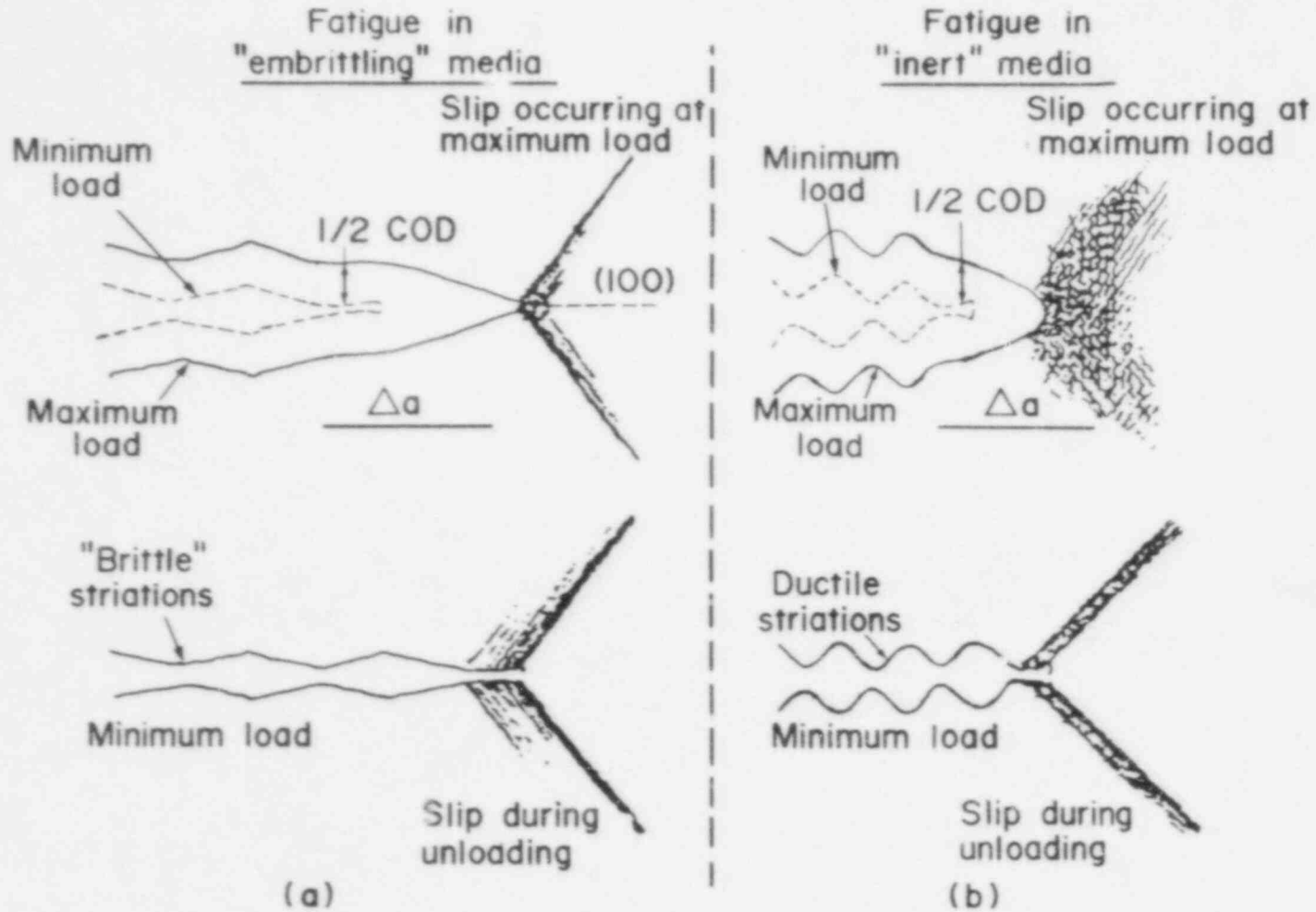


Fig. 23 Schematic illustrations of fatigue crack growth mechanism and formation of striations for (a) embrittling environments and (b) inert environments. Nucleation and growth of microvoids and cracks ahead of the main crack tip in the highly strained (shaded) areas occur during loading in many cases (Ref. 71).

striations arises because the extent of blunting during loading differs: the more blunt crack tip profile produced in inert environments concentrates slip just behind the crack tip to a greater extent during unloading. The detailed appearance of striations depends on a variety of factors (e.g., load ratio,  $\Delta K$ , orientation of slip planes with respect to crack plane, ease of dislocation egress at fracture surfaces, etc.). Environment affects the dislocation egress mechanism and this explains why well-defined striations are sometimes not observed, because oxide films can impede the dislocation egress. In the case of fatigue, sharp cracks can propagate along crystallographic planes. However, in a stress-corrosion cracking type of tension test (such as a constant extension rate test), this mechanism necessarily leads to crack blunting. Lynch (Ref. 71) proposes also that crack growth in inert environments probably occurs to a large extent by egress of dislocations at crack tips, while in embrittling environments cracks grow predominantly by nucleation and movement of dislocations from crack tips. In aqueous environments where oxide films form at crack tips, chemisorption on the metal surface cannot occur, and fracture of the oxide is necessary before crack growth promoted by chemisorption occurs. Thus, cracking can be discontinuous because competing reactions (such as repassivation) temporarily prevent adsorption and cause crack arrest. Chemisorption is here the rate-limiting step and the degree of embrittlement is a function of surface coverage of adsorbed species. Also an additional kind of fracture process ahead of the crack tip is necessary to explain the mechanistic observations, which also may operate in conjunction with alternate slip.

### 3.3 Summary and Discussion of Mechanisms

Since the mechanism of environment-sensitive cracking must be consistent with the experimental observations, some advantages and disadvantages, and the intercompatibility of the various mechanisms will be considered here. Also some important supporting, critical experiments are discussed.

In Figs. 15 and 16, a simplified illustration of the slip at the crack tip is presented. In this schematic presentation, the effects of plastic deformation on crack growth have not been taken into account. In Fig. 24, a schematic model of SCC crack growth by slip-dissolution model is presented (Ref. 72). It can be seen that alternating slip-step dissolution results in a fissure rather than a crack. Figure 23(b) shows an example of directed dissolution at the crack tip which can also take place along the slip plane. However, slip planes in many metal/environment systems are not the favored cracking planes. From this schematic picture it can be deduced that the anisotropy factor in dissolution must be rather high in order to have a sharp stress corrosion crack. Gröschel (Ref. 73) studied stress corrosion cracking of austenitic stainless steel single crystals in boiling  $MgCl_2$  solutions and came to the conclusion that the anisotropy factor should be higher than 15. In more practical stress corrosion cracking cases, the anisotropy factor is probably much higher. Thus, the precise criteria for chemical blunting in the model presented by Ford and Emigh (Ref. 39) are ill-defined at



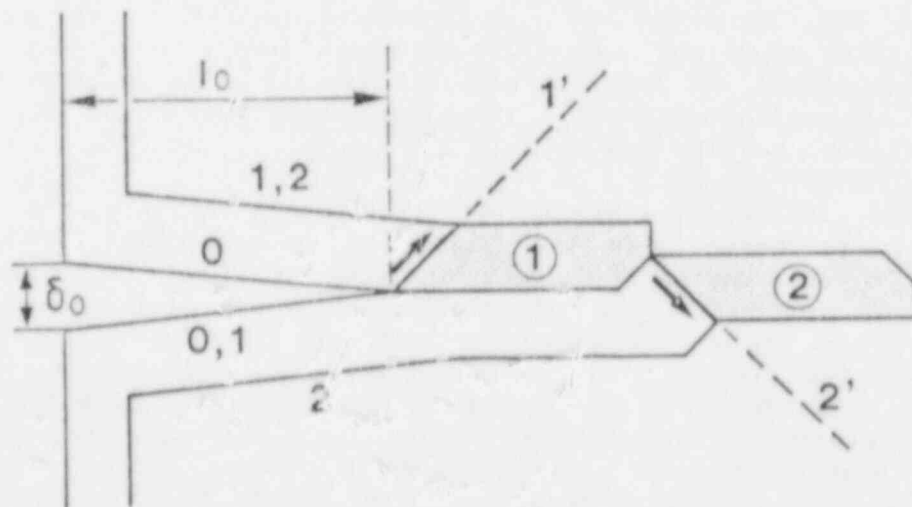
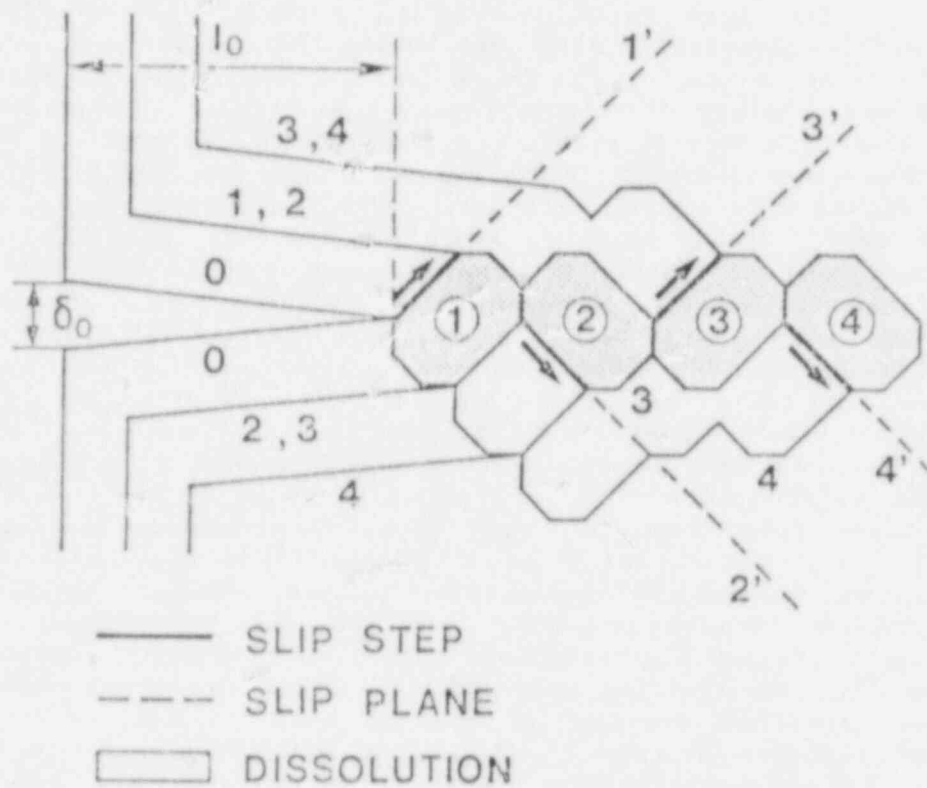


Fig. 24 Stress corrosion crack growth according to the slip-dissolution model when alternating slip is occurring at the crack tip. (a) General slip-step dissolution, and (b) directed slip-step dissolution (Ref. 72).

present. Blunting occurs when  $V_T$  is too low to offset the blunting action caused by lateral dissolution on the adjacent crack sides ( $V_S$ ). The arbitrarily chosen limiting  $V_T/V_S$  values of 5 to 10 are very low especially for sustenance a stress corrosion crack. Experimental evidence for anisotropic anodic dissolution exists only for stainless steels and noble metal alloys (Refs. 74 to 76) and has been obtained by electron microscopy, but single crystal electrochemical measurements have not revealed any indications of such kind of anisotropy (Refs. 77 and 78). Therefore anisotropic anodic dissolution should also be experimentally proven for various material/environment systems susceptible to environment-sensitive cracking. Also the cleavage component hypothesis of Sieradzki and Newman (Ref. 45) used in the model of Ford and Emigh (Ref. 39) was originally developed for Cu-base alloys in tarnishing conditions, a condition not associated with absorbed hydrogen, and as yet has no experimental support for proven hydrogen assisted crack growth phenomena. There is no reason why the Sieradzki and Newman model should not work for hydrogen assisted crack growth modeling.

In fatigue crack growth, crack tips are resharpened by reversed slip behind the crack tip during unloading and in this case the anisotropy factor may not be as critical as in the case of stress corrosion cracking. It has been proposed that in corrosion fatigue an upper limit in crack growth per cycle ( $da/dN$ ) is the maximum CTOD/2 (Ref. 79). This is a chemical blunting limitation derived from the condition at which the crack tip would lose its ability to resharpen during unloading in case of higher anodic dissolution.

When the dissolution transients have been measured during cyclic loading of A 508 Cl. 3 steel in deaerated PWR conditions at slow strain rates, compressive straining has been found to be more efficient than tensile straining in enhancing dissolution (Ref. 44). At high strain rates ( $> 5 \cdot 10^{-4} \text{ s}^{-1}$ ) however, the maximum current is obtained during tensile straining. A possible cause for enhancement of anodic dissolution during compression at slow strain rates is that in this material reversed slip is not easy and different slip planes are active during tension and compression. Since the reversed slip is occurring behind the crack tip in corrosion fatigue, this additional dissolution would further chemically blunt the crack. It should also change the crack-tip morphology markedly. One may question whether the oriented dissolution at the crack tip produces the brittle, cleavage-like crack during tensile straining; why then do the perhaps higher anodic currents during unloading not destroy the fracture surface by dissolution of the areas of reversed slip, resulting in chemical blunting?

A quantitative model for the prediction of corrosion fatigue crack growth can not be interpreted by acceleration of crack growth by localized hydrogen-induced cracking and retardation of crack growth by crack-tip blunting which is caused mainly by anodic dissolution. This type of model predicts corrosion fatigue behavior in a number of systems and successfully describes the effects of frequency, waveform and electrochemical polarization (Ref. 80). Hydrogen-induced cracking only takes place when the load is rising in the fatigue cycle and the

maximum environmental enhancement saturates when frequency is lowered to a certain level. Anodic dissolution during loading or unloading is an efficient source for hydrogen. A maximum enhancement is reached at a certain cyclic frequency and further reductions or increases in frequency usually produce less enhancement, e.g., due to extensive chemical blunting or other passivation process. Basically, the extent of hydrogen-induced cracking depends on hydrogen entry and diffusion. If the cyclic rise time is too short to allow hydrogen diffusion across the width of one fatigue striation, the embrittlement is not observed. Localized hydrogen embrittlement can be suppressed also by using square waveform cycling in which the rise time is very short. Thus it can be postulated that the mechanism of corrosion fatigue which produces environmentally-enhanced brittle, cleavage-like cracking involves a synergistic interaction between mechanical fatigue, localized hydrogen-induced cracking and crack-tip blunting as a result of anodic dissolution. In a quantitative model of corrosion fatigue crack growth, the hydrogen-induced cracking, which is discussed next in more detail, must be treated separately from the blunting effect.

Modeling of hydrogen-assisted crack growth generally recognizes (1) the processes that control the rate of supply of hydrogen to the fracture process zone, (2) the role of hydrogen/microstructure interactions which determine the partitioning of hydrogen in the structure and rate of crack growth, and (3) the critical concentration of hydrogen required for brittle fracture, which depends on the local stress (Ref. 52). The kinetics of hydrogen diffusion are complicated by the fact that the hydrogen flux is affected by stress gradients, and trapping at solutes and particles. Whether the source of hydrogen is gaseous hydrogen or an electrochemical reaction, the specific state of the surface can affect the kinetics, especially if some hydrogen recombination poisons are present. Absorbed hydrogen must reach the point at which failure occurs by diffusion or by dislocation transport (Refs. 81 to 83). In the case of high-temperature corrosion fatigue hydrogen diffusivity has a high value even when the random walk diffusion distance is used. Hydrogen diffusion rates are expected to be in the range from 20 to 200  $\mu\text{m}$  per second. Thus, hydrogen will be extremely mobile compared to typical crack-tip dimensions (Ref. 84). Even though strong hydrogen traps are still operative at 300°C, hydrogen can diffuse out of the crack tip stress field, e.g. when the stress cycle frequency is low.

Mager (Ref. 44) has not observed any marked differences between crevice conditions and conditions on free surfaces with respect to potential and pH. In crack-tip damage studies, such as that by Ford and Emigh (Ref. 39) presented in Section 3.1, the crevice effects were simulated by  $\text{SO}_4^{2-}$  additions. In the appropriate conditions  $\text{H}_2\text{S}$  and  $\text{HS}^-$  are the dissolution products from  $\text{MnS}$  inclusions but  $\text{SO}_4^{2-}$  is reduced to these species in the high-temperature water environment. However, in studies of Mager (Refs. 44, 85 and 86) very high  $\text{SO}_4^{2-}$  (1.5 ppm) contents were needed in order to obtain any effect. Presently, there is no explanation for why such a relatively large

bulk concentration of  $\text{SO}_4^{2-}$  was required to obtain a measureable effect. The local environment at the growing corrosion fatigue crack depends also on the local crack tip strain rate or more exactly on the rate of creation of fresh surface which leads to hydrolysis reactions and cathodic hydrogen evolution reactions. Transport of species between the bulk and local crack-tip environment through the pumping action of moving crack flanks during cyclic loading may not be so important, since the dissolution of exposed MnS inclusions ( $\text{H}_2\text{S}$  and/or  $\text{HS}^-$  formation) seems to play a very important local role in creating the environment conducive to brittle, cleavage-like crack growth. Crack growth acceleration due to trace amounts of  $\text{H}_2\text{S}$  has been observed in corrosion fatigue studies of low alloy steels in LWR conditions (Ref. 61). The experiments of Bamford and Moon at  $93^\circ\text{C}$  indicated that a gaseous hydrogen-sulfide containing environment can produce a lower  $\Delta K$  threshold than the high temperature PWR water environment (Ref. 61). In the hydrogen sulfide environment, no "plateau" crack growth rate was seen, probably because sufficient hydrogen can be supplied to produce the critical hydrogen concentration needed for enhanced crack growth. These corrosion fatigue cracks were completely free of micro-branching during crack growth. In general, these effects may be directly correlated with the ability of adsorbed  $\text{H}_2\text{S}$  or  $\text{HS}^-$  molecules, possibly acting as hydrogen donors (Ref. 49), to increase the rate of hydrogen absorption, but the detailed mechanisms are not understood and have been very little examined with the objective of establishing the rate-controlling mechanisms. Dissolution products of MnS ( $\text{H}_2\text{S}/\text{HS}^-$ ) also markedly increase the anodic dissolution reaction rate in oxygen-free water (Ref. 49), but there is no direct evidence available for directed anodic dissolution.

Gabetta (Refs. 87 and 88) has carried out in-situ electrochemical corrosion potential measurements within growing corrosion fatigue crack tips. These experiments monitored the transients during cyclic loading and showed that the potential becomes more negative during the rising load cycle than during unloading, which can best be interpreted by hydrogen-induced cracking mechanisms together with a reversed slip-assisted anodic dissolution component during the unloading part of the cycle.

Hydrogen entry into the lattice takes place at fresh metal surfaces produced by plastic deformation or by an electrochemical corrosion reaction. The behavior at the surface during corrosion reaction or during cathodic charging is poorly understood. Since the chemical potential of  $\text{H}^+$  at the surface during an electrochemical reaction can be extremely high, the potential for hydrogen entry is thus not a limiting factor assuming that a thermodynamically stable oxide does not inhibit such ingress. Also, high fugacity hydrogen can be produced in the metal as discussed earlier in Section 3.2.3. It is hypothesized that hydrogen embrittlement requires the development of a critical hydrogen concentration at the stress concentration site and that a uniform distribution of hydrogen below the critical concentration will not cause embrittlement. The flux of hydrogen in response to stress gradients at stress concentrations of cracks has been discussed by Gerberich (Refs. 54 and 55). The experimental basis for this work involved high-strength steels under plane-strain

conditions demonstrating the effect of stress gradient when considering the distribution of hydrogen in nonuniform stress fields.

Hydrogen entry from the gas phase consists of physisorption of  $H_2$ , molecular chemisorption, dissociation of  $H_2$  and entry of  $H^+$  into the lattice. These processes are imperfectly understood. The experiments of Mager (Ref. 44) to induce enhanced crack growth by high temperature hydrogen gas (103 bar) at 288°C even at a slow frequency of 1 cpm have not been successful. This may be due to the prohibitively low external hydrogen fugacity, which is not able to produce high fugacity hydrogen in the metal as do electrochemical reactions at the crack tip, especially near MnS inclusions where  $H_2S/HS^-$  is also produced. Atkinson and Lindley (Ref. 89), however, were able to produce hydrogen-induced enhanced crack growth in A 533-B steel in fatigue tests at 25 to 100°C, at which temperature range the environmental-enhancement factor decreased with increasing temperature in 1 bar hydrogen. Priest (Ref. 90) has additionally shown that at room temperature the influence of hydrogen pressure on acceleration of cyclic crack growth increases markedly near 100 bar. Loading frequencies less than 1 Hz did not affect the environmental-enhancement factor. It was also observed that the loading rate rather than the total cycle time is important in controlling hydrogen-induced fatigue crack growth, which produced transgranular fan-shaped fracture surface morphology. In low pressure hydrogen at room temperature the upper bound of cyclic crack growth rate equals  $3 \cdot \Delta CTOD$  and in high pressure hydrogen it may increase to  $4 \cdot \Delta CTOD$  per cycle. This is approximately 1/10th of the cyclic plastic zone size. Atkinson and Lindley (Ref. 89) suggest that there might be a mechanistic limit for hydrogen-induced cyclic crack growth rate of about  $3 \cdot \Delta CTOD$  for low pressure hydrogen. The maximum triaxiality in the crack tip stress field occurs at a distance of  $2 \cdot CTOD$  (equals  $4 \cdot \Delta CTOD$  for  $R = 0$ ) ahead of the crack tip. Thus, it is still difficult to explain mechanistically the size of this critical process zone of  $3 \cdot \Delta CTOD$ , which is much smaller than the calculated cyclic plastic zone size. The effects of hydrogen fugacity and temperature on the upper bound are also unknown. Since it is not known which of the above mentioned steps control the rate of hydrogen entry into steel, quantitative conclusions cannot be based on fatigue tests performed in hydrogen gas. The processes of hydrogen entry are most likely temperature dependent, material specific and structure sensitive. Also the hydrogen entry may be extremely sensitive to the presence of specific environmental contaminants. Inhibition of crack growth in steels in gaseous hydrogen is observed due to the presence of trace amounts of  $H_2O$ ,  $O_2$ , or  $SO_2$ , but crack acceleration due to trace amounts of  $H_2S$  has often been observed (Ref. 62).  $H_2S$  is also very important in enhancing hydrogen uptake during corrosion fatigue of low alloy steels in high temperature water (Fig. 21). Since the hydrogen diffusion rate in the lattice at about 300°C is high, it is not thought to be the rate-limiting factor. Hydrogen entry may control the crack growth rate. On the other hand, differences in hydrogen fugacities of hydrogen sources in different corrosion fatigue tests, especially in local crack-tip chemistry, determine the kinetics and even the occurrence of environmental enhancement in corrosion fatigue.

The 1 Hz low pressure hydrogen data for A 533-B steel of Atkinson and Lindley (Ref. 89) are plotted with other relevant data in Fig. 25a. For high R values, the upper bound for crack growth rates in hydrogen and H<sub>2</sub>S atmosphere at room temperature is 3 to 4 • ΔCTOD (Fig. 25b), which is less than the maximum CTOD/2, which was proposed by Tomkins (Ref. 79) for crack-tip dissolution case. In corrosion fatigue, however, crack growth rates higher than CTOD/2 per cycle have been observed (Ref. 91). It should be noted that Tomkins excluded passive material-environment combinations from the scope of the CTOD model. Tomkins (Ref. 79) suggested further that the mechanical limit in hydrogen-bearing environments was the cyclic plastic zone size per cycle, but Fig. 25 suggests that the upper bounds of the crack growth in low pressure hydrogen as a result of transgranular hydrogen-induced cracking are the ASME XI (1980) code lines developed for PWR environments. However, much additional data are needed to ascertain this, both experimentally and mechanistically. Since there are corrosion fatigue crack growth data higher than the current ASME XI (1980) code lines, the hydrogen fugacity and temperature combinations must be varied further in simulating the conditions in these cases, before the maximum theoretical environmentally-controlled crack growth rates are determined.

In hydrogen-charged iron, cleavage-like fracture on {110} and {112} planes has been observed (Ref. 92). These planes are slip planes for iron and therefore many of the above mechanisms for hydrogen embrittlement may operate. The possible role of hydrogen in corrosion fatigue needs to be examined crystallographically by comparing brittle, cleavage-like corrosion fatigue fracture surfaces to hydrogen-induced brittle fracture surfaces.

The generalized corrosion fatigue cracking mechanism involves the mutual occurrence of both hydrogen-induced cracking and anodic dissolution at the crack tip. Since there appear currently to be at least four possible mechanisms of anodic dissolution [slip-dissolution, brittle film-rupture, corrosion-tunneling, and selective-dissolution (dealloying) mechanisms] and five of hydrogen embrittlement (decohesion, pressure, adsorption, deformation and brittle hydride mechanisms) plus other adsorption models, the balance between various phenomena is very difficult to sort out. Many researchers think that dissolution and hydrogen-induced cracking processes are competitive, so that only one of them makes the major contribution to cracking, and the lesser process can be ignored. However, both processes (dissolution and hydrogen evolution) occur simultaneously at the crack tips over ranges of potential which have been measured or which are suspected to occur. If the processes were independent and were really competitive, it would only be necessary to determine which process is faster. The anodic and cathodic processes are, however, interdependent and they must operate simultaneously or sequentially and the slower process will control the overall kinetics. The crack-tip blunting and resharping can be considered similarly. If plastic flow is blunting the crack, localized-directed dissolution or hydrogen-induced cracking are needed to resharpen the crack. If chemical blunting is occurring only hydrogen-induced cracking, with the help of unloading, can keep the crack sharp.

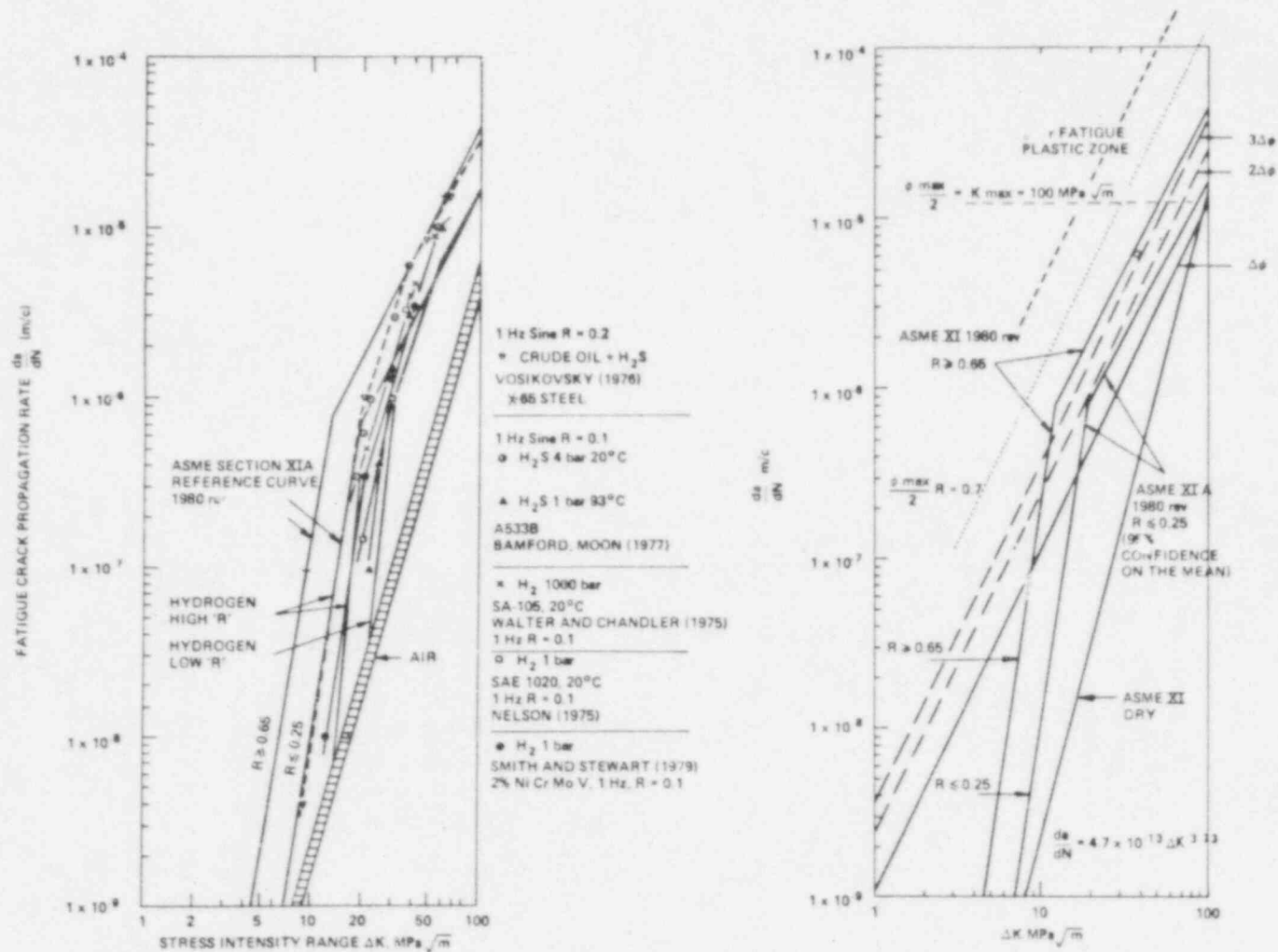


Fig. 25 (a) Comparison of fatigue crack growth data in hydrogen with data from other sources. (b) Mechanics upper bound growth predictions in relation to the ASME XI (1980) code (Ref. 89). The symbol  $\phi$  = CTOD.

Since completely adequate criteria for critical electrochemical experiments for interpretation of cracking mechanisms have not been established, the loading mode variation from Mode I (tension) to Mode III (torsion) has been thought to be a critical experiment (Ref. 93). This approach has also a weakness; it addresses a condition where hydrogen accumulates at regions of high triaxial stress, which is not unequivocally known to be either necessary nor sufficient for hydrogen embrittlement. Moreover, it is difficult to evaluate mechanistic behavior in detail because of the many uncertainties in both the currently proposed both dissolution- and hydrogen-controlled mechanisms. It therefore appears premature to try to select the best mechanism based on existing evidence. More indirect, but mechanisms-oriented work is needed, in which the environmental conditions at the crack tip are verified, the crack-tip strain conditions analysed and effects of hydrogen on deformation and fracture properties of these materials are determined in the appropriate temperature range. Detailed direct observations by fractography and high voltage electron microscopy of the phenomena occurring in the crack-tip process zone are most helpful in increasing the understanding of corrosion fatigue mechanisms.

#### 4.0 COMPUTATIONAL MODELS FOR ENVIRONMENTALLY-ASSISTED CRACK GROWTH RATE

Whatever mechanism is responsible for environmentally-enhanced crack growth, either anodic dissolution or cathodic reactions (such as hydrogen evolution), the fundamental rate-determining factors are oxide rupture rate, repassivation rate and solution-renewal rate in the crack enclave (Ref. 94). Plastic deformation in the metal substrate will give rise to metal-oxide debonding and oxide film rupture perhaps, as shown in Fig. 26 for a flat surface (Ref. 95). Therefore, it is clear that the strain rate ( $\dot{\epsilon}$ ) of the metal is an important parameter in environmentally-enhanced subcritical crack growth, because it directly influences oxide rupture rate and bare surface creation. Strain rate is in fact widely used as a determining parameter to study stress corrosion susceptibility of a given material in a given environment (Ref. 96). For this purpose constant extension rate tests on smooth specimens are often performed. Specimens are loaded at a constant displacement rate, so that strain rate is determined as displacement rate divided by a gage length, as shown in Fig. 27. In general, maximum severity of the corrosion effect is observed within a critical  $\dot{\epsilon}$  range and the susceptibility decreases at faster and slower strain rates; a too rapid strain rate results in ductile fracture of the specimen before deep stress-corrosion cracks can be created to a degree which affects the tensile properties, while a very low strain rate often allows repassivation and suppresses SCC. For many material-solution systems, the maximum in the degradation of tensile ductility is found at a strain rate of about  $10^{-6} \text{ s}^{-1}$  (Ref. 97); for A 508 pressure vessel steel tested in pure water at a strain rate of  $10^{-6} \text{ s}^{-1}$ , the susceptibility has been found to be related to the oxygen content in water (i.e. on  $E_{\text{corr}}$ ); no SCC has been found at oxygen concentrations lower than  $\sim 5$  ppb oxygen, corresponding to an  $E_{\text{corr}} < -200\text{mV}_{\text{SHE}}$ , SCC was present at 400 ppb oxygen (Ref. 98).



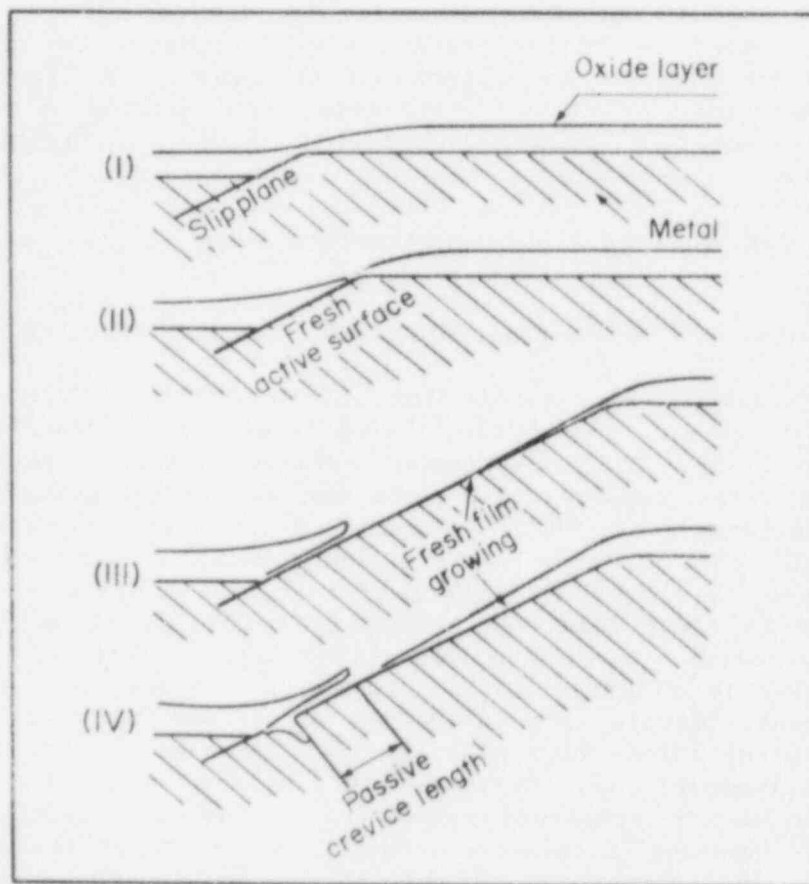


Fig. 26 Schematic representation of the formation of a micronotch from underfilm crevice attack: (I) emergence of a slip step with a necking effect on the oxide film. (II) rupture of the oxide film at the leading edge and crevice activation. (III) partial passivation of the crevice area and (IV) notching penetration at the active foot of the slip step (Ref. 95).

In the study of cyclic crack growth in these environments, it is customary to assume that strain rate at the crack tip plays a similar role on oxide rupture and bare surface creation as on smooth specimens. It is then important to evaluate crack-tip strain rates in the different strain conditions, not only to quantify and to predict the presence of SCC during environmental fatigue, but also with the purpose of correlating results obtained on smooth and notched specimens in (a) constant extension rate, (b) monotonic load, and (c) fatigue load tests at different values of load ratio and test frequency.

#### 4.1 Crack-Tip Strain Rate

Two different steps are necessary to evaluate crack-tip strain rate: strain must be calculated, and its dependence on time has to be derived. The calculation of local crack-tip strain is difficult due to the presence of a mathematical singularity in elastic analyses of the material, i.e., the crack tip, where the theoretical stress and strain go to infinite values. What happens in reality is the creation of a plastic zone which increases in size as the applied  $K$  increases.

Going back to a smooth specimen (Fig. 27), it is important to remember that in this case the strain value ( $\Delta G/G$ ) is an average value; the strain is considered as equally distributed along the completed gage length ( $C$ ); no effect is generally assumed on  $\dot{\epsilon}$  distribution due to the presence of one or more cracks. So, to correlate smooth specimens with notched specimens in terms of strain, it is possible to:

- (a) Treat a smooth specimen in the same way as a notched one, taking into account the presence of a small crack in it.
- (b) Treat a notched specimen as a smooth one, considering the strain as equally distributed in a large process zone.

The two different approaches are shown in Figs. 28 and 29. In the first case, the strain is calculated in a very small region ahead of the crack tip by using a fracture mechanics approach; in the second one, the strain is considered as evenly distributed on a large process zone by using an approach that has already shown to be useful in traditional stress corrosion tests.

Assuming now that it is possible to compute the strain distribution at a given point of the notched specimen, its dependence on time during a fatigue test must be evaluated. In Fig. 30 a plot of strain as a function of time during fatigue load cycle is shown. Two possible  $\dot{\epsilon}$  evaluations are indicated: that for a single cycle (designated  $\dot{\epsilon}_{sc}$ ), or following the variation of the maximum strain values (the "envelope") of strain (designated  $\dot{\epsilon}_e$ ). Several models for computing crack tip strain rates have been proposed up to now; they will be described in the following. Table I shows the proposed models listed according to the different approaches used.

G = GAGE LENGTH

$$\epsilon = \frac{\Delta G}{G}$$

$$\dot{\epsilon} = \frac{d}{dt} \left( \frac{\Delta G}{G} \right)$$

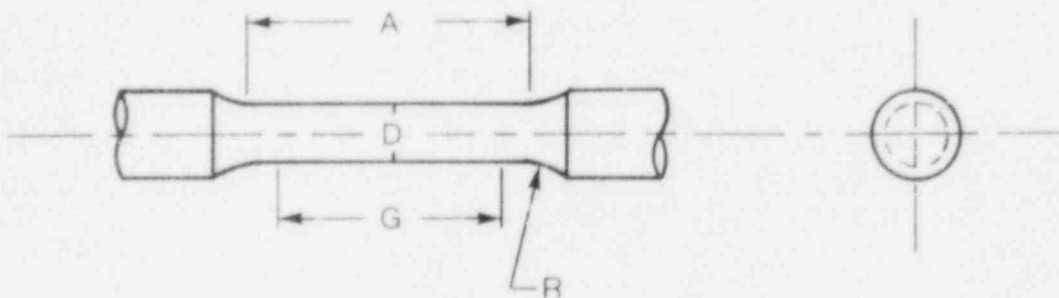


Fig. 27 A cylindrical slow strain rate specimen and the  $\dot{\epsilon}$  calculation for it.

TREATING A SMOOTH SPECIMEN AS  
A NOTCHED ONE: IN A SMALL  
ZONE.

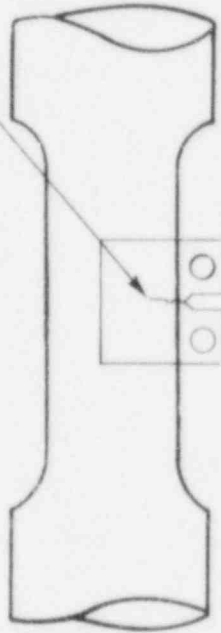
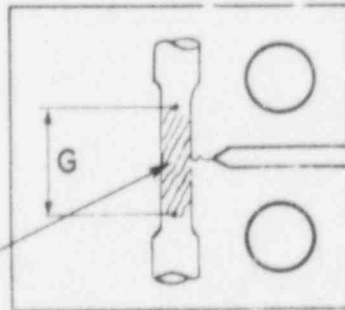


Fig. 28 The first of two different approaches for strain evaluation in both notched and smooth specimens.



TREATING A NOTCHED SPECIMEN  
AS A SMOOTH ONE: IN A  
LARGE PROCESS ZONE.

Fig. 29 The second of two different approaches for strain evaluation in both notched and smooth specimens.

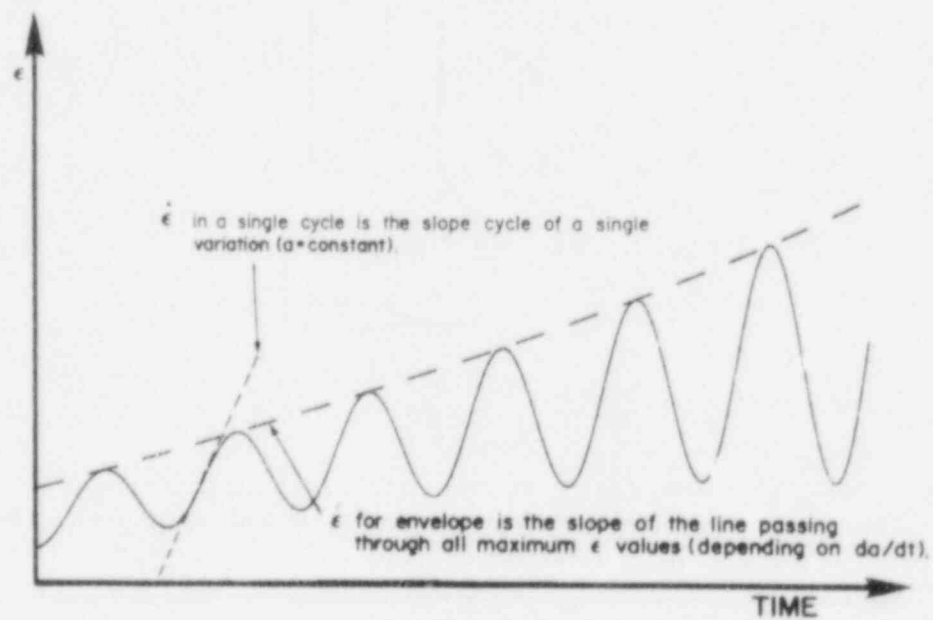


Fig. 30 Strain versus time in a fatigue test and two constructions of the  $\dot{\epsilon}$  formulation.

Table 1 Different Crack Tip Strain Rate Calculation Methods Proposed

Time Regime	Calculation Zone	
	Small Zone Ahead of the Crack Tip	Whole Process Zone
Single Cycle	Scott (Ref. 99)	Gabetta (Ref. 101)
Single Cycle	Lidbury (Ref. 100)	Atkinson (Ref. 12)
Envelope	Shoji (Ref. 94)	Gabetta (Ref. 101)

#### 4.1.1 Single-Cycle Strain Rate, $\dot{\epsilon}_{sc}$

When  $\dot{\epsilon}$  is calculated as strain variation during the loading part of a single cycle, the crack length is assumed to be constant, so that no dependence on  $da/dt$  is taken into account. In summary,  $\dot{\epsilon}$  in a single cycle is:

- A few orders of magnitude greater than  $\dot{\epsilon}$  calculated using the envelope technique
- Dependent on frequency (or rise time)
- Directly dependent on mechanical and geometrical parameters through  $K_{app}$ .

It is moreover possible to compute  $\dot{\epsilon}_{sc}$ , using one of the following models, from the mechanical parameters of the test. The model proposed by Scott and Truswell (Ref. 99) in 1981, and further developed by Lidbury to compute the shear strain at the crack tip (Ref. 100), assumes that the strain rate at the crack tip can be estimated from the rate of change of crack-tip opening displacement,  $\delta$ . Crack-tip opening displacement has been used also as a gage length, so that crack-tip strain rate,  $\dot{\epsilon}_{sc}(t)$ , is

$$\dot{\epsilon}_{sc}(t) = \frac{1}{\delta} \cdot \frac{d\delta}{dt} \quad (4-1)$$

In the case of small scale yielding, crack-tip opening displacement is

$$\delta = \frac{K^2}{E\sigma_y} \quad (4-2)$$

where  $E$  = elastic modulus and  $\sigma_y$  = yield strength.

Since the stress intensity factor is a function of time, it is possible to calculate  $\dot{\epsilon}_{sc}$  during a single cycle. In Fig. 31, plots of crack-tip strain rate vs. time during the loading parts of the sinusoidal and triangular wave forms at different load ratios are shown. In a sinusoidal wave,  $\dot{\epsilon}_{sc}$  is zero at minimum and maximum load, while in the middle of the rise time it reaches a maximum whose value increases as  $R$  ratio decreases. During a ramp, the strain rate is quite constant at  $R > 0.5$ , but at low  $R$  ( $\sim 0.2$  or less) and minimum load,  $\dot{\epsilon}_{sc}$  tends to very high values, due to the small  $\delta$ .

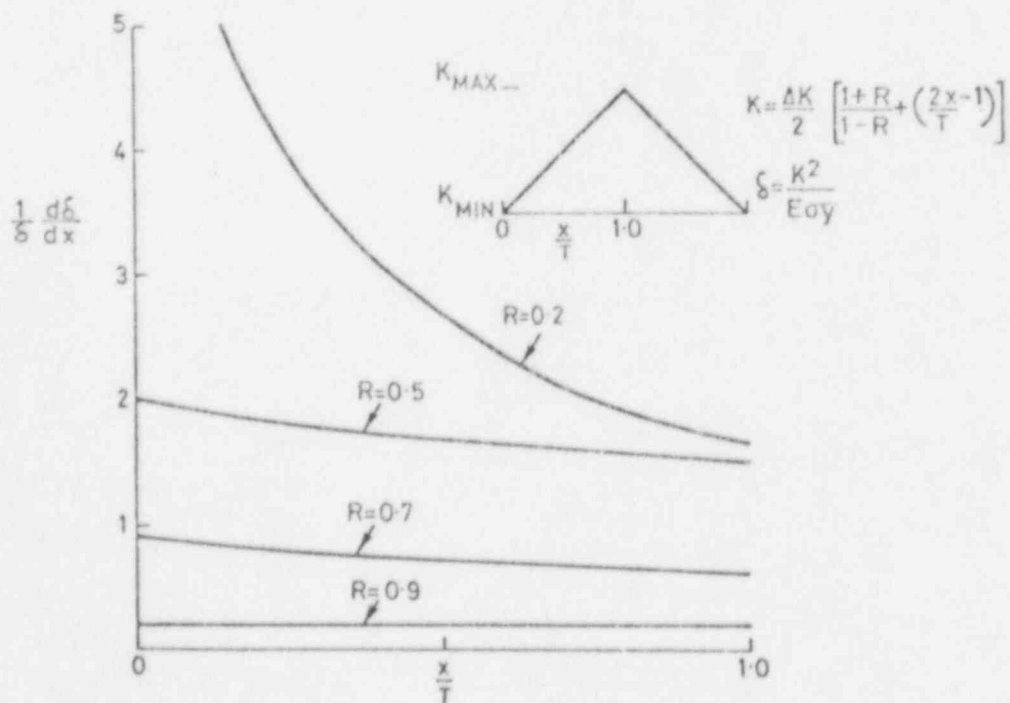
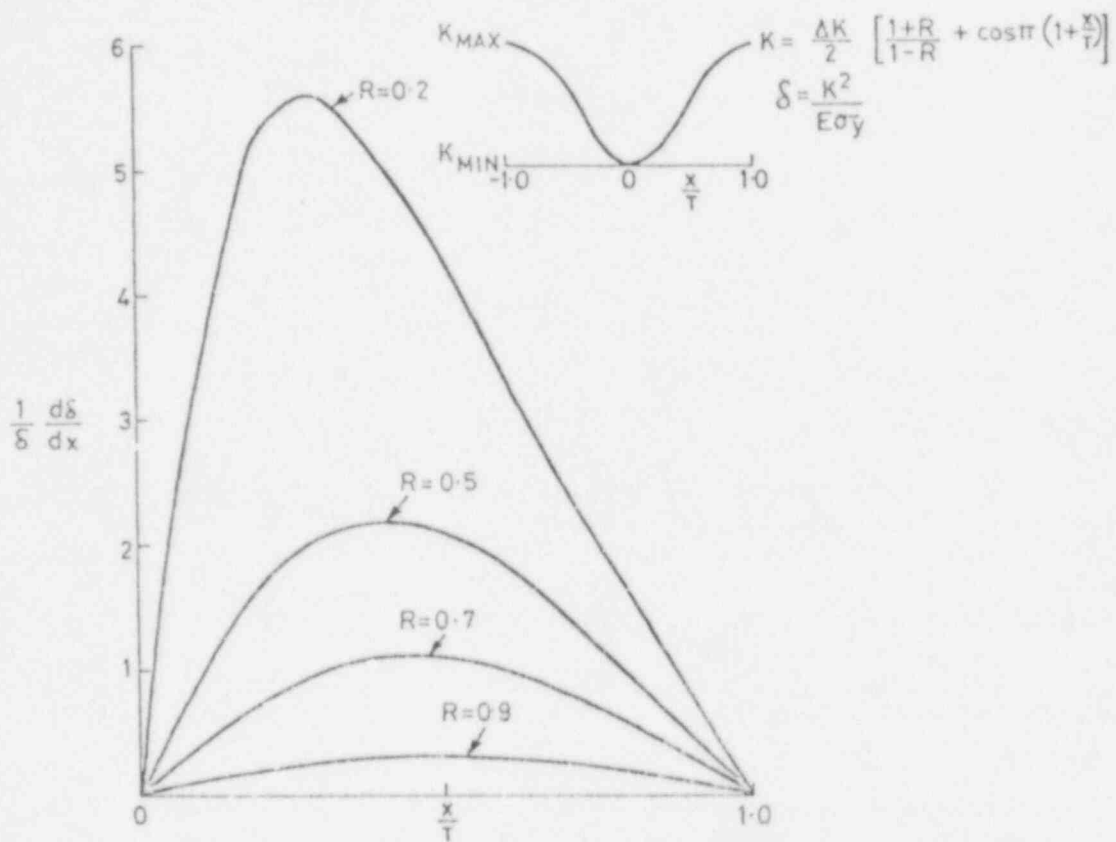


Fig. 31 Crack tip strain rates during sinusoidal and triangular fatigue cycles for a range of load ratios (Ref. 99).

The average strain rate during the loading part of a cycle with rise time,  $T$ , is the following:

$$\dot{\epsilon}_{avg} = \frac{1}{T} \int_{\delta_{min}}^{\delta_{max}} \frac{1}{\delta} d\delta = \frac{2}{T} \ln \frac{1}{R} \quad (4-3)$$

Figure 32 shows average, maximum and minimum strain rates as a function of time, during sinusoidal and ramp loading, at different  $R$  values. Here again it turns out that  $\dot{\epsilon}_{avg}$  is the correct value to use at  $R$  ratio  $> 0.5$ . It is important to note now that the strain rate calculated this way is independent of crack length,  $a$ , so that  $\dot{\epsilon}_{avg}$  is assumed to be constant during the complete test.

During fatigue tests, the occurrence of a plateau in crack growth rate has been often reported. It is possible to say that a stress corrosion cracking process superposed on pure fatigue is responsible for the onset of the plateau, the position of which in the  $da/dN$  vs.  $\Delta K$  plot is dependent on and rate-controlled by an interaction between cyclic rupture of the protective oxide film and its repair by passivation. The strain rate is supposed to play an important role in this corrosion process. In Fig. 33, "plateau" crack growth rates vs. strain rate ( $\dot{\epsilon}_{avg}$ ) are reported for several tests (every point is representative of a test). It has been found (Ref. 2) that the crack growth rate depends on  $\dot{\epsilon}_{avg}$ , according to the equation:

$$\frac{da}{dt} = 1.6 \times 10^{-3} \times \dot{\epsilon}_{avg}^{1/2} \quad (4-4)$$

in the case of low water flow rate (laminar flow on the specimen). For high flow rate tests (turbulent flow):

$$\frac{da}{dt} = 10^{-3} \times \dot{\epsilon}_{avg}^{1/2} \quad (4-5)$$

Moreover, crack growth rate upper limits depending on experimental electrochemical conditions have been found (see horizontal lines in the plot). These results have been verified for relatively high frequencies ( $> 0.25$  Hz) and  $R$  ratios (0.7 to 0.9).

Atkinson, et al. (Ref. 12) proposed that the frequency of crack-tip oxide rupture events is correlated to crack-tip opening displacement rate, rather than to the strain rate defined by Eq. 4-1. This statement amounts to adopting a definition of crack-tip strain rate in which the crack-tip opening displacement rate  $\dot{\delta}(t)$ , is normalized with respect to a constant characteristic length  $B$ , instead of the variable quantity  $\delta$ . Thus, for the loading part of a fatigue cycle

$$\dot{\epsilon}_{sc}(t) = \frac{1}{B} \frac{d\delta}{dt} \quad (4-6)$$

A possible physical significance of the length,  $B$ , has been proposed by Gabetta (Ref. 101), considering the complete zone ahead of the crack tip which experiences a tensile stress, i.e., the zone between the crack tip and the specimen center of rotation,  $x_0$  (see Fig. 34). The position of the center of rotation depends on crack length and can be computed by means of a polynomial, as suggested by Saxena and Hudak (Ref. 102).



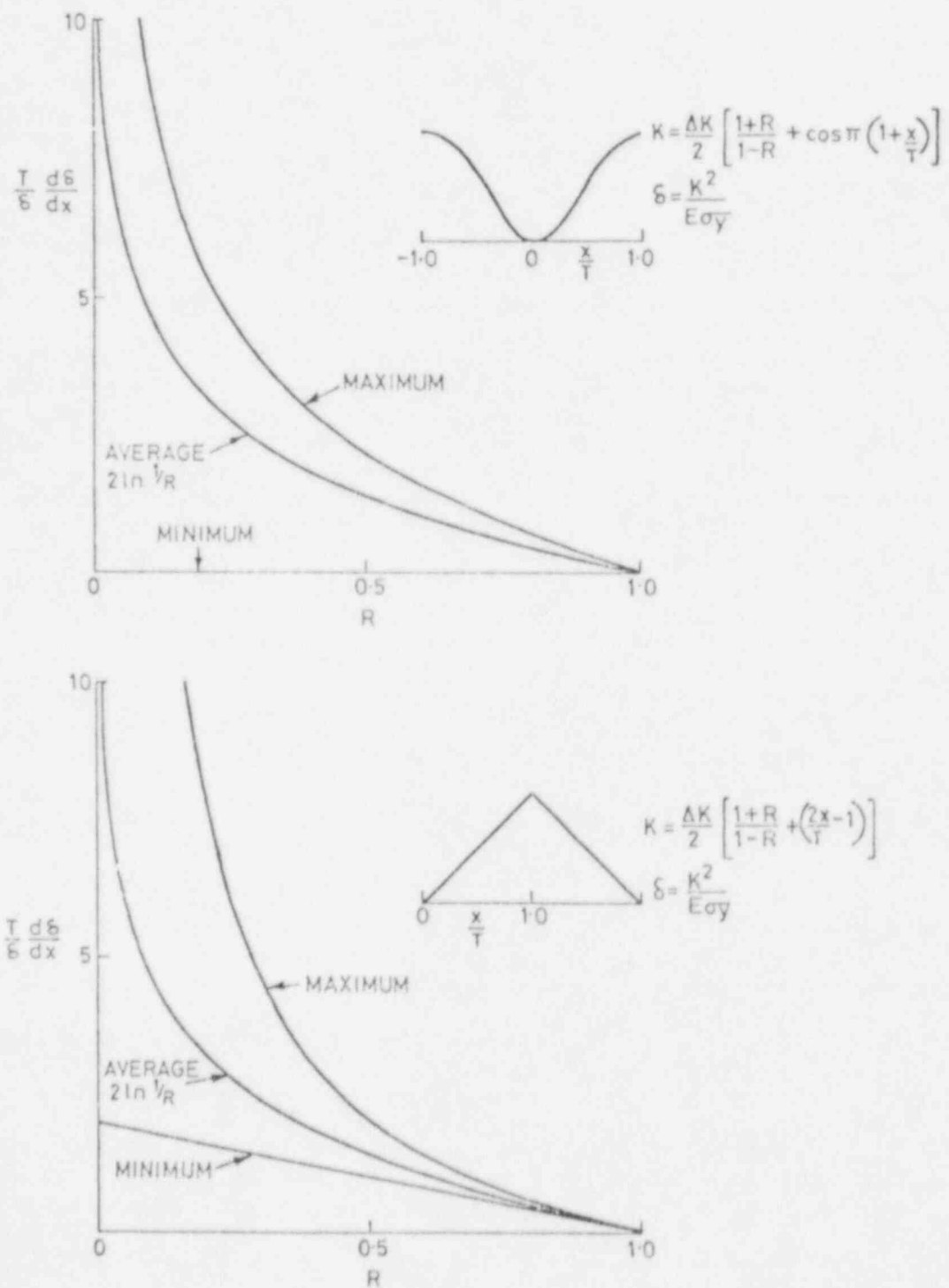


Fig. 32 Average, maximum and minimum crack tip strain rates during sinusoidal and triangular fatigue cycles as a function of load ratio (Ref. 99).

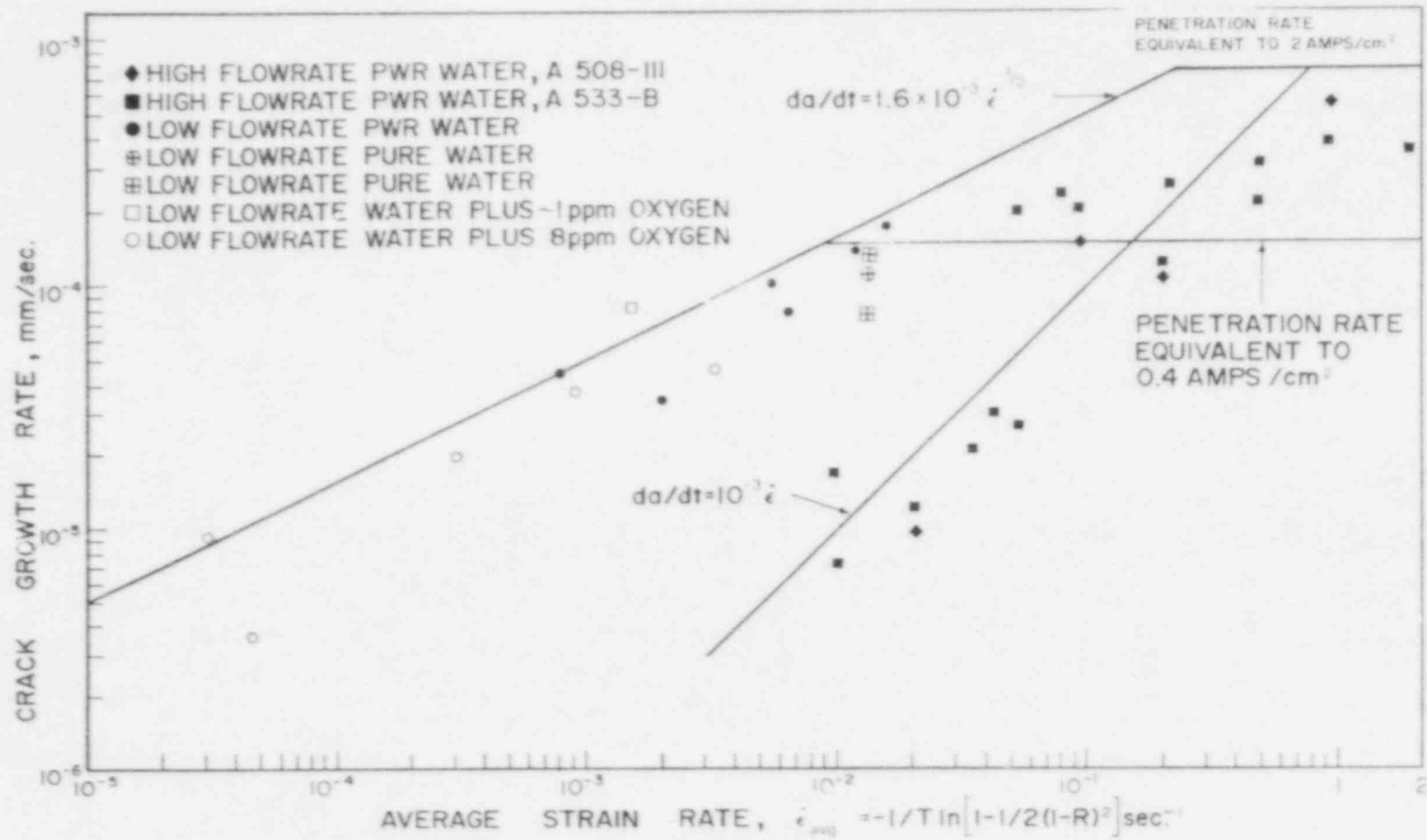


Fig. 33 "Plateau" rates of environmentally-assisted crack growth as a function of crack tip strain rate, from the Scott model (Ref. 99).

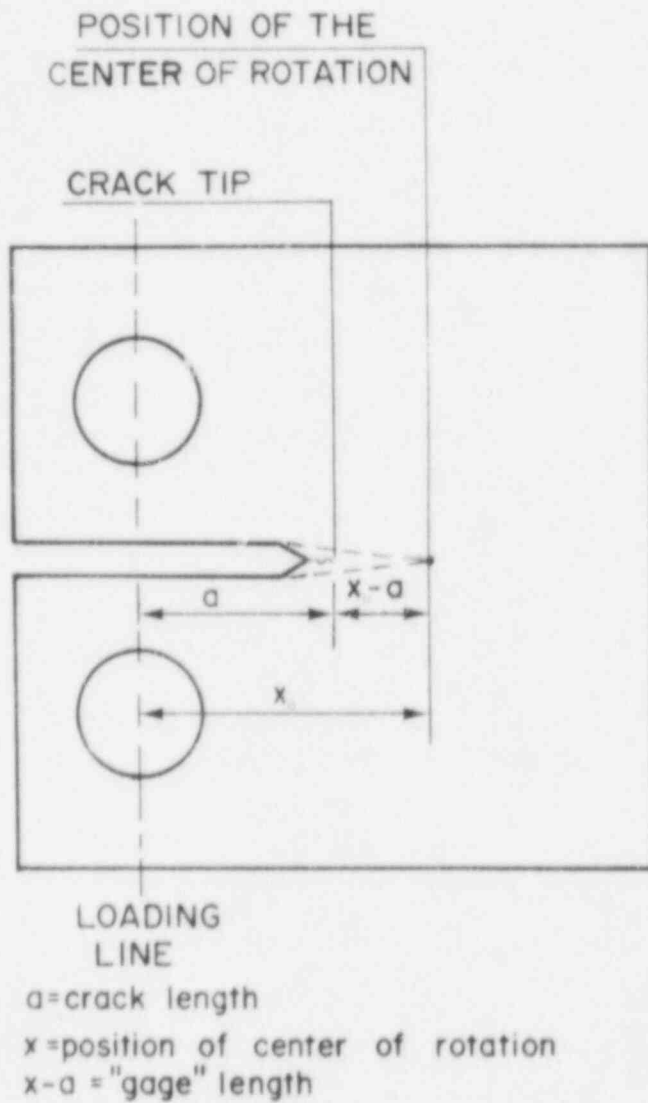


Fig. 34 A schematic of a compact fracture specimen showing the position of the center of rotation and its use as a gage length for strain rate calculations (Refs. 103 and 104).

Considering that CTOD has a component in x-direction ( $\theta = 0$ )

$$\text{CTOD}_x = \alpha_1 \delta \quad (4-7)$$

the strain in this direction is

$$\epsilon_x = \alpha_1 \frac{\delta}{x_0 - a} \quad (4-7a)$$

which is correlated to  $\epsilon_y$  by plasticity equations.

It follows that

$$c = \alpha \frac{\delta}{x_0 - a} = \frac{K^2}{\sigma E (x_0 - a)} \quad (4-7b)$$

and

$$\dot{c} = \alpha \frac{d\delta}{dt} \cdot \left[ \frac{1}{x_0 - a} \right] \quad (4-7c)$$

In Eqs. 4-7,  $\alpha$  and  $\alpha_1$ , are multiplying factors, and  $c$  and  $\dot{c}$  are generic quantities representing x- or y-components of strain.

In Fig. 35, the trends of  $K$ ,  $\delta$  and  $\dot{\delta}$  are shown for a sinusoidal wave (loading part) and a ramp with the same rise time ( $T$ ) and the same  $\Delta K$ .  $\dot{\epsilon}_{sc}$  can be obtained as  $\dot{\delta}$  divided by the gage length,  $(x_0 - a)$ , which is constant for  $a = \text{constant}$ . The maximum in  $K$ ,  $\delta$  or  $\dot{\delta}$  during a sine wave is only slightly higher than the corresponding maxima for a ramp. In any case, as a first approach, an average value independent of the wave form can be calculated:

$$\dot{\epsilon}_{avg} = \frac{1}{T} \cdot \left[ \frac{\delta_{max} - \delta_{min}}{x_0 - a} \right] \quad (4-8)$$

Using this model,  $\dot{\epsilon}_{avg}$  may be calculated in a large zone ahead of the crack tip; the value obtained increases during a constant load test, as the crack grows. In Fig. 36, a plot of  $\dot{\epsilon}_{avg}$  as a function of crack length during a test is shown.

The  $\dot{\epsilon}_{avg}$  computed in this way has been correlated to the purely environmental part of crack growth rate (Ref. 99), obtained by subtracting the corresponding value of ASME XI air curve from the measured  $da/dN$ :

$$\left( \frac{da}{dt} \right)_{env} = \left[ \left( \frac{da}{dN} \right) - \left( \frac{da}{dN} \right)_{air} \right] \frac{1}{T} \quad (4-9)$$

In Fig. 37, the environmental crack growth rate is plotted against  $\dot{\epsilon}_{sc}$  for several specimens tested in the same water chemistry conditions; it is interesting to note that the environmental effect tends to a maximum within the midrange of  $\dot{\epsilon}_{sc}$ , and decreases to very low values for  $\dot{\epsilon}_{sc}$  exceeding about  $10^{-3} s^{-1}$ . Moreover, the maximum  $da/dt$  is about

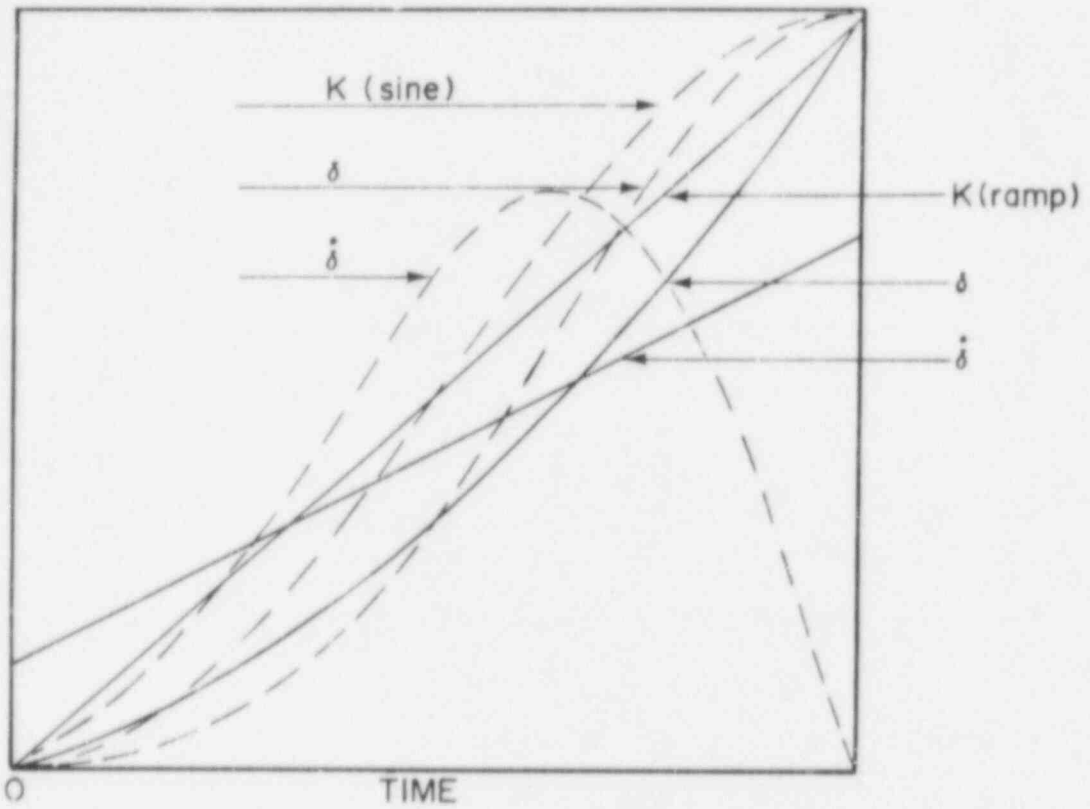


Fig. 35 The behavior of  $K$ ,  $\delta$ , and  $\dot{\delta}$  during the loading part of sine and ramp cycles with the same  $\Delta K$  and load ratio = 0.2. The solid lines are for ramp waveforms and the dotted lines are for sinusoidal waveforms.

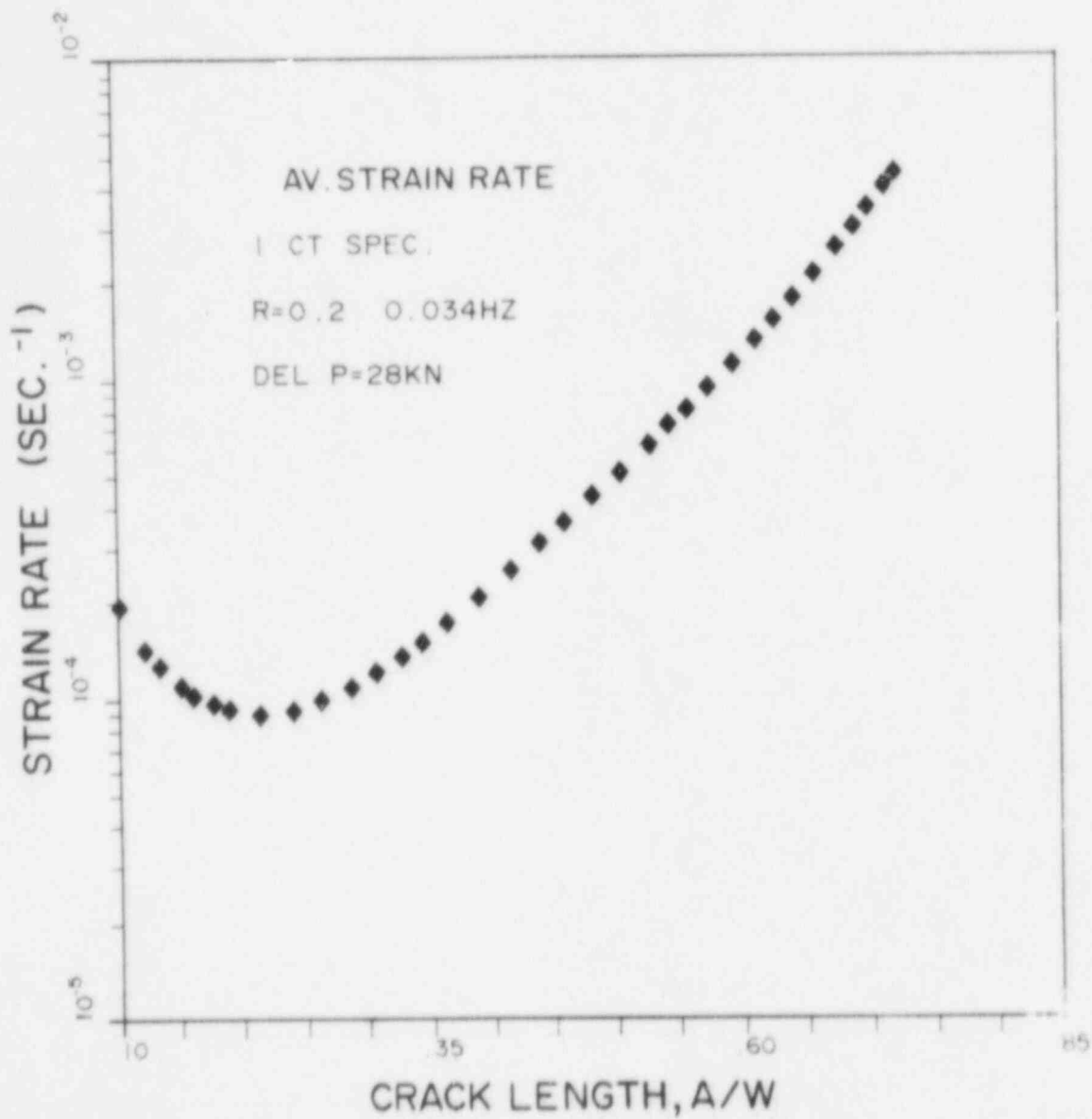


Fig. 36 Plot of the average  $\dot{\epsilon}$  as a function of  $a/W$  for a 1T-CT specimen tested at constant load amplitude frequency.

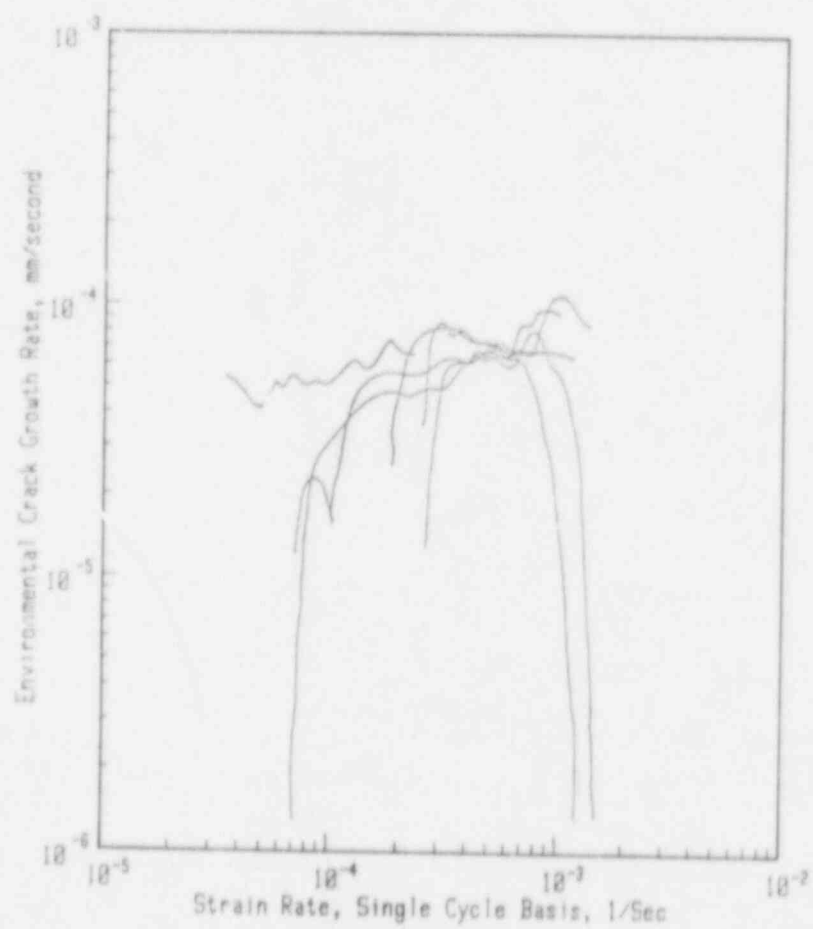


Fig. 37 Environmental  $da/dt$  plotted versus  $\dot{\epsilon}_{sc}$  calculated on a single cycle basis (Ref. 103) for several tests.

$10^{-4}$  mm/s and is frequency independent, at least in the range 0.1 to 0.017 Hz. It has been postulated that the corrosion process is superposed on a mechanical fatigue which follows the ASME XI air line. The corrosion process does not have a linear (on a log/log plot) dependence on  $\Delta K$ ; its maximum rate on a time basis is  $10^{-4}$  mm/s. By adding this maximum rate to the ASME XI air line, a family of limit curves for  $da/dN$  (at different frequencies) can be proposed (Ref. 104). They are shown in Fig. 38. Equations 4-1, 4-6, and 4-8 are representative of models proposed up to now for  $\dot{\epsilon}$ . No matter what is the numerical value obtained (which is different for each model), the physical meaning is straightforward and can be attributed to mechanical oxide rupture. Moreover, the maximum shown by  $\dot{\epsilon}$  in the middle of sine wave rise time can account for the more detrimental effect of the sinusoidal wave with respect to ramp loading. However, it is important to take into account the effects of crack propagation in a model for  $\dot{\epsilon}$ . Models in which the strain rate,  $\dot{\epsilon}_{sc}$ , is a function of crack growth rate,  $da/dt (= \dot{a})$  depend on computation of the strain envelope which characterizes a growing crack, as shown in Fig. 30.

#### 4.1.2 Envelope Strain Rate, $\dot{\epsilon}_{en}$

Such a model was proposed by Shoji (Ref. 94) in 1981, by using a classical fracture mechanics approach, where crack opening rate ( $\delta$ ) is regarded as proportional to  $K \cdot K$  in the elastic case, and to  $J$  in the elastic-plastic case. In both cases, it is possible to demonstrate that  $\dot{\epsilon}_{en}$  is proportional to  $\dot{a}$ . In this way it is possible to take the crack growth rate  $da/dt|_{inert}$ , produced mechanically, as a parameter representative of the crack-tip strain rate.

The same approach can be used to evaluate crack-tip strain rates for a growing crack under cyclic, monotonic (Refs. 105 and 106) or static load. In the case of corrosion fatigue (Ref. 107),  $\dot{\epsilon}$  at the crack tip is:

$$\dot{\epsilon} = A \cdot f + B \cdot \dot{a} \quad (4-10)$$

where  $f$  is the frequency,  $A$  and  $B$  are constants only slightly dependent on the applied  $K$ ,  $\dot{a}$  is the  $da/dt|_{inert}$ .

A schematic representation of how plastic strain at one point in the specimen  $\epsilon_p$  changes during crack growth is shown in Fig. 39. A sharp increase of  $\epsilon_p$  occurs for locations near the crack tip (pos. 3). At the same time or at the same point, the environmental effect starts to have an influence. Moreover, in the situation where  $\dot{\epsilon}_p$  is a maximum, it is possible to calculate  $\dot{\epsilon}_{sc}$  during a single cycle, and an average or global  $\dot{\epsilon}_{avg}$  using the envelope of mean  $\dot{\epsilon}_p$  values as shown in Fig. 40. It has been demonstrated that

$$\dot{\epsilon}(\Delta K, f, R) = \frac{\dot{a}(\Delta K, f, R)|_{inert}}{a_0} \quad (4-11)$$

where  $\dot{a}$  = crack growth rate in an inert environment =  $da/dt|_{inert}$ , and  $a_0$  is a constant.



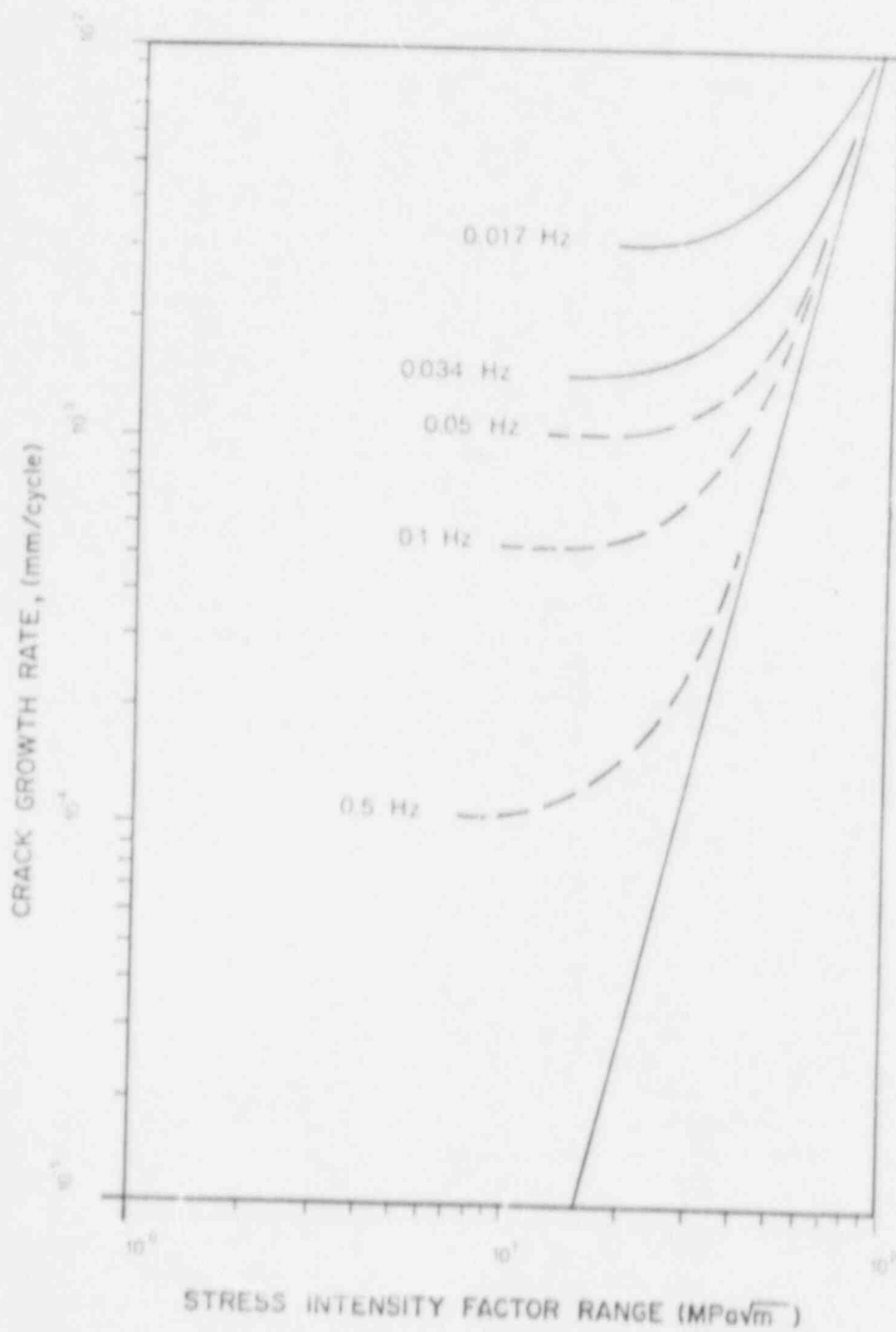


Fig. 38 Limit crack growth rate curves for different frequencies calculated from the single cycle strain rate model.

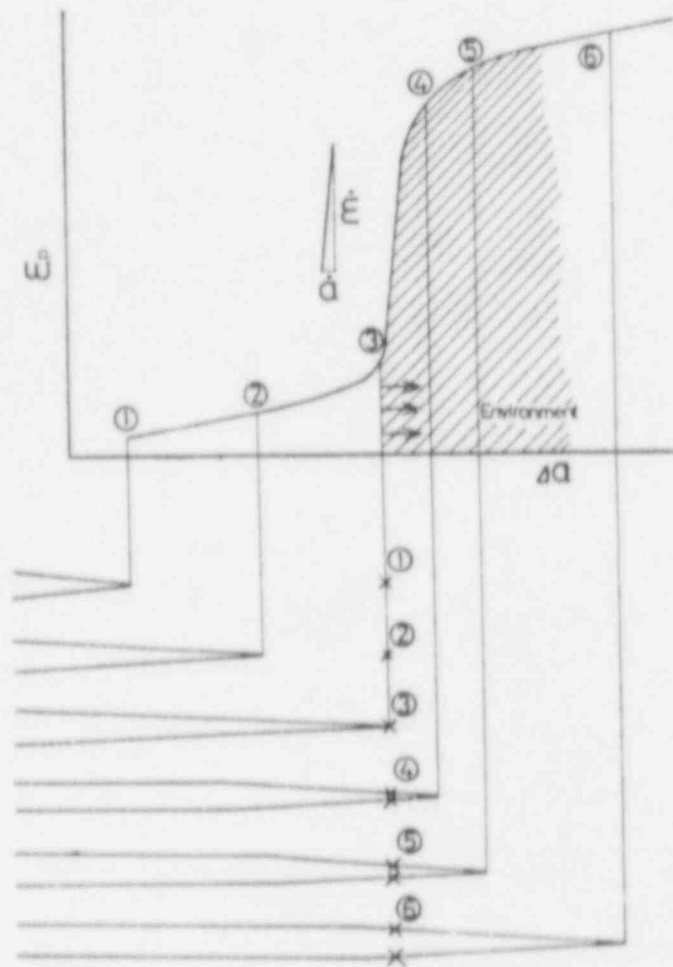


Fig. 39 Plastic strain at different positions (labeled 1 through 6) with respect to the crack tip (Ref. 107).

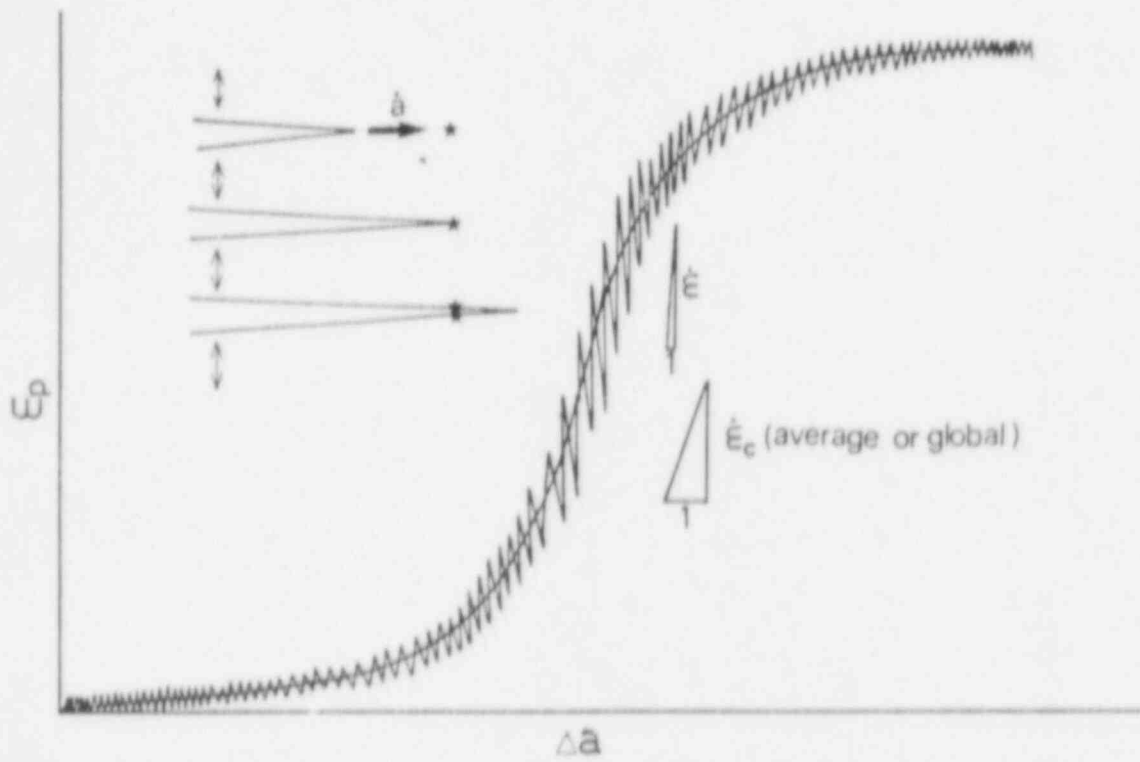


Fig. 40 Plastic strain and  $\dot{\epsilon}$  as a function of crack length (Ref. 107).

It is possible to plot environmental fatigue data as crack growth in environment  $(da/dt|_{env})$  vs.  $\dot{\epsilon}$  (or  $da/dt|_{inert}$ ), in the form  $\dot{\epsilon}_{en}$  ( $= \dot{\epsilon} a/a_0$ ) from Eq. 4-11. The plotting is shown in Fig. 41. It is interesting to notice that the environmental effect is higher at low  $\dot{\epsilon}_{en}$  and decreases gradually at high strain rates. Moreover, it is important to notice that  $da/dt|_{env}$  increases as the sulphur content of the material increases, while the shape of  $da/dt|_{env}$  vs.  $\dot{\epsilon}_{en}$  curve is still the same.

With the hypothesis that crack growth in an environment is the sum of a purely mechanical  $da/dt|_{inert}$ , plus a purely environmental  $da/dt|_{env}$  and assuming moreover a dependence of  $da/dt|_{env}$  on  $da/dt|_{inert}$  through  $\dot{\epsilon}_{en}$ , it is possible to obtain limit curves for crack growth rates which are shown in Fig. 41. Note that the curves are very similar to those presented in Fig. 37, which were obtained using a different model.

The general concept of the strain rate envelope can be applied to any calculation. As an example, Gabetta (Ref. 104) proposed the use of the derivative of Eq. 4-6 to calculate  $\dot{\epsilon}_e$ . In this case,  $\dot{\epsilon}_{en}$  is proportional to the actual  $da/dt$ , as obtained in environment, rather than to  $da/dt|_{inert}$  as proposed by Shoji.

$$\dot{\epsilon}_{en} = \frac{d}{da} \left[ \frac{\dot{\epsilon}}{(x - a_0)} \right] \cdot \frac{da}{dt} \quad (4-12)$$

Some results are worth mentioning because of their order of magnitude since with this last model  $\dot{\epsilon}$  ranges between  $10^{-6} s^{-1}$  to  $10^{-10} s^{-1}$  for typical crack growth rates. By using the same approach in treating data that have been presented by the same author using  $\dot{\epsilon}_{sc}$ , it has been shown (Ref. 104) that the purely environmental effect tends to become very small (Fig. 42) at  $\dot{\epsilon}_{en}$  values ranging between  $10^{-6} s^{-1}$  and  $10^{-7} s^{-1}$ , with oxygen < 180 ppb. These values are of the same order of magnitude as those of a typical constant extension rate test (CERT). In an ICCGR CERT round robin (Ref. 94), using smooth A 508 specimens, an environmental effect was noticed at  $\dot{\epsilon} = 10^{-6} s^{-1}$ , with an oxygen content of about 400 ppb, while no environmental effect was observed at lower oxygen content and the same applied strain rate. The interesting aspect of the strain rate envelope approach can be found in its dependence on crack growth rate; in fact, a corrosion process is likely to be dependent on the bare surface creation at the crack tip. It follows that the environmental enhancement of crack growth rate during fatigue depends on crack growth rate, at least up to a point; this conclusion seems to be demonstrated also by experimental results.

#### 4.1.3 Summary of Strain Rate Models

Four different models for the evaluation of strain rate at the crack tip have been described. They are quite different from each other in the numerical results, giving strain rate values ranging from  $10^{-10} s^{-1}$  to  $1 s^{-1}$ , depending on the model.

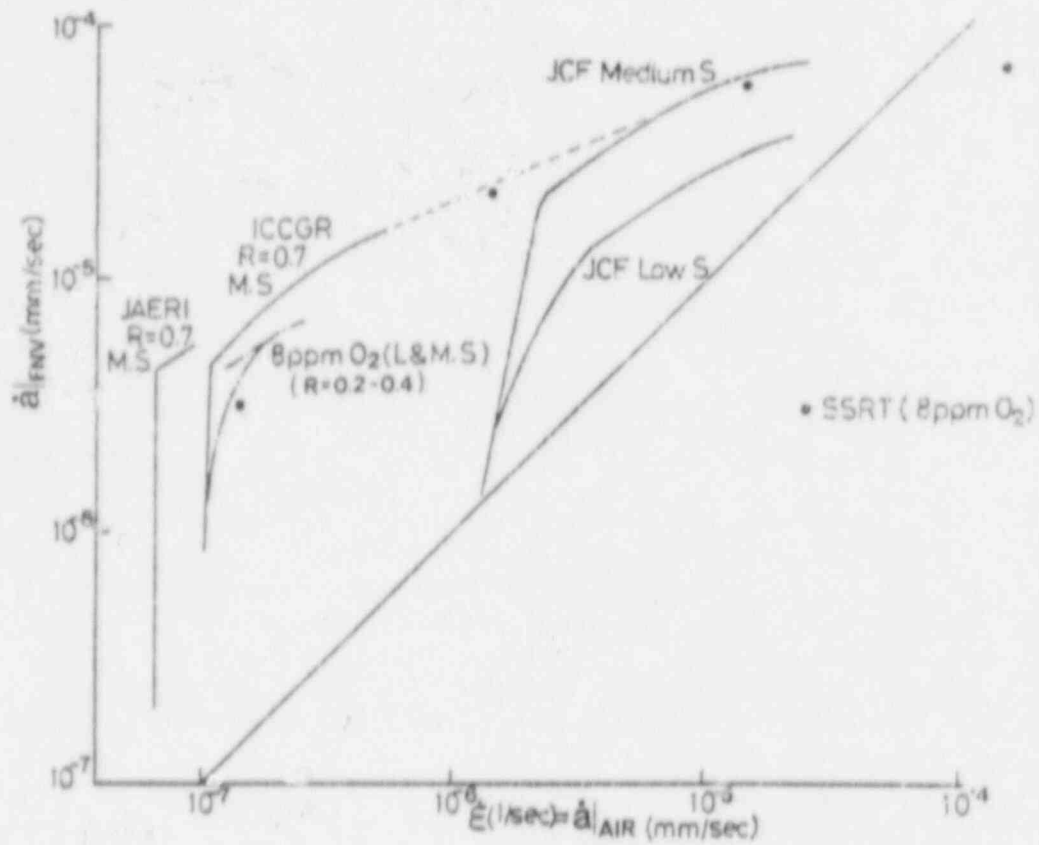


Fig. 41 Crack growth rate as a function of  $\dot{a}$  (Ref. 107).

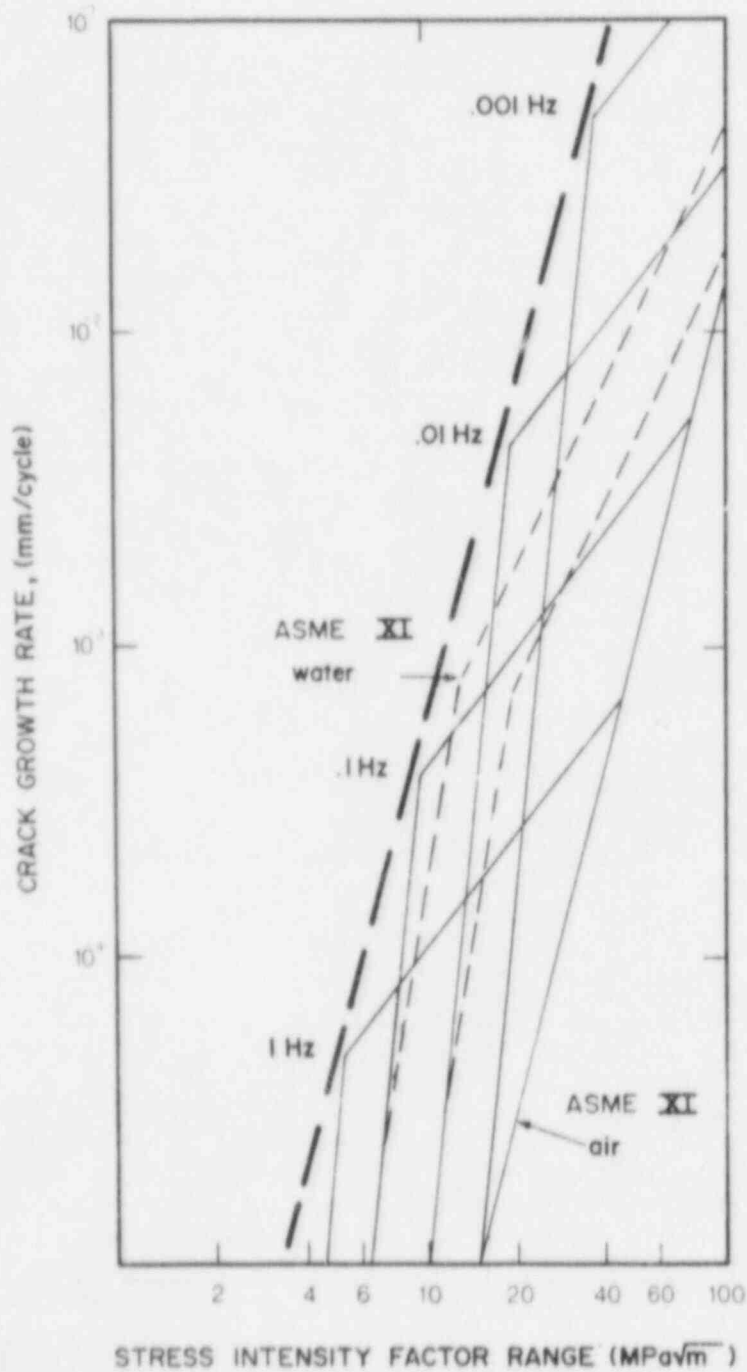


Fig. 42 Bounding crack growth curves based on a hypothetical relationship between  $\dot{a}_l$  and  $\dot{a}_e$  (Ref. 107).

Two different approaches have been outlined, single cycle strain rate models (Eqs. 4-1, 4-6, 4-8) and envelope strain rate models (Eqs. 4-11 and 4-12). Physically, it is possible to say that single cycle strain should be seen as responsible for oxide film rupture, so that it can be seen to be a much more "mechanical" parameter, while  $\dot{\epsilon}_{en}$  envelope, being dependent on  $da/dt$ , i.e., on bare surface creation rate due to the growing crack, can be considered as a "corrosion" parameter. As the same method has been used by Gabetta to calculate both  $\dot{\epsilon}_{sc}$  and  $\dot{\epsilon}_{en}$  (Eqs. 4-8 and 4-12), it is interesting now to compare the two models. It is clear from Figs. 37 and 43, where the same data are reported using the two different approaches, that differences between the effects of the choice of  $\dot{\epsilon}_{sc}$  and  $\dot{\epsilon}_{en}$  are small. It is important, however, to note that all tests were at a frequency of 1 or 2 cpm. When changing frequency over a wider range (for example, by conducting a test at 6 cpm), the corresponding change in strain rate is different, depending on the approach employed. In Figs. 44 and 45, a test at 6 cpm, with the same water chemistry as in the others, has been added to the plots already presented in Fig. 37 ( $\dot{\epsilon}_{sc}$ ) and Fig. 43 ( $\dot{\epsilon}_{en}$ ). When results are plotted as a function of  $\dot{\epsilon}_{en}$  (Fig. 45), the added curve of  $(da/dt)_{en}$  matches quite well with the other tests, while using  $\dot{\epsilon}_{sc}$ , the effect of the frequency change is clearly seen as a shift of the curve with respect to the others. In fact,  $\dot{\epsilon}_{sc}$  has by definition a direct dependence on frequency:

$$\dot{\epsilon}_{sc} \propto \frac{1}{T} \sim f \quad (4-13)$$

where,  $T$  = rise time and  $f$  = frequency so that, with the same loading conditions, a direct proportionality between  $\dot{\epsilon}_{sc}$  and frequency can be found. In case of  $\dot{\epsilon}_{en}$  this parameter is related to the time, through  $da/dt$ , but not directly to the frequency, so that  $\dot{\epsilon}_{en}$  can have the same value over a wide frequency range if the loading conditions are suitable and the crack growth rate is the same. It is obvious that to apply single cycle models over a large frequency range, some additional hypothesis on frequency must be added to the model, since crack growth rates seldom scale exactly with the frequency, as the proportionality (Eq. 4-13) suggests.

It can be said as a conclusion that, in spite of the large difference in computed values (depending on the model) the crack tip strain rate is a suitable parameter to describe at least the stress corrosion side of the environmental fatigue processes. A larger effort needs to be carried out in order to achieve better understanding of the real physical meaning of this parameter, not only in environmental fatigue on notched specimens, but also in CERT on smooth specimens. This understanding will give the possibility of comparing results obtained with different techniques, and of choosing which one of the proposed models is more suitable for use for data reduction.

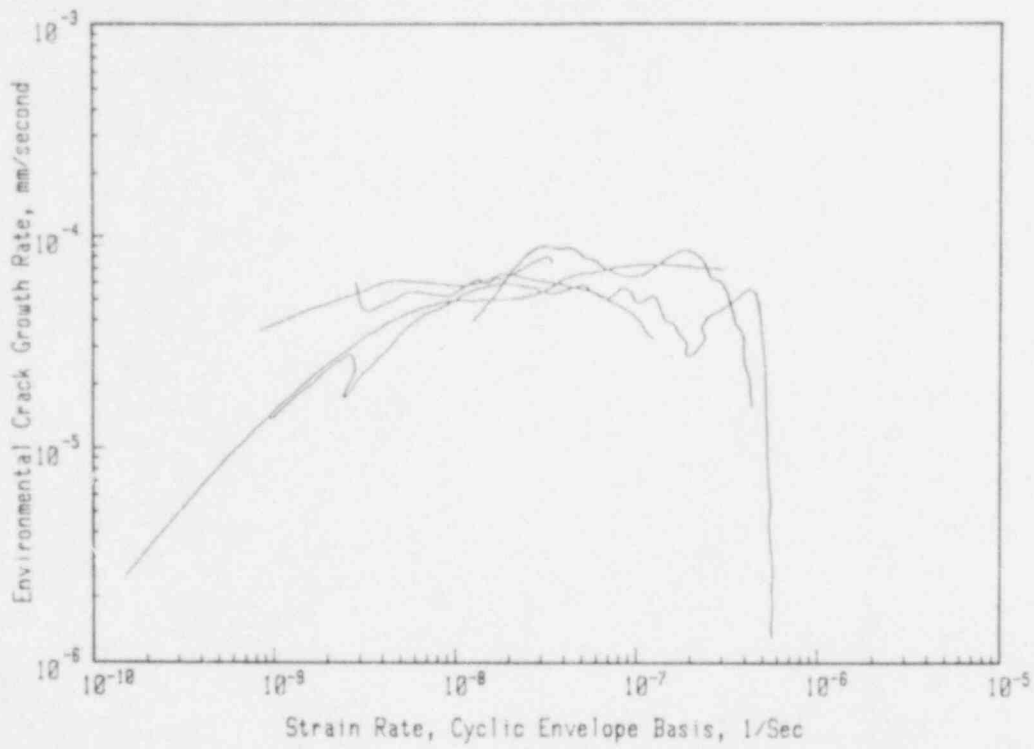


Fig. 43 The environmental component of crack growth rate ( $da/dt_{env.}$ ) plotted versus  $\dot{\epsilon}$  (Ref. 104). Compare with Fig. 37 in which the abscissa is  $\dot{\epsilon}$  single cycle.



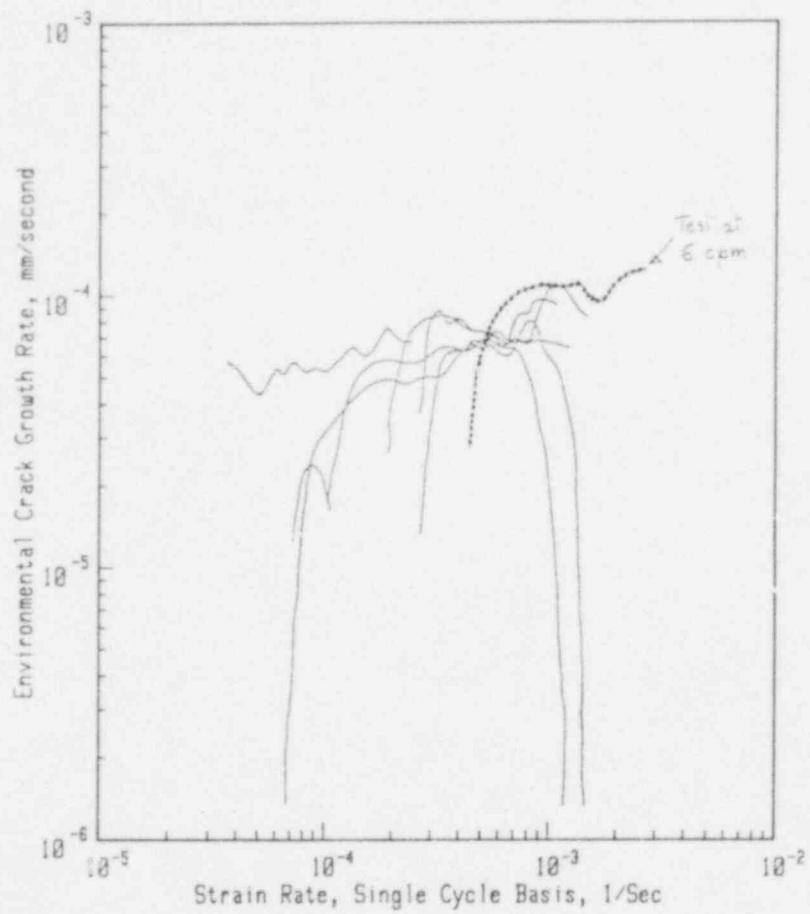


Fig. 44 The same results as in Fig. 37, with  $\dot{\epsilon}_{\text{single cycle}}$  as abscissa, with one added set of test results for a frequency of 0.10 Hz.

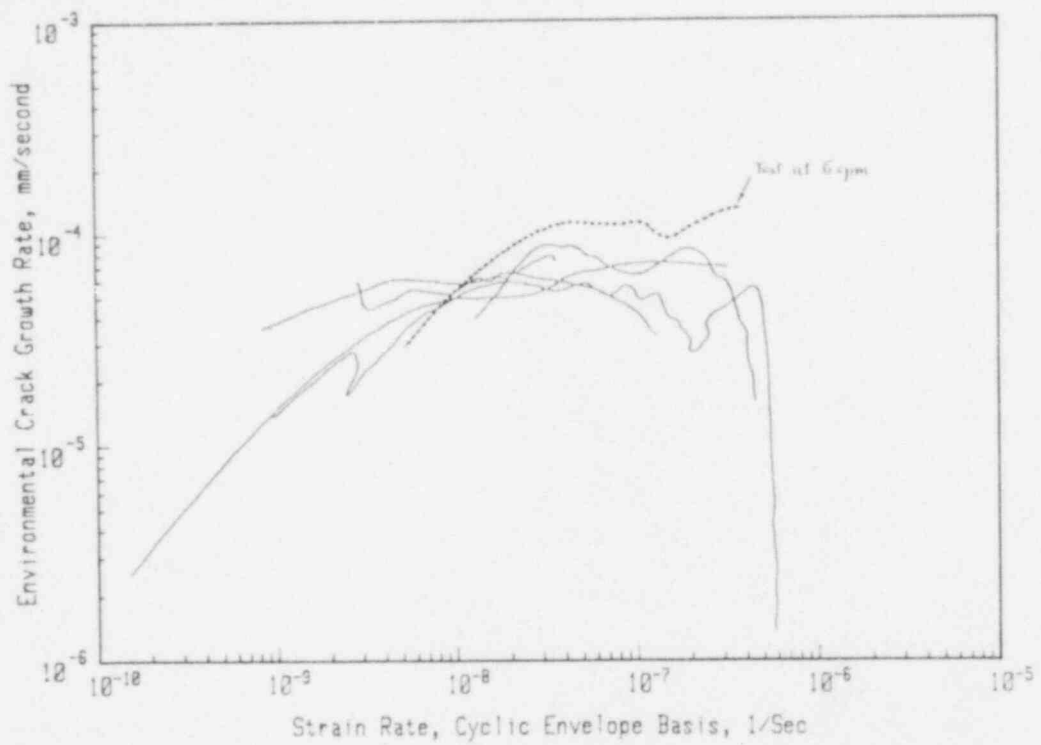


Fig. 45 The same results as in Fig. 43, with  $\dot{\epsilon}_{env.}$  as abscissa, with one added set of test results for a frequency of 0.10 Hz.

#### 4.2 Finite Element Model (FEM) Calculations

Models described up to now have been formulated by using simple physical approaches to the strain calculation in a notched specimen. Through use of stress analysis, the presence of a singularity in the stress and strain field at the crack tip in elastic-plastic materials, particularly for the plane strain case, has been pointed out by several authors (Refs. 108 to 111). Other authors have suggested a design of finite elements which allows accurate replication, in terms of numerical solutions, of the principal features of the near crack-tip stress and strain fields (Ref. 112). By using a finite element code, in fact, it is possible to attain reasonable numerical accuracy near singularities. Rice and Johnson (Ref. 113) have recently emphasized the importance of accurate determinations of the stress and deformation state very near the crack tip in connecting continuum analyses with microstructural separation mechanisms. Many numerical elastic-plastic solutions for cracked or sharply notched bodies have been published, employing finite element and finite difference methods (Refs. 114 to 117), while the strain rate near the crack tip has been evaluated with numerical methods by Wilson, et al. (Refs. 118 and 119) and will be described in the following section.

To obtain a correct solution of the problem, the following input parameters must be evaluated:

- (a) Crack tip size and shape
- (b) Constitutive equations of the material, under the appropriate environmental conditions.

The analysis has been performed by using a computer code with large deformation and large geometry change capability. The geometry of the crack-tip model used for small scale yielding condition (which should be representative of the majority of environmental crack growth conditions in nuclear components) is that of a cylindrical body with outside radius,  $R_0$ , as shown in Fig. 46.

The cylinder contains a radial crack whose tip is located at the center of the cylinder and which extends to the outer surface. The crack-tip radius is  $\rho_0$  in the undeformed state. The boundary conditions (strain in x direction (u) and y direction (v)) are the following:

$$u = \frac{K_I}{2\mu} \left[ \frac{r}{2\pi} \right]^{1/2} \cos\left(\frac{\theta}{2}\right) \left[ \kappa - 1 + 2 \sin^2\left(\frac{\theta}{2}\right) \right] \quad (4-14a)$$

$$v = \frac{K_I}{2\mu} \left[ \frac{r}{2\pi} \right]^{1/2} \sin\left(\frac{\theta}{2}\right) \left[ \kappa + 1 - 2 \sin^2\left(\frac{\theta}{2}\right) \right] \quad (4-14b)$$

where,  $\kappa = 3 - 4\nu$ ,  $\mu = E/[2(1 + \nu)]$ , and  $r = R$ . The crack-tip opening is presumed to change due to loading without changing its shape, as shown in Fig. 47.

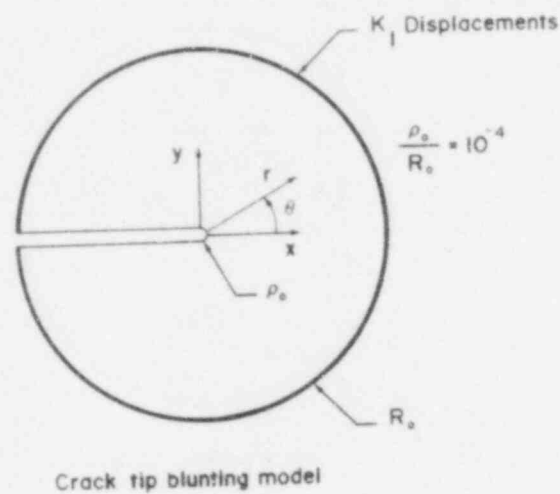


Fig. 46 Coordinate scheme for a crack tip blunting model (Ref. 108).

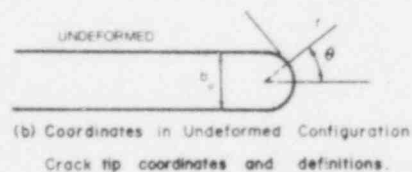
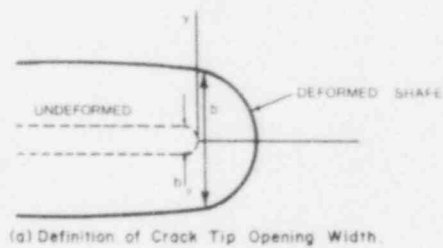


Fig. 47 Coordinates and definitions relating to the undeformed and deformed crack tip (Ref. 109).

The fine mesh model of the crack-tip region used in this study is shown in Fig. 48. The dimension of this mesh at the crack tip is small with respect to the crack-tip root radius,  $\rho$ . A wider mesh has been used for the region far from the crack tip.

To obtain the constitutive equations of the material, results of tests performed at room temperature and at 300°C on A 508 in air have been used. In Fig. 49, as an example, the cyclic stress-strain curve for A 508 at room temperature is shown.

Based on the hypothesis of a blunt crack, the shape of the crack tip for A 508 steel at 300°C can be drawn as shown in Fig. 50. The deformation in the blunted region (b) is a function of crack opening displacement. Calling  $b_0$  the initial crack-tip opening width, ( $= 2\rho_0$ , using the nomenclature of Fig. 46), the relationship between crack-tip root strain and crack-tip opening width for A 508 steel at 300°C is obtained as shown in Fig. 51. As a further step, cyclic loading could be considered. During a loading sequence (such as: load, unload, reload), the shape of a blunted crack in A 508 at 300°C is calculated to be modified as shown in Fig. 52. In Fig. 53, the value of crack-tip strain is shown as a function of opening width,  $b/b_0$ . The same plot shows a comparison with results obtained by Scott, using his previously described model (Ref. 2). The two results are in good agreement. The strain situation at the crack tip was calculated for a stationary crack; however, both experiments and theoretical considerations show that crack growth must be allowed in these computer simulations (Ref. 119). In order to simulate crack growth in an FEM analysis, a relaxation of the nodal force at the crack tip has to be provided. In the Wilson model, to obtain the strain rate value, the relaxation is assumed to follow a creep law which has been arbitrarily chosen by the author; this creep law is shown in Fig. 54. It is interesting to note at this point that the strain rate (being similar, in a way, to  $\dot{\epsilon}$  envelope) is not related to the externally applied load variation during fatigue, but to the crack growth rate through the creep properties of the material.

The  $\dot{\epsilon}_y$  value obtained in this way is shown in Fig. 54.  $\dot{\epsilon}_y$  tends to a constant value of  $\sim 10^{-5} \text{ s}^{-1}$ , after about 10 minutes of elapsed time.

The model described here involves only a calculation of strain rate at the crack tip; no hypothesis has been made by the authors on the influence of strain rate on the environmental crack growth rate. It is possible, however, to make a few comments about the results obtained. As in every problem solved by finite element method, the most important factor in determining the order of magnitude of the final result is the physical approach employed, which in this case can be seen to be similar to the one previously described in Fig. 29a: strain and strain rate have been determined in a very small zone ahead of the crack tip (the mesh used at the crack tip was small with respect to the crack-tip radius,  $\rho$ ). Moreover, as pointed out by the author himself (Ref. 109), the physical meaning and the real value of the crack opening in the unloaded situation ( $b_0$ ) is not clearly understood.

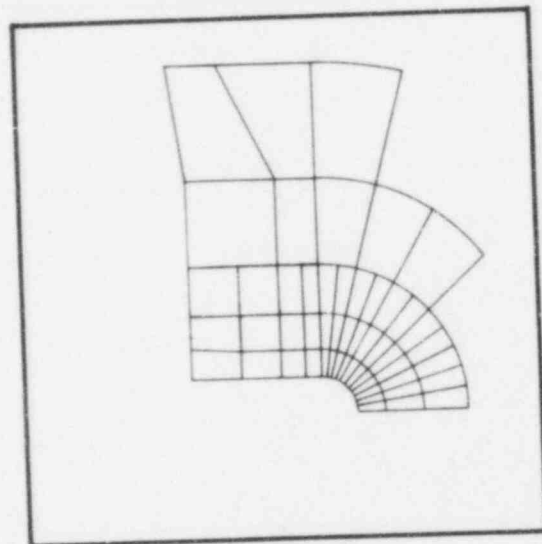


Fig. 48 Fine mesh finite element model of a crack tip region (Ref. 108).

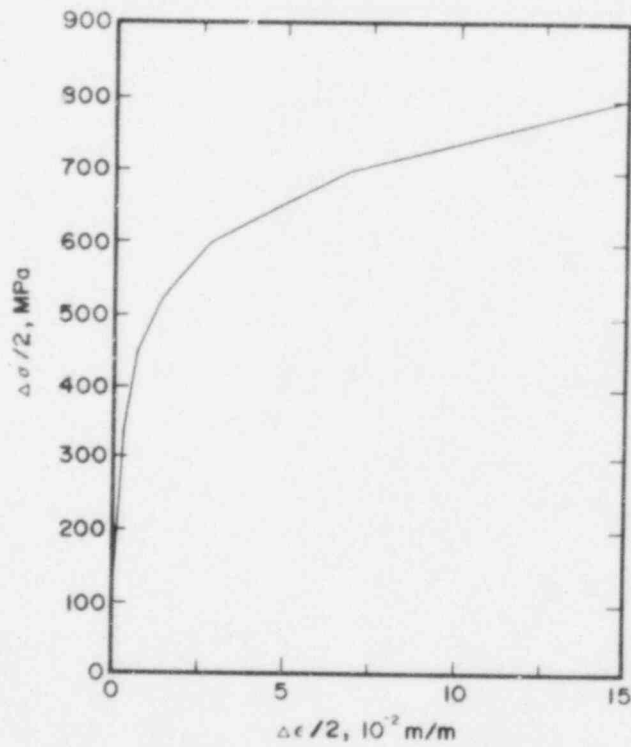
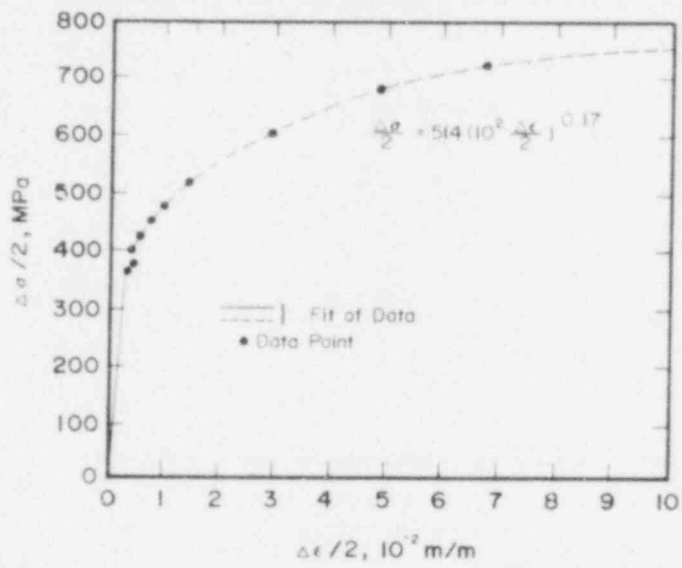


Fig. 49. Cyclic stress-strain curve (a) for A 508 steel at ambient temperature, and its piecewise representation (b) used in the finite element analysis (Ref. 109).

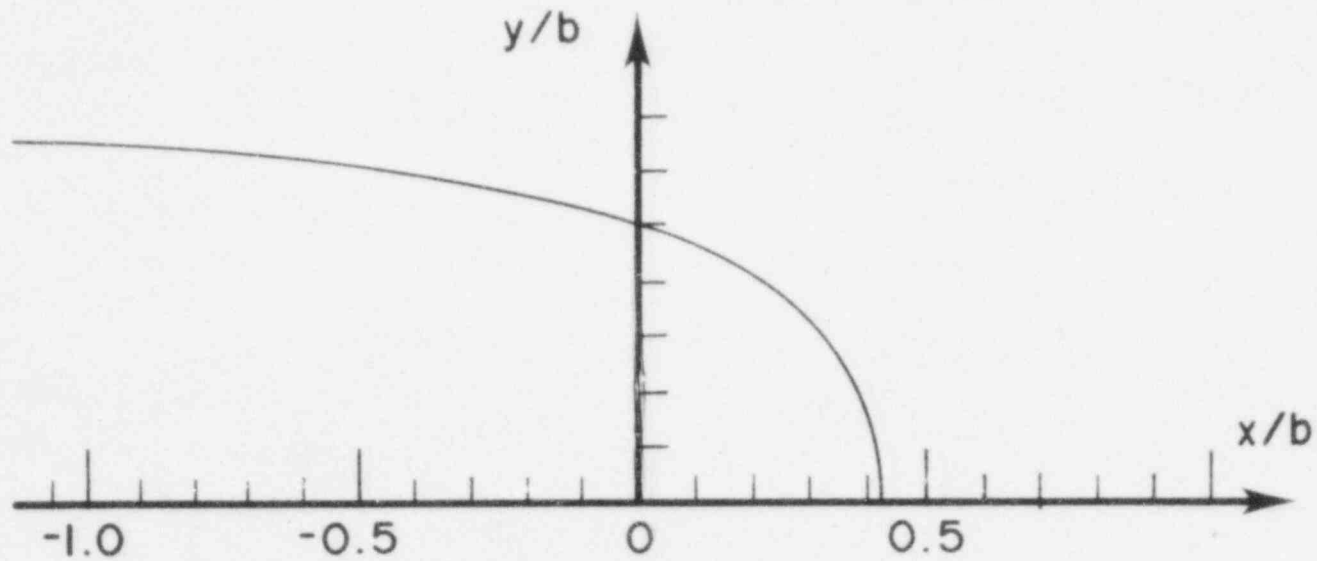


Fig. 50 Shape of a blunted crack in A 508-2 steel at 300°C. Displacement in x-direction are relative to a point at a distance  $2b$  ahead of the root of the blunted crack (Ref. 108).



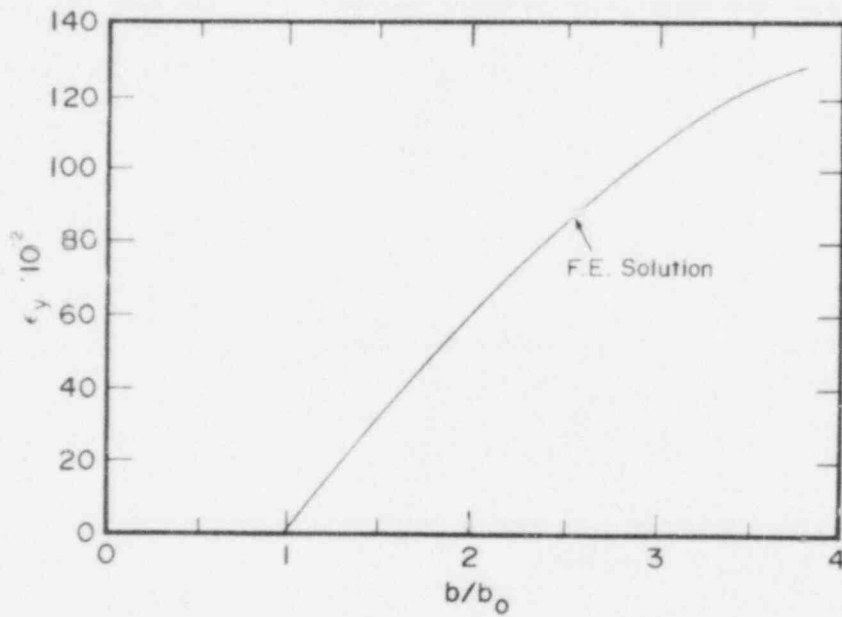


Fig. 51 Relationship between crack tip root strain and crack tip opening width for A 508 steel at 300°C, calculated from a finite element model (Ref. 108).

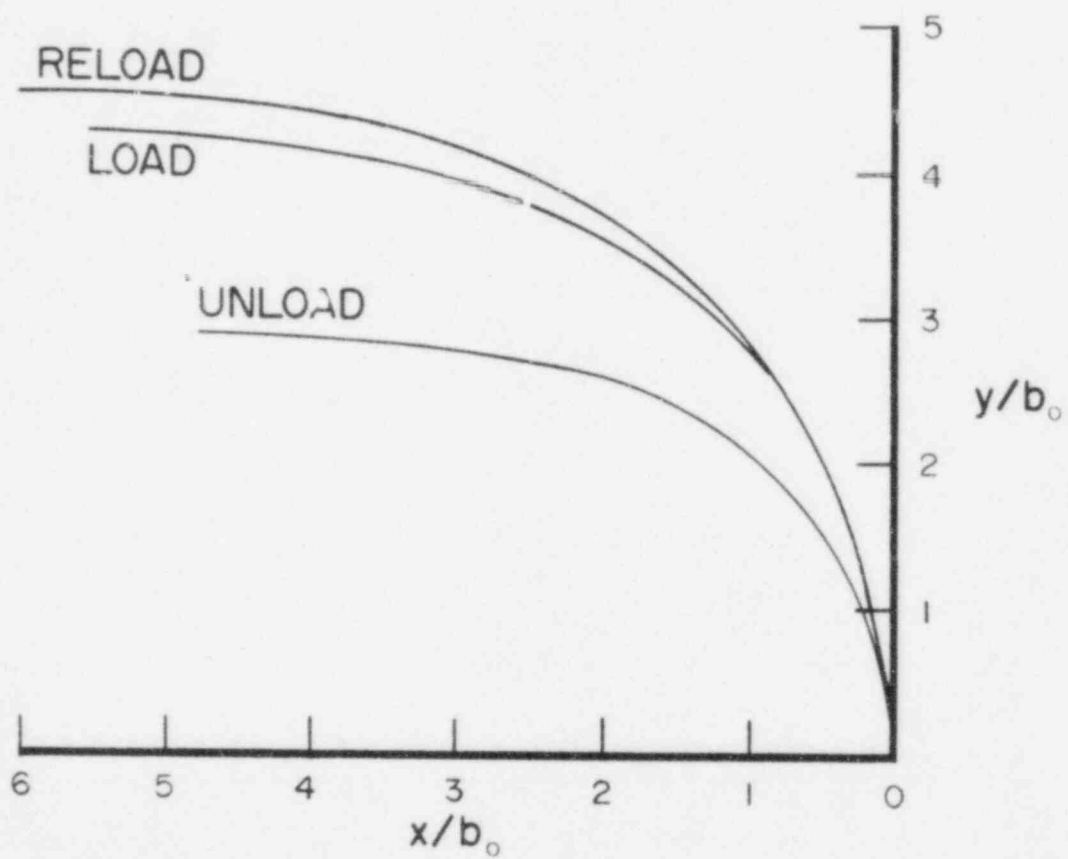


Fig. 52 Shapes of blunted crack in A 508 steel at 300°C. The loading sequence is load, unload and reload (Ref. 108).

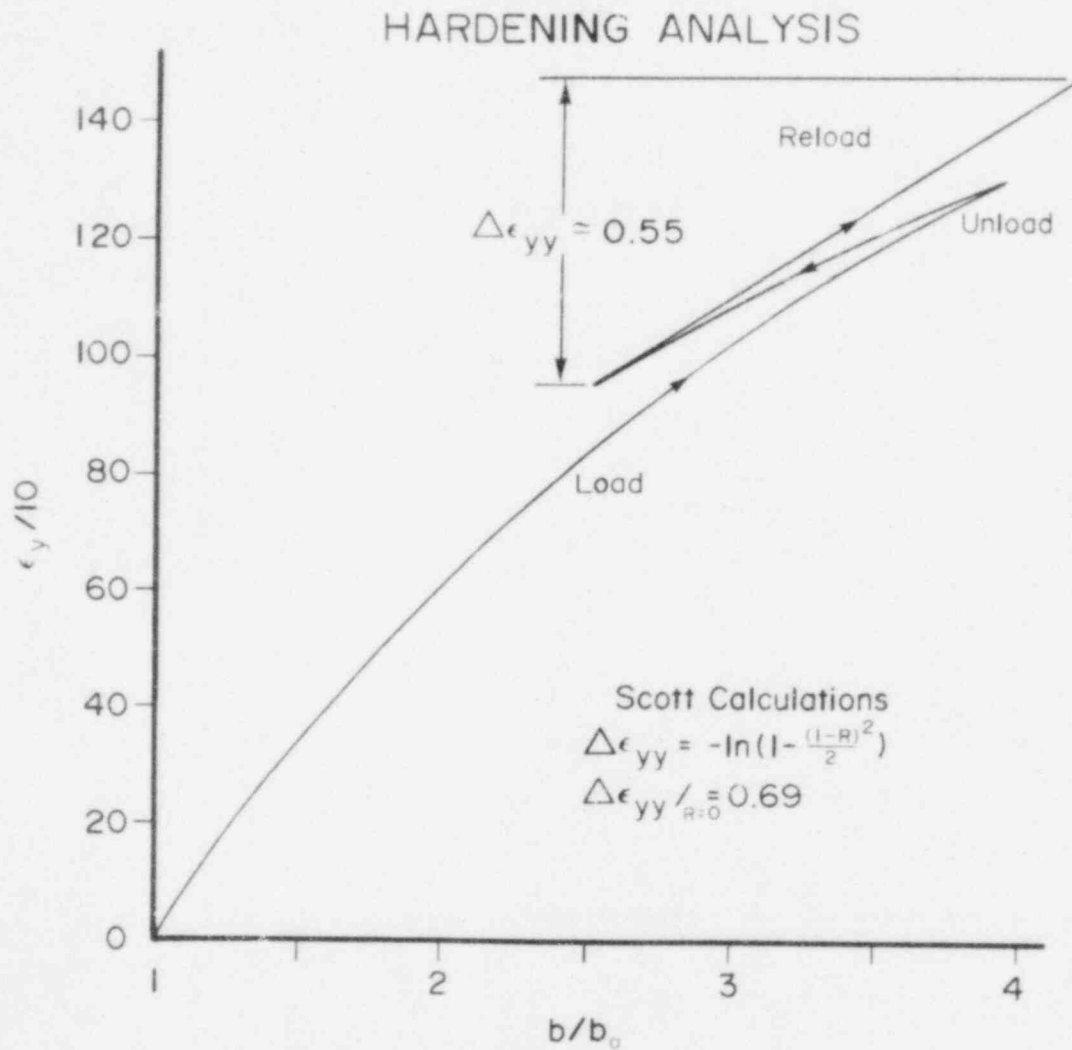


Fig. 53 Crack tip root strain as a function of opening width for A 508 steel at 300°C. The loading sequence is load, unload and reload (Ref. 109).

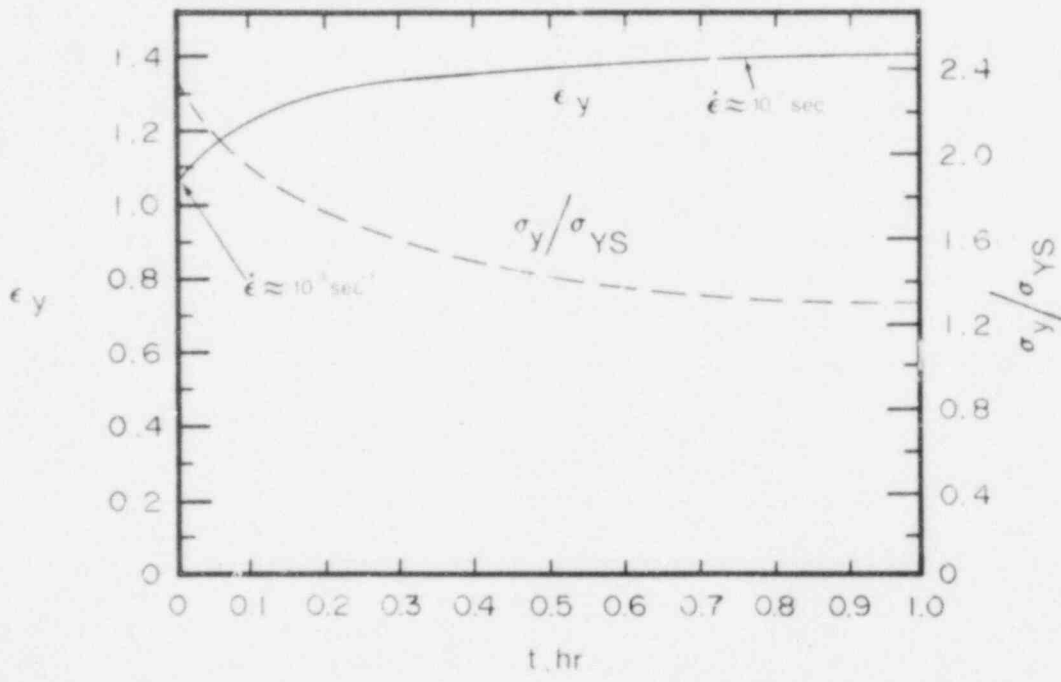


Fig. 54 Blunted crack tip root stress and strain as a function of time for A 508 steel using the arbitrarily assumed creep law (Ref. 109).

The comparison of this model with the one proposed by Scott, et al. (Refs. 2, 99, 100), described above is meaningful because the same physical approach has been used in both cases. In fact, the numerical value obtained for the strain at the crack tip is reasonably similar in both methods, as shown in Fig. 52. Therefore, it is possible to say that the physical approach is the most important factor affecting the results in crack-tip strain evaluation, regardless of the numerical analysis method used. However, when strain rate ( $\dot{\epsilon}_{sc}$ ) is calculated, a large difference (about 3 orders of magnitude) can be found between the results obtained with the Scott model (Refs. 2 and 99) and the finite element approach (Ref. 119). This is due to the hypothesis of relaxation at the crack tip, which corresponds to the physical assumption that the crack does grow during a single fatigue cycle.

A comparison of strain rate models should be of interest at this point. Shoji's model (Ref. 107) is expected to be the most similar to the finite element method, due to the physical approach used by this author which takes the  $da/dt$  influence into the proper consideration. It is possible to see in Fig. 41 that the values of strain rate obtained by Shoji range between  $10^{-4} s^{-1}$  to  $10^{-7} s^{-1}$ . This corresponds to finite element results rather well.

It is clear that the understanding of the physical meaning of the different models is an important step in the understanding of environmental crack growth phenomenon. An accurate study and comparison of differently obtained results can be useful for this purpose.

#### 4.3 Slip-Controlled (Deformation) Models

A simple model to describe the rate of fatigue crack growth must incorporate a cycle-dependent criterion for crack advance based on crack-tip micromechanics. The effect of plasticity at the crack tip can be taken into account by either crack-tip blunting models (Refs. 120 to 122) or damage accumulation models (Refs. 123 to 125). Both of these consider crack-tip opening displacement (CTOD) to be due to dislocations moving on slip planes, and that a number of cycles are required to reach a maximum CTOD, which causes a crack growth rate proportional to CTOD itself.

Crack-tip blunting models are aimed at finding the relationship between  $da/dN$  and  $\Delta K$  through a measure of crack-tip opening displacement (CTOD) and striation spacing (Ref. 126). The simplest way to visualize such a model is through the hypothesis that the amount of crack growth in a single cycle is equal to half the measured CTOD increment. Unfortunately, this statement is correct only in particular  $da/dN$  ranges, and for a limited number of materials. In the same way, the spacing of striations observed on the fracture surface is equal to macroscopic crack growth rate only in a limited  $\Delta K$  range. Moreover, in some materials (particularly pressure vessel steels), the measurement of fatigue striations is a quite difficult task, due to the complicated microstructure and to the fatigue process characteristics. As a consequence, crack-tip blunting models have been used successfully up to now to explain fatigue crack growth rates

in air on materials with a simple microstructure, such as aluminum and stainless steel. This crack-tip blunting model can be further developed by using damage accumulation models, which are based on the assumption that crack growth does not occur on each cycle. Crack blunting is assumed to occur, and to increase in magnitude on each successive cycle, resulting finally in crack advance. Thus,  $N$  cycles are required for the sudden advance of a crack by an increment,  $\Delta a$ . This physical model led to the conclusion that fatigue crack growth can be treated in the same way as failure of a low cycle fatigue specimen. The models correlate the increment of crack advance,  $\Delta a$ , to the microstructural parameters of the material, such as slip length and dislocation pile-up characteristics (Refs. 127 to 129). Other models (Ref. 130) do not explicitly define a slip length, but instead use the concept of a process zone, defined as the region in which metallurgical factors are important. The size of the process zone for crack growth at near-threshold stress intensity factor levels has been correlated with either subcell size or grain size (Ref. 130).

Figures 55 and 56 show the crack advance mechanism for low  $\Delta K$  (where only a slip plane is supposed to act) and high  $\Delta K$  (with several active slip planes), respectively. The accumulated damage is due to the incomplete reversibility of the dislocation formation process. On succeeding cycles, it is likely that an increasing difference will occur between the number of dislocations generated at the crack tip during the loading and the number which return during the unloading. This process lowers the effective driving stress by shielding the crack tip, and at the same time causes a strain-induced softening of the material. The slip distance,  $r_s$ , can also change with the increasing number of cycles, due to the slip characteristics of the material. It is possible to correlate in a simple way (Ref. 131) the length of slip lines,  $r_s$ , the number of dislocations on the slip plane,  $D_N$ , and the stress on the slip plane. For the simple case of a single slip line, the relationship is

$$D_N b = \left[ \frac{\pi (1 - \nu)}{\mu} \right] \Delta \tau r_s \quad (4-15)$$

where,  $b$  = Burger's vector,  $\mu$  = shear modulus,  $\nu$  = Poisson ratio, and  $\tau$  = shear stress on the slip plane.

Based on the model described in Fig. 56,

$$CTOD_x = D_N b \sin \theta \quad (4-16)$$

and the increment of crack advance along the slip line is:

$$\Delta a = D_N b \cos \theta \quad (4-17)$$

It follows that calculation of the shear stress at the crack tip is necessary to apply this model. Therefore, the importance of a correct evaluation of the crack-tip stress and strain situation is emphasized once again.

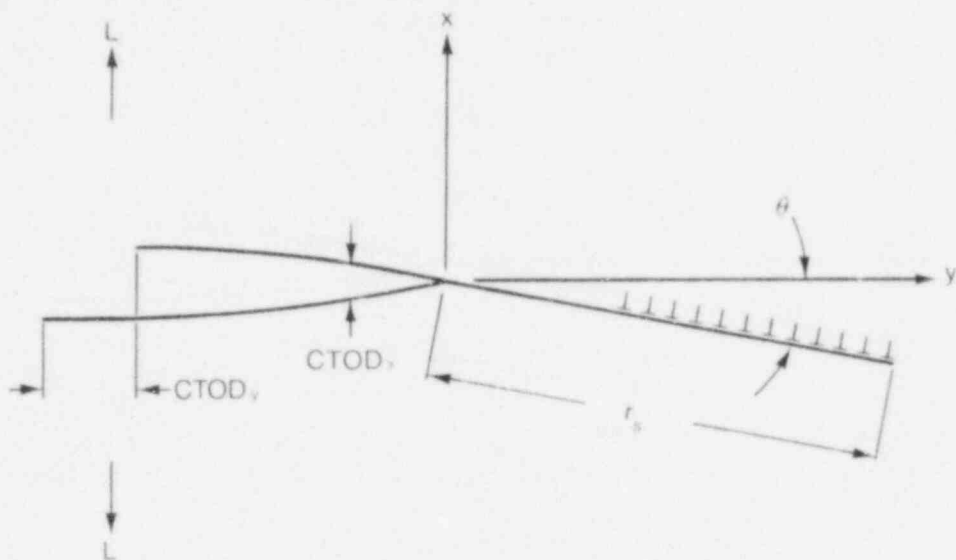


Fig. 55 Crack tip at the  $\Delta K_{eff}$  just exceeding the threshold. The crack has one slip plane coming from the crack tip at an angle ( $\theta$ ) to the growth direction (Ref. 133).

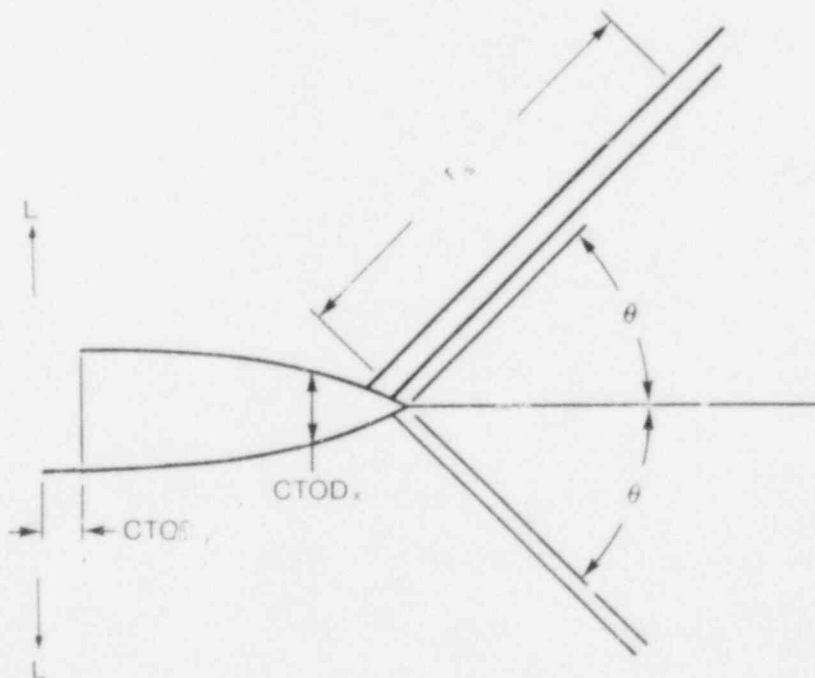


Fig. 56 Crack tip at a large  $\Delta K_{eff}$  showing four and a half slip lines at the angle ( $\theta$ ) to the direction of crack growth. Slip lines are assumed to be separated by the distance  $D_N b$  (Ref. 133).

Davidson and Lankford (Ref. 131) have determined the shear stress at the crack tip for low carbon steel through the size of the subgrains which form during fatigue crack growth. Moreover, the analysis of fatigue cracks by using stereoimaging techniques has allowed the same authors (Ref. 132) to obtain direct measurement of CTOD and through computation from the measured displacements, the crack-tip near field strain.

This experimentally-determined crack tip strain has been applied to results previously obtained on 7075-T651 aluminum (Ref. 132). The model can be used to derive the length of slip lines and their angle to the direction of crack growth, when the crack growth increment is measured, or to predict the increment of crack growth, when the length of slip lines is known. This has been verified for the aluminum alloy examined, where slip line length appears to be related to the mean free path between dispersoids. The author recognizes this model as having limitations (Ref. 133), the most serious of them being that not all the factors associated with fatigue crack growth under constant cyclic load are accounted for in the model. For example, neither the threshold effect or crack closure, nor their relationship with metallurgical parameters, are included. Both crack closure and threshold effect have been accounted for in ongoing research on the effect of environment on fatigue. This study has been performed by Davidson, et al. (Ref. 134), Hudak and Davidson (Ref. 135), Hudak, Davidson and Page (Ref. 136), on low carbon steel and A 304 steel, exposed respectively, to pure aqueous and dilute sulphate environments.

Independent of the proposed model, two points are of importance:

- (1) The capability of stereoimaging technique to be used for a correct estimate of crack-tip strain rate.
- (2) The effect of environment on crack-tip strain rate measured with stereoimaging.

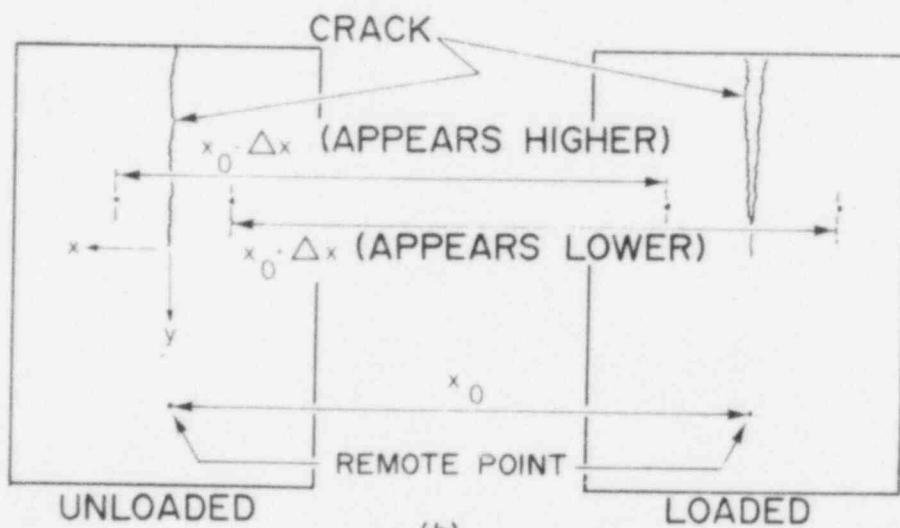
In Fig. 57, a schematic of the stereoimaging technique is shown. In Fig. 58, measured values of effective strain range (i.e., taking into account the presence of crack closure) ahead of the crack tip in environmental fatigue are reported as a function of the distance from the crack tip. The decreasing slope of this line shows once again, as seen for previously discussed models, that the distribution of strain depends on the position where the strain is calculated, so that the gage length chosen is still an important parameter for the evaluation of the stress and strain distribution. Strain rate values computed by using the stereoimaging strain measurement technique are shown in Fig. 59. As the gage length is small and  $\dot{\epsilon}$  is computed during a single cycle, these values are comparable with those obtained by Scott's ( $\dot{\epsilon}_{sc}$ ) model (Refs. 2 and 99). Once again, this is a demonstration of the importance of a physical approach, much more than the computational method, on the order of magnitude of the results obtained.

The effect of environment on strain rate is not important for 304 stainless steel in aqueous sulphate (Ref. 135). On the other hand, for low carbon steel exposed to water (Ref. 134), the environment





(a)



(b)

Fig. 57 Schematic of the measurement method used to quantify the stereoiaged displacements (Ref. 134).

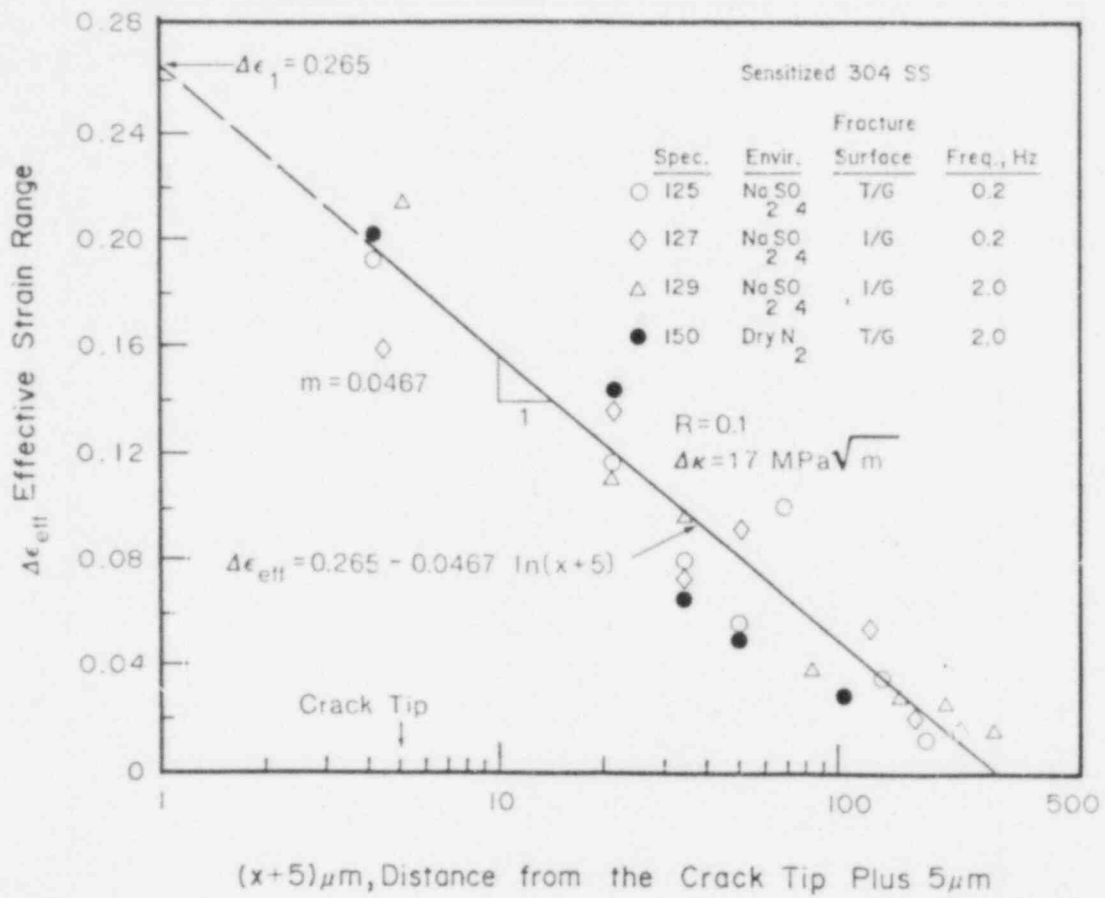


Fig. 58 Distribution of effective strain range ahead of the crack in sensitized 304 stainless steel for various environments, fracture surface morphologies, and cyclic frequencies (Ref. 136).

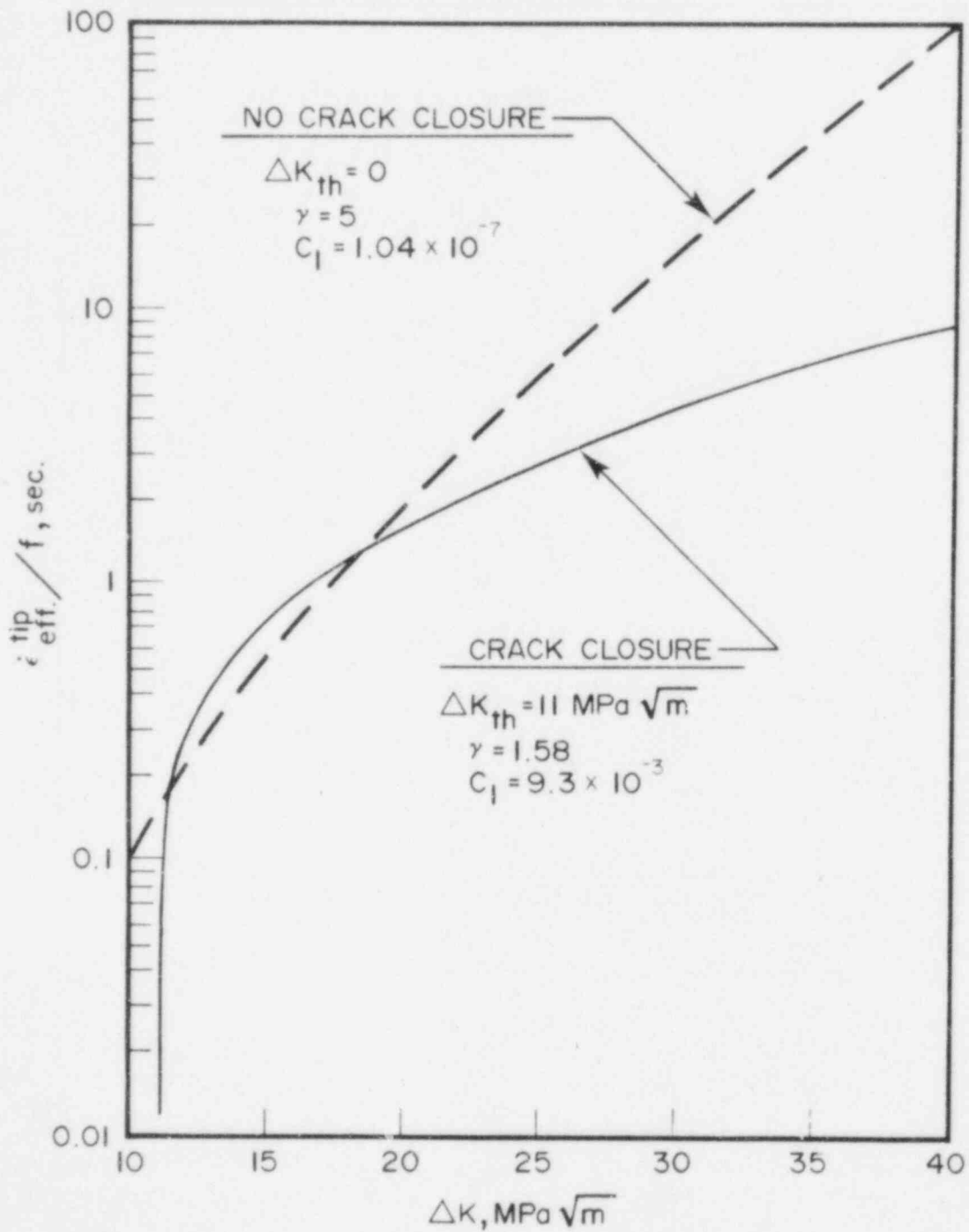


Fig. 59 Computed crack-tip strain rates for various assumptions regarding crack closure and threshold stress intensity values (Ref. 135).

produces a significant lowering of the strain that is measured at the crack tip. These results seem to indicate that different mechanisms can be active in corrosion fatigue, due to the characteristics of the environment/material couple which is considered. This effect needs to be studied further.

The use of this model for corrosion fatigue requires the calculation of crack-tip strain and strain rate; therefore, a method for direct measurement of strain rate during tests has been proposed. Values obtained are in good agreement with those obtained by other models, provided that the same physical approach is used. With this technique, moreover, the values of strain rate obtained can be used as a measure of the environmental effect.

#### 5. SUMMARY OF MECHANISMS AND MODELS

Both the anodic dissolution and hydrogen-assisted crack growth models have been described in some detail. Both have certain advantages and disadvantages which more or less reflect the state of development of each.

The anodic dissolution mechanism has the strong advantage that it is conceptually easier to comprehend than the hydrogen assistance mechanism, has been under active development for a longer period of time, and may have a larger contingent of followers. There is little doubt or argument that anodic dissolution is the probable dominant mechanism for a large number of metals/environment combinations. It can be quantified in a straightforward and understandable way, thus increasing its appeal enormously. The mathematics lend themselves to a superposition treatment of fatigue crack growth, in which the environmental component is simply added to the mechanical component to obtain the total environmentally-assisted crack growth rate. The first quantified analysis of fatigue crack growth, while not mentioning anodic dissolution *per se*, was a superposition method, which received some acclaim, and is still in widespread use (Ref. 137). As the anodic dissolution concepts became more heavily utilized, they were often incorporated in the superposition model, thus heightening the visibility of both. The fact that the anodic dissolution mechanism lends itself to superposition treatments so well makes it intrinsically well-tailored for incorporation in the more-recently developed strain rate models discussed in Section 4.

On the other hand, anodic dissolution fails to account for several phenomenological observations, especially in the fractographic arena. The brittle-like appearance of fatigue fracture surfaces, including fan-shaped features emanating from manganese sulfide inclusions and brittle striations on the fans, are difficult to reconcile with the lateral dissolution velocity,  $V_s$  concept that is an integral part of the anodic dissolution mechanism description. In an attempt to account for the fractographically obvious, but to retain the calculational advantages noted above, Ford and Emigh have attempted to marry the cleavage concept and the basic dissolution parameters (Ref. 39). Of equal concern is that the dissolution mechanism cannot account for the observed threshold behavior and

frequency dependence of fatigue crack growth rates without invoking a strong competitive process. For low load ratios, ( $R \sim 0.1$  to  $0.2$ ) it has been demonstrated that very long cyclic periods produce little or no environmental assistance (Ref. 3), while for very high load ratios ( $R \sim 0.8$  to  $0.9$ ), the maximum in growth rate enhancement comes at high frequencies, up to about 10 or 20 Hz (Ref. 2). On its own, anodic dissolution would predict a continuing increase in growth rates for increasing cyclic periods. Advocates of the dissolution mechanism usually invoke creep and crack blunting arguments to help handle the low frequency problem.

The hydrogen assistance mechanism has the advantage that it can account for the fractographic features, but in most other respects is not nearly as well-developed or well-conceptualized, and is certainly not as amenable to quantification as is the anodic dissolution mechanism. At this point in time, there are several pieces of isolated evidence which tend to point in the direction of the existence of hydrogen assistance, but none are conclusive, and in order to account for all the phenomena which are experimentally observed, the hydrogen assistance model must be combined with crack tip passivation and filming mechanisms. Perhaps the most convincing evidence is that crack growth rates and fractographic features are very similar for tests of low alloy steels conducted at low temperatures in hydrogen-bearing environments other than water, such as dry, highly purified hydrogen gas, and hydrogen sulfide gas. The fact that hydrogen can have so many different effects on the metal matrix serves to diffuse the amount of attention which any one hydrogen effect receives, to the detriment of hydrogen mechanism development as a whole. It will be very difficult to measure hydrogen effects directly, since these are probably bulk effects, rather than surface effects. It is likely that the effects of hydrogen are only manifested under the conditions of triaxiality and electrochemistry which are found at the tip of a crack, suggesting that all critical or supporting experiments may have to be performed with cracked specimens, which are far more difficult to analyze than uniaxial test specimens.

The development of calculational models is really still in its infancy. Although the strain rate model is a vast improvement over its predecessors, it must be remembered that it too is no more than another curve-fitting procedure, albeit one with a more physical basis. It is difficult to envision how the strain rate model is going to be generalized to the case of variable load/frequency situations; it is much better suited to the constant amplitude/constant frequency test analysis. At present, it is used most convincingly for the calculation of maximum environmental effects, which are, generally speaking, not appropriate to combinations of more modern, less-sensitive steels or well-regulated water quality.

It seems intuitive that some cycle-by-cycle integration would offer the most promising hope for calculational success. As input, the user would have to know exactly what happens to hydrogen accumulations in the metal matrix following an overload, and what that does to the plastic zone shape and size, and how the crack tip deformation rates

result in breakup of the oxide film, thus establishing the conditions for hydrogen adsorption and assumption into the matrix. While cycle-by-cycle summations are exceptionally time-consuming computationally, and will be even more so when combined with environmental effects, this may be the only feasible approach. With the astounding growth in supercomputer capabilities, computational speed, coupled with a possible large number of model parameters may not be the overwhelming problem in the future that they are today.

Lastly, a very pragmatic look at the future requirements for mechanistic development for the PWR situation should be established. It is apparent that only the older steels, those with higher sulfur and processing which is less effective in controlling inclusion shape, are overly susceptible to environmental enhancement. More modern steels generally appear to have growth rates which are a simple factor of two or three faster in growth than air environment rates, and this can be dealt with quite simply. Since it will require many more years of development before a mechanism/model can be developed and brought to convincing calculational accuracy, the industry must look at a time-line analysis to determine if any of these older, more susceptible steels will still remain in service at the time an effective model will be approved. If it might be twenty or more years before a model acceptable to the regulatory agencies can be developed, and if the cost of model development, integrated over all the sponsoring agencies and vendors, is going to outweigh the potential gain, then those research funds would be much better spent in areas which offer more immediate return for the investment.

Along this line, it may be more realistic to pursue model development with the motivation that understanding of a model might show the research community where the problem areas may reside, and then to pursue those areas with increased experimental research budgets.

## 6. RECOMMENDED RESEARCH

One of the most significant concerns in this field is that the  $\Delta K$  range which has been experimentally investigated, and over which the available models are claimed to work, is really the tail-end of the total fatigue cracking process. As such, it may account for a few percent of component life, and because of that, may be within a range which is unacceptable for operation in the eyes of regulatory agencies. A far greater percentage of the component lifetime is consumed by the crack nucleation and near-threshold growth phases, which have not been well-investigated experimentally, and which have virtually zero development on the environmentally-assisted mechanisms front. This is an exceptionally difficult area to investigate experimentally, and development of experimental techniques is slow and expensive. However, neglect of this area should not be continued. Based on what little research is available on environmental effects in the near-threshold regime (Refs. 138 to 141), indications are that the phenomena are very different from those which act over the better-investigated, higher  $\Delta K$  range. We may find that all the current energy and resources, human and financial, are addressing the ten percent of the problem beyond the safe operation cut-off point.

Historically, the driving energy for the development of concepts concerning mechanisms has been the development of some experimental result. The first hint that hydrogen assistance could be responsible for increased crack growth rates came from fractographic observations. The change in slope of crack growth rates as a function of temperature (Fig. 6) suggests that there may be competing contributions to the mechanistic processes. The role of ionic species in the formation of crack tip oxides can be evaluated by various spectroscopic techniques. The conditions for oxidation or reduction reactions can be measured by pH and electrochemical potential probes. The list could go on, but the point is that experimental evidence has been of crucial importance in achieving proper mechanistic concepts, and is likely to continue to be the major influence on continued development and improvement of the existing models.

One of the more promising of the experiments being prepared is the measurement of crack enclave pH and potential, which will be performed at CISE during 1985-86. This initial phase of the work will be conducted at temperatures less than 100°C, but if successful, it might be expected that attempts to perform these measurements near 300°C would be attempted. If it can be shown that crack tip potentials are low ( $< -500 \text{ mV}_{\text{SHE}}$ ), and if the pH is nearly neutral, then it becomes very difficult to postulate that anodic dissolution can provide the full amount of environmental enhancement which is observed.

Experiments to measure the effect of hydrogen on mechanical properties would be especially helpful to a wide variety of scientists. The flow curves are required input for finite element and plasticity modeling, and changes in elastic modulus and ductility are helpful parameters for understanding the crack tip mechanics. Currently there appears to be conflicting evidence on the effects of hydrogen on certain mechanical properties, and the incorporation of uniaxial mechanical property data to what in a triaxial situation is always a questionable procedure.

From a crack growth standpoint, it was pointed out that the near threshold regime is far more influential in determining component lifetime than the higher  $\Delta K$  regime which is the current subject of most experimental and conceptual modeling attention. But as suggested above, first we need to have the experimental results before we can make any realistic attempt to conceptualize a model. Therefore, we would encourage that a considerably higher level of effort should be directed toward the measurement of environmental effects for crack nucleation processes and near-threshold growth rates.

Allied with this concern is the question of crack closure effects. There are two types of closure with which we might be concerned. The first is mechanically induced closure caused by plastic deformation along the flanks of the crack, preventing full closure of the crack tip when loads are reduced to zero. The second is oxide-induced closure caused by oxide forming on the flanks of the crack, thus keeping the crack wedged open. Both phenomena effectively lower the applied  $\Delta K$  for all loadings involving compressive loads or near-zero

tensile loads. Since reactor pressure vessels often have a high tensile mean load, this may ameliorate the crack closure problems.

We also need to be concerned with the question of the usefulness of compact specimen data. There are two questions here: the first is the question of stress field similarity, and the second is the question of environmental access. Since most cracks in real structures are assumed to be two-dimensional with a roughly semi-elliptical shape, there will be relatively little bending moment at the crack tip, which will have some effect on the triaxial stress state. If the changes in stress state range and amplitude are sufficiently different, and if internal hydrogen effects are responsible for environmental enhancement, then we could expect changes in the results produced by either compact tension or center-cracked tension specimens for otherwise identical experimental variables. If crack enclave flushing or bulk environment flow rates are important in controlling crack growth rates, then the much reduced environmental access, through the much smaller aperture of a two-dimensional semi-elliptical crack will be of some importance.

Lastly, it is important to not develop a mindset about a particular experimental direction along which to proceed. It has been more than obvious over the last few years that for every seeming advance in the development of mechanistic concepts, there will be new experimental results which strongly influence or even negate those conclusions. There is no substitute for good, carefully executed studies of the effects of critical variables on crack growth rates.



## REFERENCES

1. W. H. Cullen and K. Torronen, "A Review of Fatigue Crack Growth of Pressure Vessel and Piping Steel in High Temperature, Pressurized, Reactor-Grade Water," USNRC Report NUREG/CR-1576, NRL Memorandum Report 4296, Sept. 1980.
2. P. M. Scott and A. E. Truswell, "Corrosion Fatigue Crack Growth in Reactor Pressure Vessel Steels in PWR Primary Water," Journal of Pressure Vessel Technology, Vol. 105, 1983, pp. 245-254.
3. W. Van Der Sluys and R. Emanuelson, "Overview of Data Trends in Cyclic Crack Growth Results in LWR Environments," in Proceedings of Second IAEA Specialists' Meeting on Subcritical Crack Growth, Sendai, Japan, May 15-17, 1985. To be published as USNRC Conference Proceeding.
4. J. M. Barsom, "Effect of Cyclic Stress Form on Corrosion Fatigue Crack Propagation Below  $K_{Isc}$  in a High Yield Strength Steel," in Corrosion Fatigue: Chemistry, Mechanics and Microstructures, NACE-2, O. Devereaux, A. J. McEvily and R. W. Staehle, eds., National Association of Corrosion Engineers, 1972, pp. 424-433.
5. G. Slama and P. Rabbe, "French Approach and Results in Cyclic Crack Growth," in Proceedings of the 5th SMIRT (Structural Mechanics in Reactor Technology) Post-Conference Seminar, Paris, France, Aug. 1981, pp. 311-325.
6. W. H. Cullen, et al., "Fatigue Crack Growth of A 508-2 Steel in High-Temperature, Pressurized Reactor-Grade Water," USNRC Report NUREG/CR-0969, Sept. 1979.
7. W. H. Bamford, L. J. Ceschini and R. J. Jacko, "Environmentally Assisted Crack Growth Studies," in Heavy Section Steel Technology Report for July-September 1983, USNRC Report NUREG/CR-3334, Vol. 3, March 1984, pp. 97-114.
8. W. H. Cullen, et al., "The Effects of Sulfur Chemistry and Flow Rate on Fatigue Crack Growth Rates in LWR Environments," USNRC Report NUREG/CR-4121, Feb. 1985.
9. W. H. Bamford, "Environmentally Assisted Crack Growth Studies," in Heavy Section Steel Technology Report for October-December 1982, USNRC Report NUREG/CR-2751, Vol. 4, May 1983, pp. 139-161.
10. H. Hanninen, K. Torronen, M. Kemppainen and S. Salonen, "On the Mechanisms of Environment Sensitive Cyclic Crack Growth of Nuclear Reactor Pressure Vessel Steels," Corrosion Science, Vol. 23(6), 1983, pp. 663-679.
11. W. H. Cullen, K. Torronen and M. Kemppainen, "Effects of Temperature on Fatigue Crack Growth of A 508-2 Steel in LWR Environment," USNRC Report NUREG/CR-3230, Apr. 1983.

12. J. D. Atkinson, S. T. Cole, and J. E. Forrest, "Corrosion Fatigue Mechanisms in Ferritic Pressure Vessel Steels Exposed to Simulated PWR Environments," in Proceedings of IAEA Specialists' Meeting on Subcritical Crack Growth, Sessions III, IV and V, USNRC Conference Proceeding NUREG/CP-0044, Vol. 2, May 1983, pp. 173-197.
13. T. A. Prater and L. F. Coffin, "Crack Growth Studies on a Carbon Steel in Oxygenated High-Pressure Water at Elevated Temperatures," in Proceedings of IAEA Specialists' Meeting on Subcritical Crack Growth, Sessions III, IV and V, USNRC Conference Proceeding NUREG/CP-0044, Vol. 2, May 1983, pp. 355-370.
14. W. H. Cullen, et al., "Fatigue Crack Growth Rates of Irradiated Pressure Vessel Steel in Simulated Nuclear Coolant Environment," J. Nuclear Materials, Vol. 96, 1981, pp. 261-268.
15. T. Kondo, et al., "Corrosion Fatigue of ASTM A 302B Steel in High Temperature Water -- The Simulated Nuclear Reactor Environment," in Corrosion Fatigue: Chemistry, Mechanics and Microstructure, NACE-2, O. Devereaux, et al., eds., National Association of Corrosion Engineers, Houston, TX, pp. 539-556.
16. N. Nagata, presentation at ICCGR meeting, Tokai-mura, Japan, May 21, 1985.
17. T. Kikuyama, presentation at ICCGR meeting, Tokai-mura, Japan, May 20, 1985.
18. K. Torronen, M. Kemppainen and H. Hanninen, "Fractographic Evaluation of Specimens of A 533B Pressure Vessel Steel," EPRI Report NP-3483, Electric Power Research Institute, May 1984.
19. T. Boniszewski and J. Moreton, "Effect of Micro-Void and Manganese Sulphide Inclusions in Steel on Hydrogen Evolution and Embrittlement," British Welding Journal, Vol. 14, 1967, pp. 321-333.
20. K. Klemetti et al., "On the Role of Inclusions in Environment Sensitive Cracking of Reactor Pressure Vessel Steels," in Proceedings of the International Conference on Environmental Degradation of Materials in Nuclear Power Systems - Water Reactors, 22-25 August 1983, Myrtle Beach, South Carolina.
21. M. Iino, "Trapping of Hydrogen by Sulfur-Associated Defects in Steel," Metallurgical Transactions, Vol. 16A, 1985, pp. 401-409.
22. G. Gabetta, et al., "Prediction of Cyclic Crack Growth in LWR Environments," in Proceedings of Second IAEA Specialists' Meeting on Subcritical Crack Growth, to be published as USNRC Conference Proceeding.
23. S. P. Lynch, "Environmentally Assisted Cracking -- Fractographic and Mechanistic Aspects," Advances in the Mechanics and Physics of Surfaces, Vol. 2, R. M. Latanision and T. E. Fischer, eds., 1983, pp. 264-364.

24. F. P. Ford, "Mechanisms of Environmental Cracking in Systems Peculiar to the Power Generation Industry," EPRI Final Report, NP-2589, Menlo Park, CA, 1982.
25. F. A. Champion, "Effects Associated with Internal Stresses - Discussion," Internal Stresses in Metals and Alloys, Inst. of Metals, London, 1948, pp. 468-469.
26. H. L. Logan, "Film-Rupture Mechanism of Stress Corrosion," J. Res. Nat. Bur. Std., Vol. 48, 1952, pp. 99-105.
27. T. P. Hoar and J. G. Hines, "The Stress-Corrosion Cracking of Austenitic Stainless Steels: Part I - Mechanism of the Process in Hot Magnesium-Chloride Solutions," J. Iron St. Inst. 182, 1956, pp. 124-143.
28. T. P. Hoar and J. M. West, "Mechano-Chemical Anodic Dissolution of Austenitic Stainless Steel in Hot Chloride Solution," Proc. Royal Soc., A268, 1962, pp. 304-315.
29. T. P. Hoar and J. C. Scully, "Mechanochemical Anodic Dissolution of Austenitic Stainless Steel in Hot Chloride Solution at Controlled Electrode Potential," J. Electrochem. Soc., Vol. 111, 1964, pp. 348-352.
30. P. R. Swann and J. D. Embury, "Microstructural Aspects of Stress-Corrosion Failure," High Strength Materials, V. F. Zackay ed., Wiley, New York, 1965, pp. 327-362.
31. T. J. Smith and R. W. Staehle, "Role of Slip Step Emergence in the Early Stages of Stress Corrosion Cracking in Face Centered Iron-Nickel-Chromium Alloys," Corrosion, Vol. 23 (5), 1967, pp. 117-129.
32. J. C. Scully, "Kinetic Features of Stress Corrosion Cracking," Corros. Sci., Vol. 7, 1967, pp. 197-207.
33. J. C. Scully, "Stress Corrosion Crack Propagation: A Constant Charge Criterion," Corros. Sci., Vol. 15, 1975, pp. 207-224.
34. J. C. Scully, "The Interaction of Strain-Rate and Repassivation Rate in Stress Corrosion Crack Propagation," Corros. Sci., Vol. 20, 1980, pp. 997-1016.
35. R. N. Parkins, "Stress Corrosion Spectrum," Br. Corros. J., Vol. 7(2), 1972, pp. 16-28.
36. R. N. Parkins, "Environment Sensitive Fracture and Its Prevention," Br. Corros. J., Vol. 14, 1979, pp. 5-11.
37. R. W. Staehle, "Stress Corrosion Cracking of the Fe-Cr-Ni Alloys System," The Theory of Stress Corrosion Cracking in Alloys, ed., J. C. Scully, NATO, Brussels, 1971, pp. 223-288.

38. R. W. Staehle, "Predictions and Experimental Verification of the Slip Dissolution Model for Stress Corrosion Cracking of Low Strength Alloys," Stress Corrosion Cracking and Hydrogen Embrittlement of Iron-Base Alloys, R. W. Staehle, et al. eds., NACE, Houston, 1977, pp. 180-207.
39. F. P. Ford and P. W. Emigh, "Prediction of the Maximum Corrosion Fatigue Crack Propagation Rate in the Low Alloy Steel/Deoxygenated Water System at 288°C," submitted for publication in Corrosion Science, 1984.
40. R. N. Parkins, "Predictive Approaches to Stress Corrosion Cracking Failure," Corrosion Science, Vol. 20, 1979, pp. 147-166.
41. D. A. Vermilyea, "A Film Rupture Model for Stress Corrosion Cracking," Stress Corrosion Cracking and Hydrogen Embrittlement of Iron Base-Alloys, R. W. Staehle, et al. eds., NACE, Houston, 1977, pp. 208-217.
42. D. A. Vermilyea and R. B. Diegle, "Concerning Strain-Enhanced Corrosion Mechanisms of SCC," Corrosion, Vol. 32, 1976, pp. 26-29.
43. P. M. Scott and A. E. Truswell, "Corrosion Fatigue Crack Growth in Reactor Pressure Vessel Steels — Measurement and Application," Structural Integrity of Light Water Reactor Components, eds., L. E. Steele, et al., Applied Science Publishers, 1982, pp. 287-309.
44. T. R. Mager, G. P. Sabol and G. Slama, "Prediction of Environmental Crack Growth in Nuclear Power Plant Components," EPRI Semiannual Technical Progress Report No. 4, Palo Alto, CA, 1984.
45. K. Sieradzki and R. C. Newman, "Brittle Behavior of Ductile Metals During Stress-Corrosion Cracking," Phil. Mag., Vol. 51 (1), 1985, pp. 95-132.
46. E. Lenz, A. Liebert, B. Stellwag, and N. Wieling, "Einflussgrößen der Dehnungsinduzierten Risskorrosion an Niedriglegierten Stählen in Hochtemperatur-Wasser," 8, MPA-Seminar, Stuttgart, Oct. 14-15, 1982.
47. T. Kobayashi and D. A. Schockey, "Environmentally-Accelerated Cyclic Crack Growth Mechanisms in Reactor Steel Determined from Fracture Surface Topography," SRI International Technical Report 002-84, Menlo Park, CA, 1984, p. 20.
48. J. H. Bulloch and L. W. Buchanan, "Fatigue Crack Growth Behaviour of A 533-B Steel in Simulated PWR Water," Corrosion Science, Vol. 24(8), 1984, pp. 661-674.
49. H. Illi, E. Chanfreau and H. Hänninen, "Application of Miniature Autoclaves in the Study of Crevice Chemistry at High Temperatures," Conference on Corrosion Chemistry Within Pits, Crevices and Cracks, Teddington, Oct. 1-3, 1984.
50. A. R. Troiano, "The Role of Hydrogen and Other Interstitials in the Mechanical Behavior of Metals," Trans. ASM, Vol. 52, 1960, pp. 54-80.

51. R. A. Oriani, "A Mechanistic Theory of Hydrogen Embrittlement of Steels," Ber. Bunsenges. Phys. Chem., Vol. 76, 1972, pp. 848-857.
52. R. A. Oriani and P. H. Josephic, "Equilibrium Aspects of Hydrogen-Induced Cracking in Steels," Acta Met., Vol. 22(9), 1974, pp. 1065-1074.
53. W. A. Tiller, "Thermodynamic-Kinetic Model of Stress Corrosion," Stress Corrosion Cracking and Hydrogen Embrittlement of Iron Base Alloys, R. W. Staehle, et al. eds., NACE, Houston, pp. 332-350.
54. W. W. Gerberich and Y. T. Chen, "Hydrogen-Controlled Cracking -- An Approach to Threshold Stress Intensity," Met. Trans., Vol. 6A(2), 1975, pp. 271-278.
55. R. A. Page and W. W. Gerberich, "The Effect of Hydrogen Source on Crack Initiation in 4340 Steel," Met. Trans., Vol. 13A(2), 1982, pp. 305-311.
56. J. R. Rice, "Hydrogen and Interfacial Cohesion," Effect of Hydrogen on Behavior of Materials, A. W. Thompson and I. M. Bernstein eds., AIME, New York, 1976, pp. 455-466.
57. N. J. Petch and P. Stables, "Delayed Fracture of Metals Under Static Load," Nature, Vol. 169, 1952, pp. 842-843.
58. N. J. Petch, "Lowering of the Fracture Stress Due to Surface Adsorption," Phil. Mag., Vol. 1, 1956, pp. 331-335.
59. C. A. Zapffe and C. E. Sims, "Hydrogen Embrittlement, Internal Stress and Defects in Steel," Trans. AIME, Vol. 145, 1941, pp. 225-259.
60. J. P. Hirth and H. H. Johnson, "Hydrogen Problems in Energy Related Technology," Corrosion, Vol. 32(1), 1976, pp. 3-25.
61. W. H. Bamford and D. M. Moon, "Some Mechanistic Observations on the Crack Growth Characteristics of Pressure Vessel and Piping Steels in PWR Environment," Corrosion, Vol. 36(6), 1980, pp. 289-298.
62. H. K. Birnbaum, "Hydrogen Related Failure Mechanisms in Metals," Environmental-Sensitive Fracture of Engineering Materials, Z. A. Foroulis ed., TMS-AIME, Warrendale, PA, 1979, pp. 326-460.
63. C. D. Beachem, "A New Model for Hydrogen Assisted Cracking (Hydrogen "Embrittlement")," Met. Trans., Vol. 3A(2), 1972, pp. 437-451.
64. C. D. Beachem, "Electron Fractographic Support for a New Model for Hydrogen-Assisted Cracking," Stress Corrosion Cracking and Hydrogen Embrittlement of Iron Base Alloys, R. W. Staehle, et al. eds., NACE, Houston, 1977, pp. 376-381.
65. T. Tabata and H. K. Birnbaum, "Direct Observations of the Effect of Hydrogen on the Behavior of Dislocations in Iron," Scripta Met., Vol. 17, 1983, pp. 947-950.

66. T. Tabata and H. K. Birnbaum, "Direct Observations of Hydrogen Enhanced Crack Propagation in Iron," Scripta Met., Vol. 18, 1984, pp. 231-236.
67. A. W. Thompson, "Effect of Metallurgical Variables on Environmental Fracture of Engineering Materials," Environment-Sensitive Fracture of Engineering Materials, Z. A. Foroulis ed., TMS-AIME, Warrendale, PA, 1979, pp. 379-410.
68. F. E. Fujita, "Theory of Hydrogen Induced Delayed Fracture of Steel," Second International Congress on Hydrogen in Metals, ed., P. Azou, Paris, Paper 2B10, 1977.
69. A. R. C. Westwood, C. M. Preece and M. H. Kamdar, "Application of a Crack Propagation Criterion to Liquid-Metal Embrittlement; Cleavage of Aluminum Monocrystals in Liquid Gallium," Trans. ASM, Vol. 60, 1967, pp. 763-765.
70. H. H. Uhlig, "Applying Critical Potential Data to Avoid Stress Corrosion Cracking of Metals," Journal of Applied Electrochemistry, Vol. 9, 1979, pp. 191-199.
71. S. P. Lynch, "Mechanisms of Fatigue and Environmentally Assisted Fatigue," Fatigue Mechanisms, J. T. Fong ed., ASTM STP 675, American Society for Testing and Materials, Philadelphia, PA, 1979, pp. 174-213.
72. T. Hakkarainen and H. Hänninen, On the Slip-Dissolution Stress Corrosion Mechanism, to be published, 1985.
73. F. Gröschel, "Untersuchungen zur Rolle der Plastizität bei der Spannungsrisskorrosion in FeCrNi-Einkristallen," Doktor-Ingenieurs Dissertation, Fakultät für Bergbau und Hüttenwesen der Rheinisch-Westfälischen Technischen Hochschule, Aachen, 1981, p. 84.
74. J. Silcock and P. R. Swann, "Microstructural Aspects of Environment Sensitive Failure of Austenitic Stainless Steels," Mechanisms of Environment Sensitive Cracking of Materials, P. R. Swann, F. P. Ford and A. R. C. Westwood eds., The Metals Society, London, 1977, pp. 66-80.
75. G. M. Scamans and P. R. Swann, "High Voltage Electron Metallography of Stress Corrosion Cracking of Austenitic Stainless Steels," Corros. Sci., Vol. 18, 1978, pp. 983-995.
76. N. A. Nielsen, "Observations and Thoughts on Stress Corrosion Mechanisms," J. Mater., Vol. 5(4), 1970, pp. 794-829.
77. S. Tähtinen, H. Hänninen and T. Hakkarainen, "Electrochemical Measurements of Low-Index Planes of a Fe-14.5Cr.14.5Ni-2.5Mo Single Crystal," Thin Films Science and Technology, Passivity of Metals and Semiconductors, ed., M. Froment, Elsevier, Amsterdam, 1983, pp. 695-700.
78. S. Tähtinen, H. Hänninen and T. Hakkarainen, "On the Role of Anisotropic Electrochemical Properties in Stress Corrosion Cracking of Austenitic Stainless Steel," Conference on Stainless Steels '84, Gothenburg, Sept. 3-5, 1984.

79. B. Tomkins, "Role of Mechanics in Corrosion Fatigue," Metal Science, Vol. 13(1), 1979, pp. 387-395.
80. I. M. Austen, Quantitative Understanding of Corrosion Fatigue Crack Growth Behaviour, Commission of the European Communities, London, 1983, p. 130.
81. M. R. Louthan, Jr., G. R. Caskey, Jr., J. A. Donovan and D.E. Rawl, Jr., "Hydrogen Embrittlement of Metals," Mat. Sci. Eng., Vol. 10, 1972, pp. 357-368.
82. J. A. Donovan, "Accelerated Evolution of Hydrogen from Metals during Plastic Deformation," Met. Trans., Vol. 7A(11), 1976, pp. 1677-1683.
83. J. K. Tien, A. W. Thompson, I. M. Bernstein and R. J. Richards, "Hydrogen Transport by Dislocations," Met. Trans., Vol. 7A(5), 1976, pp. 821-829.
84. T. R. Mager, G. P. Sabol and G. Slama, "Prediction of Environmental Crack Growth in Nuclear Power Plant Components," EPRI Semiannual Technical Progress Report No. 1, Palo Alto, CA, 1982.
85. T. R. Mager, G. P. Sabol and G. Slama, "Prediction of Environmental Crack Growth in Nuclear Power Plant Components," EPRI Semiannual Technical Progress Report No. 2, Palo Alto, CA, 1983.
86. T. R. Mager, G. P. Sabol and G. Slama, "Prediction of Environmental Crack Growth in Nuclear Power Plant Components," EPRI Semiannual Technical Progress Report No. 3, Palo Alto, CA, 1983.
87. G. Gabetta and R. Rizzi, "Electrochemical Potentials Measured at the Tip of a Growing Fatigue Crack in Demineralized Water 93°C: The Effect of Frequency, Wave Form and Oxygen Content," Corrosion Science, Vol. 23(6), 1983, pp. 613-621.
88. G. Gabetta and E. Caretta, "Electrochemical Potential Measurements Inside and Outside a Growing Crack During Environmental Fatigue Tests at 288°C, With Different Oxygen Contents," Conference on Corrosion Chemistry Within Pits, Crevices and Cracks, Teddington, Oct. 1-3, 1984.
89. J. D. Atkinson and T. C. Lindley, "The Effect of Hydrogen Gas on Fatigue Crack Propagation in A 533-B Steel Below 100°C and Its Relevance to Environmentally Assisted Cracking in Aqueous Environments," CERL Memorandum, TPRD/L/MT/0212/M84, 1984, p. 25.
90. A. H. Priest, Fatigue Crack Growth and Fracture Resistance of Steels in High-Pressure Hydrogen Environments, Commission of the European Communities, London, 1983, p. 47.
91. C. Amzallag, J. L. Bernard, G. Slama, "Effect of Loading and Metallurgical Parameters on the Fatigue Crack Growth Rates of Pressure Vessel Steels in Pressurized Water Reactor Environment," Environmental Degradation of Materials in Nuclear Power Systems - Water Reactors, J. T. A. Roberts and W. Berry eds., NACE, Houston, 1983, pp. 727-745.

92. F. Nakasato and I. M. Bernstein, "Crystallographic and Fractographic Studies on Hydrogen-Induced Cracking in Purified Iron and Iron-Silicon Alloys," Met. Trans., Vol. 9A(9), 1978, pp. 1317-1326.
93. H. W. Hayden and S. Floreen, "Effect of Various Modes of Loading on the Stress Corrosion Cracking of a Maraging Steel," Corrosion, Vol. 27(10), 1971, pp. 429-433.
94. T. Shoji, et al., "Role of Loading Variables in Environment Enhanced Crack Growth for Water Cooled Nuclear Reactor Pressure Vessel Steels," IAEA Specialists' Meeting on Subcritical Crack Growth, Freiburg, FRG, 1981.
95. G. Bombara, "Review of Surface Factors in Stress Corrosion Cracking of Alloys," Metallurgical Science and Technology, Vol. 2(2), Aug. 1984.
96. Stress Corrosion -- New Approaches, ASTM STP 610, American Society for Testing and Materials, Philadelphia, 1976.
97. J. H. Payer, W. E. Berry and W. K. Boyd, "Constant Strain Rate Technique for Assessing Stress Corrosion Susceptibility," Stress Corrosion -- New Approaches, ASTM STP 610, American Society for Testing and Materials, Philadelphia, 1976.
98. Round Robin on Slow Strain Rate Tests, ICCGR Meeting, Daresbury, UK, Spring 1984.
99. P. M. Scott and A. E. Truswell, "The Influence of Water Chemistry on Fatigue Crack Propagation in LWR Pressure Vessel Steels," In Proceedings of IAEA Specialists' Meeting on Subcritical Crack Growth, Sessions III, IV and V, U.S.N.R.C. Conference Proceeding NUREG/CP-0044, Vol. 2, May, 1983, pp. 91-126.
100. D. P. G. Lidbury, "The Estimation of Crack Tip Strain Rate Parameters Characterizing Environment Assisted Crack Growth Data," Proceedings of TMS-ASME Symposium Localized Chemistry and Mechanics in Environment Assisted Fracture, Oct. 4-5, 1983.
101. G. Gabetta, Presentation at ICCGR Spring Meeting 1984, Risley, UK.
102. A. Saxena and S. J. Hudak, "Review and Extension of Compliance Information for Common Crack Growth Specimens," Int. Jour. of Fracture, Vol. 14(5), Oct. 1978, pp.
103. G. Gabetta and C. Rinaldi, "Environmental Fatigue Tests at Different Starting Crack Length and Applied Load," Conference on Environment Sensitive Cracking Problems in Nuclear Installations Containing High Temperature Water, Munich, FRG, Sept. 18-20, 1984.
104. G. Gabetta, Presentation at the ICCGR Fall Meeting 1984, Akron, OH.
105. T. Shoji and J. Congleton, "Evaluation of Crack Opening Rate in SSRT by Elastic-Plastic Fracture Mechanics," Presentation at ICCGR Spring 1983 meeting in Milano, Italy.



106. W. J. Shack, "Phenomenological Model for Strain Rate Effects on IGSCC in CERT Tests," Presentation at the ICCGR Spring 1984 meeting in Risley, UK.
107. T. Shoji, "Evaluation of Crack Tip Strain Rates and Crack Growth Mechanisms," Presentation at ICCGR Spring 1984 meeting in Risley, UK.
108. G. C. Cherepanov, "Crack Propagation in Continuous Media," Appl. Math. Mech (PMM), Vol. 31, 1967, p. 476.
109. J. W. Hutchinson, "Plastic Stress and Strain Field at a Crack Tip," J. Mech. Phys. Solids, Vol. 16, 1968, p. 337.
110. J. R. Rice, "Mathematical Analysis in the Mechanics of Fracture," Fracture, An Advance Treatise, Vol. II, Chp. 3, ed., H. Leibowitz, Academic Press, NY, 1968.
111. J. R. Rice and A. L. Rosengren, "Plane Strain Deformation Near a Crack Tip in Power Law Hardening Material," J. Mech. Phys. Solids, Vol. 16, 1968, p. 1.
112. N. Levy, P. V. Marchal, W. J. Ostergren and J. Rice, "Small Scale Yielding Near a Crack in Plane Strain: A Finite Element Analysis," Int. J. Fracture Mech., Vol. 16, 1971, p. 143.
113. J. R. Rice and M. A. Johnson, "The Role of Large Crack Tip Geometry Changes in Plane Strain Fracture," Inelastic Behavior of Solids, M. F. Kanninen, et al. eds., McGraw Hill, NY, 1969.
114. P. V. Marcal and I. P. King, "Elastic-Plastic Analysis of Two-Dimensional Stress Systems by the Finite Element Method," Int. J. Mechanical Sciences, Vol. 9, 1967, p. 143.
115. A. Mendelson, Plasticity: Theory and Application, The MacMillan Company, NY, 1968.
116. J. L. Sweldlow, "Elasto-Plastic Cracked Plates in Plane Strain," Int. J. Fracture Mech., Vol. 5, 1963, p. 33.
117. I. S. Tuba, "A Method of Elastic-Plastic Plane Stress and Strain Analysis," J. of Strain Analysis, Vol. 1, 1966, p. 115.
118. W. L. Wilson, et al., "Crack Tip Strain and Strain Rates," Presentation at the ICCGR meeting in Risley, UK, Spring 1984.
119. G. Wästberg, "A Finite Element Analysis of a Crack Growing Under Cyclic Loading," Fat. of Eng. Mat. and Structures, Vol. 6, 1983, p. 149.
120. C. Laird and G. C. Smith, "Crack Propagation in High Stress Fatigue," Phil. Mag., Vol. 7, 1962, p. 847.
121. B. Tomkins and W. D. Biggs, "Low Endurance Fatigue in Metals and Polymers," J. Mater. Sci., Vol. 7, 1969, p. 544.

122. P. Newmann, "New Experiments Concerning the Slips Processes at Propagating Fatigue Crack," Acta Metall., Vol. 22, 1974, p. 1155.
123. F. A. McClintock, "On the Plasticity of the Growth of Fatigue Cracks," Fracture in Solids, J. J. Gilman and D. C. Drucker eds., Wiley, NY, 1963.
124. J. Weertman, "Fatigue Crack Propagation Theories," Fatigue and Microstructure, American Society for Metals, 1978.
125. A. J. McEvily, Jr., "On the Quantitative Analysis of Fatigue Crack Propagation," Fatigue Mechanisms: Advances in Quantitative Measurement of Physical Damage, ASTM STP 811, American Society for Testing and Materials, Philadelphia, 1983, p. 283.
126. K. Tanaka, T. Hoshide and N. Sakai, "Mechanics of Fatigue Crack Propagation by Crack-Tip Plastic Blunting," Engineering Fracture Mechanics, 19 (5), 1984, p. 805.
127. G. Terlinde and G. Luetjering, "Influence of Grain Size and Age-Hardening on Dislocation Pile-Up and Tensile Fracture for a Ti-Alloy," Metall. Trans. A., Vol. 13A, 1982, p. 1283.
128. S. B. Chakraborty, "A Model Relating Low-Cycle Fatigue Properties and Microstructure to Fatigue Crack Propagation Rates," Fatigue Engrg Mater. Struct., Vol. 2, 1979, p. 331.??
129. H. W. Liu and N. Ino, Fracture, Chapman and Hall, London, 1969, p. 812.
130. J. Lanteigue and J. P. Bailon, "Theoretical Model for FCGR Near the Threshold," Metall. Trans. A., Vol. 6A, 1981, p. 459.
131. D. L. Davidson and J. Lankford, "The Effect of Water Vapor on Fatigue Crack Tip Stress and Strain Range Distribution and the Energy Required for Crack Propagation in Low-Carbon Steel," Int. J. Fract., Vol. 17, 1981, p. 257.
132. D. L. Davidson and J. Lankford, "The Effect of Water Vapor on Fatigue Crack Tip Mechanics in 7075-T651," Fatigue Engrg. Mater. Struct., Vol. 6, 1983, p. 241.
133. D. L. Davidson, "A Model for Fatigue Crack Advance Based on Crack Tip Metallurgical and Mechanics Parameters," Acta Metall., Vol. 32, 1984, p. 707.
134. D. L. Davidson, et al., "Crack Tip Plasticity Associated with Corrosion Fatigue," Interim Report for Period June 1978 - June 1979, N00014-75-C-1038, May 31, 1979.
135. S. J. Hudak, Jr., D. L. Davidson, "The Role of Crack-Tip Deformation on Environment-Enhanced Crack Growth," Interim Progress Report no. 2, EPRI Contract RP-2006-7, March 1984.

136. S. J. Hudak, Jr., D. L. Davidson and R. A. Page, "The Role of Crack-Tip Deformation on Environment-Enhanced Crack Growth," Interim Progress Report no. 1, EPRI Contract RP-2006-7, Dec. 1983.
137. R. Wei and J. Landes, "The Kinetics of Subcritical Crack Growth and Deformation in a High-Strength Steel," Trans ASME, J. Eng. Mat. Tech., Series H, 95, (1973) pp. 2-9.
138. R. O. Ritchie, "Near-Threshold Fatigue Crack Propagation in Steels," International Metals Reviews, 1979, No. 5 and 6, pp. 205-230.
139. P.C. Paris et al., "An Extensive Study on Low Fatigue Crack Growth Rates in A533B and A508 Steels," Westinghouse Technical Document 71 - 1E7-FMPWR-P7, Westinghouse Research Laboratories, 1971.
140. R. A. Schmidt and P. C. Paris, "Threshold for Fatigue Crack Propagation and the Effects of Load Ratio and Frequency," in Progress in Flaw Growth and Fracture Toughness, ASTM STP 536, 1973, pp. 79-94.
141. P. K. Liaw, J. Anello and J. K. Donald, "Influence of Corrosive Environments on Near-Threshold Fatigue Crack Growth in 403 Stainless Steel," Met. Trans A, 13A, 1982, pp. 2177-2189.

U.S. NUCLEAR REGULATORY COMMISSION  
BIBLIOGRAPHIC DATA SHEET

1. REPORT NUMBER (Assigned by DDC)

NUREG/CR-4422  
MEA-2078

4. TITLE AND SUBTITLE (Add Volume No., if appropriate)

A Review of the Models and Mechanisms for Environmentally-Assisted Crack Growth of Pressure Vessel and Piping Steels in PWR Environments

2. (Leave blank)

3. RECIPIENT'S ACCESSION NO.

7. AUTHOR(S)

W. Cullen, G. Gabetta, H. Hanninen

5. DATE REPORT COMPLETED

MONTH | YEAR  
September | 1985

9. PERFORMING ORGANIZATION NAME AND MAILING ADDRESS (Include Zip Code)

Materials Engineering Associates, Inc.  
9700-B George Palmer Highway  
Lanham, MD 20706

DATE REPORT ISSUED

MONTH | YEAR  
December | 1985

6. (Leave blank)

8. (Leave blank)

12. SPONSORING ORGANIZATION NAME AND MAILING ADDRESS (Include Zip Code)

Division of Engineering Technology  
Office of Nuclear Regulatory Research  
U.S. Nuclear Regulatory Commission  
Washington, D. C. 20555

10. PROJECT/TASK/WORK UNIT NO.

11. FIN NO

B8900

13. TYPE OF REPORT

Technical Report

PERIOD COVERED (Inclusive dates)

15. SUPPLEMENTARY NOTES

14. (Leave blank)

16. ABSTRACT (700 words or less)

The crack-tip micromechanisms and the computational models for environmentally-assisted cracking in pressure vessel and piping steels in high-temperature, low-oxygen (PWR), reactor-grade water are described and evaluated in this report. The micromechanistic models are discussed in some detail, with anodic dissolution and hydrogen assistance being the prime candidates for the successful explanation of the observed phenomena. The anodic dissolution model offers far better quantification of the environmentally-assisted crack growth rates, but tends to overpredict the rates for a large number of conditions. The hydrogen assistance models qualitatively could account for a wider range of effects, but quantification of the model is virtually nonexistent. A variety of calculational models are in various stages of development; all of them are far from use as a predictive tool. Crack-tip strain rate models have received the most attention, and the approach to their use has been to partition the environmentally-assisted growth rates into a mechanically-driven component, with the environmental enhancement superposed. The environment component is then correlated with a calculated crack-tip strain rate.

17. KEY WORDS AND DOCUMENT ANALYSIS

17a DESCRIPTORS

Corrosion Fatigue, Stress-Corrosion Cracking, Hydrogen Assisted Cracking, Anodic Dissolution, Film Rupture, Crack Tip Strain Rate, Crack Tip Opening Displacement, Hydrogen Absorption, Load Ratio Effects, Frequency Effects, Passivation, Oxidation, Hydrolysis, Fractography, Finite Element Method

17b. IDENTIFIERS/OPEN ENDED TERMS

18. AVAILABILITY STATEMENT

Unlimited

19. SECURITY CLASS (This report)

Unclassified

21. NO. OF PAGES

20. SECURITY CLASS (This page)

Unclassified

22. PRICE

5

UNITED STATES  
NUCLEAR REGULATORY COMMISSION  
WASHINGTON, D.C. 20555

OFFICIAL BUSINESS  
PENALTY FOR PRIVATE USE, \$300

120555079877 1 1A1RFR1R5  
US NRC  
ADM-DIV OF TIDC  
POLICY & PUB MGT BR-PDR NUREG  
W-301  
WASHINGTON DC 20555

FOURTH CLASS MAIL  
POSTAGE & FEES PAID  
USNRC  
WASH DC  
PERMIT No. G 87

CRACK GROWTH OF PRESSURE VESSEL AND PIPING STEELS IN PWR ENVIRONMENTS